1-1-2010

Fabrication of microfluidic channels via Two Photon Absorption (TPA) polymerization

Samir Jariwala
Ryerson University

FABRICATION OF MICROFLUIDIC CHANNELS VIA TWO PHOTON ABSORPTION (TPA) POLYMERIZATION

by

Samir Jariwala
Bachelor of Engineering (Mechanical)
Ryerson University, 2010

A Thesis
presented to Ryerson University
in partial fulfillment of the requirement for the degree of
Master of Applied Science
in the program of
Mechanical Engineering

Toronto, Ontario, Canada, 2010

AUTHOR'S DECLARATION

I hereby declare that I am the sole author of this thesis report.

I authorize Ryerson University to lend this thesis to other institutions or individuals for the purpose of scholarly research.

Samir Jariwala
Department of Mechanical Engineering
Ryerson University

I further authorize Ryerson University to reproduce this project by photocopying or by other means, in total or in part, at the request of other institutions or individuals for the purpose of scholarly research.

Samir Jariwala
Department of Mechanical Engineering
Ryerson University

ABSTRACT

FABRICATION OF MICROFLUIDIC CHANNELS VIA TWO PHOTON ABSORPTION (TPA) POLYMERIZATION

Samir Jariwala, Master of Applied Science, 2010

Mechanical Engineering, Ryerson University

Lab-on-a-chip (LOC) and Micro Total Analysis System (μTAS) devices have attracted a great deal of research because of its potential to be cost effective for onsite biomedical and chemical analyses. Developing low-cost fabrication techniques is the key in transferring TAS from the research labs to the consumer applications. This research focuses on the invention of fluidic channels fabrication processes suitable for rapid prototyping.

Three distinctive and novel processes, each suitable for different channel dimensions and structures, have been developed based on two photon absorption (TPA) polymerization using a high repetition rate femtosecond laser. The first process creates channels as small as a few nanometers in width. Any two dimensional channels can be easily fabricated with the second process. And the last process can be used to fabricate self-enclosed channels. A feasibility study of the proposed techniques and the analysis of control parameters, such as the repetition rates, number of effective pulses, scan speed and pulse energy, are also presented.

Unlike existing lithography-based processes, the proposed processes do not require a mask. Micro/nano Fluidic channels can be generated in a single-step formation. Hence, these processes are cost efficient, fast, simple, and particularly suitable for rapid prototyping.

ACKNOWLEDGMENTS

I would like to thank my research supervisors Dr. K. Venkatakrishnan and Dr. Bo Tan, for their outstanding supervision and guidance. Their unconditional support, advice and constructive criticism throughout my research study have been invaluable.

I would like to thank Dr. Greg Kawall, Director of the Mechanical Engineering Graduate program, all the faculty members, the technical officers and the administrative staff members for their kind support and cooperation throughout all the time during my stay at Ryerson University.

I am also very grateful to my family for their continued support, prayers and love. Deepest gratitude to my parents, sisters and wife, who had to sacrifice their time and needs to support me in successfully finishing my studies.

Finally, I am grateful to the Grace of God for the countless blessings I have received.

DEDICATION

The author hereby would like to dedicate this thesis to his parents, sisters and wife as a token of humble and sincere appreciation for their invaluable love and support.

TABLES OF CONTENTS

LIST OF TABLES

LIST OF FIGURES

NOMENCLATURE

ps	picosecond (10^{-12} s)
fs	femtosecond (10^{-12} s)
µm	micrometer (10^{-6} m)
MHz	megahertz (10^{6-} Hz)
nm	nanometer (10^{-9} m)
W	watt
mW	milli-Watt (10^{-3} W)
µJ	micro-Joule (10^{-6} J)
mJ	milli-Joule (10^{-3} J)

T_g	transition temperature of substrate
E_g	energy bandgap
$h\nu$	photon energy
R	free radicals
I	photoinitiators; intensity of excitation source
k_{i1}	first reaction rate constant
k_{i2}	second reaction rate constant
k_p	propagation rate constant
k_t	termination rate constant
M	monomer molecules
P_1	active, growing free-radical polymer
P_N	free-radicals polymer attach to form macroradical
S	photosensitizer molecule
$n^{(1)}$	number of molecules excited by SPA
$n^{(2)}$	number of molecules excited by TPA
N_g	density of molecules in the ground state
$\sigma(\nu)$	cross section of absorption process at frequency ν
$\delta(\nu)$	TPA cross section at frequency ν

z	distance from the focal plane
ρ_0	primary particle density
$\rho(r, t)$	locally generated density of radicals
ρ_{th}	minimum density of radicals
$N(r, t)$	photon flux
N_0	Constant photon flux
σ_2	effective two photon cross section
σ^a_2	Ordinary two photon absorption cross section
η	efficiency of the initiation process
d	voxel diameter
l	voxel length
t	total irradiation time
τ_L	laser pulse width
n	number of pulses
z_R	Rayleigh length
f	effective focal length; laser repetition rate
λ_0	laser wavelength
D	laser beam diameter
$2\omega_0$	theoretical laser spot size
DOF	depth of focus
Φ_0	maximum laser fluence
Φ_{th}	threshold laser fluence
$\Phi(N_{eff})$	laser fluence at N_{eff}
E_{pulse}	measured laser pulse energy
N_{eff}	effective number of pulses
v	scan speed
R	scanning resolution
%Overlap	Spot-overlap as a percentage of focal spot diameter

µTAS	micro total analysis system
CAD	computer aided drawing
DUV	deep UV lithography
EBL	electron beam lithography
EUV	extreme UV
FIB	focused ion beam
IC	Integrated Circuit
IR	Infrared
LOC	lab on a chip
MEMS	micro-electro-mechanical system
MPA	multi photon absorption
NIL	nano-imprinting lithography
PC	polycarbonate
PDMS	polydimethylsiloxane
PECVD	plasma enhanced chemical vapour deposition
PMMA	poly(methyl methacrylate)
SEM	scanning electron microscope
SPA	single photon absorption
TPA	two photon absorption
UV	ultraviolet
XRL	X-ray lithography

CHAPTER 1

INTRODUCTION TO MICROSYSTEMS, MICROFLUIDIC DEVICES AND MICROFULIDIC CHANNEL FABRICATION PROCESSES

1.1 MICROSYSTEMS AND MICROFLUIDIC DEVICES

Microelectronics and semiconductors have become a foundation of all modern high-tech industries. Integrated circuits (ICs) have penetrated into every aspect of modern life in the form of consumer electronics, computers and communication devices. Over the last few decades, there has been rapid advancement seen in modern Integrated Circuit (IC) Technology. The world total IC sales of $234.3 billion are projected in 2008 and forecasted the growth rate of 16% by 2012 [1]. While the IC industry has witnessed phenomenal growth in the last few decades, a comparable revolution is quietly gaining attention is microsystems technology. Microsystem is a broad name for all miniaturized non-electronic systems such as MEMS (Micro-Electo-Mechanical System), lab-on-a-chip (LOC) [2-4], micro-total analysis system (μTAS) [5, 6], and biochips. μTAS may be hybrids of multiple chips, integrated electronics, and external supports. LOC on the other hand, refers more specifically to a microfluidic chip, and the biochips more generically include the LOC devices and microarray devices. These non-electronic systems have been envisioned for about the last two decades and are almost ready to transform the concepts into reality.

1.2 CONCEPT OF MICRO-TOTAL ANALYSIS SYSTEM (μTAS)

In 1979, S. C. Terry et al. presented "a gas chromatographic air analyzer fabricated on silicon wafer using integrated circuit technology" [7]. This was the first publication that discussed the use of IC fabrication techniques in fabricating structures for chemical analysis. Later in 1990, Manz and coworkers proposed for the first time the concept of μTAS [8]. But why has it attracted so much interest from the scientific and the industrial community? It is because the conventional approach to chemical analysis can no longer meet all the requirements that many applications demand. With rapid developments and growing interest in e.g., medicine, drug discovery, biotechnology, and environmental monitoring, we have become more and more dependent on chemical analysis. Traditionally, chemical analyses have been performed in central laboratories because of the requirements of skilled personnel, specialized equipments, and controlled testing environment. However, the trend is to move chemical analysis closer to the 'customer' to reduce the overall cost, increase flexibility and speed up the detection and treatment process. Today, many examples of such testing devices can be seen, for example, pregnancy test, blood glucose concentration tests, and analysis of soil and water samples. Decentralization of such chemical analyses means that the users can acquire test kits off the shelf and they can be used in the home without any special training in chemistry. For this to happen, we need to make analytical equipment small and thus portable, reliable and easy to operate. Microfabrication allows us to reproduce the same carefully designed μTAS and biochips many times with the same specification. At the heart of each μTAS is a chip, in which fractions of microliters of samples and reagents are moved around with very high accuracy. Traditionally chemical analyses are performed by mixing milliliters of samples and reagents in conventional test tubes and analyzing the product in an analytical instrument. Especially, when the samples

and reagents are in short supply or very expensive, μTAS offers a significant decrease in costs by dramatically reducing the volume of samples and reagents that are needed to perform a chemical analysis. The capability of producing microsturctures in large numbers opens up the possibility of processing samples in parallel, which is very useful and ideal for drug discovery when the same chemical analyses must be performed over many times.

Apart from portability and easiness, online monitoring capability is also desirable. Often, we want to know how the concentration of an analyst changes in time. It is better to continuously monitor the concentration of glucose in the blood of a diabetes patient than to measure the glucose concentration time to time. Similarly, continuous analysis of ammonium in wastewater is more valuable for controlling a sewage-treatment plant than a measurement only 2 or 3 times a day. With the conventional methods of chemical analysis, it is difficult to implement online chemical analyses. Characteristics such as sample handling and processing, the chemical analysis, and data processing are integrated in μTAS, which makes it very well suited for online measurements.

The advantages of μTAS can be summarized as follows: it offers portability, reliability, reduction of sample and reagent consumption, automation of chemical analysis, high-throughput screening, and online analysis. However, more research and advancement is necessary in fabrication techniques of the microfeatures, interconnection and packaging. In addition, the biochip at the heart of the μTAS must be interfaced to the macroworld of the user. For μTAS, this requires fluidic, mechanic, optical, and electronic interconnection. In fluidic devices, many components such as fluidic channels, micropumps, micromixers, filters, reservoirs, valve, nozzle diffusers etc. must be carefully designed and fabricated. Figure 1-1 is an example of the LOC,

which consist of a network of fluidic channels including a sample loading compartment, a chamber for DNA amplification, and channels for separation of the DNA molecules by capillary electrophoresis [9]. Fluidic channels are the most essential component in any fluidic device, therefore should carefully be fabricated incorporating with design requirements.

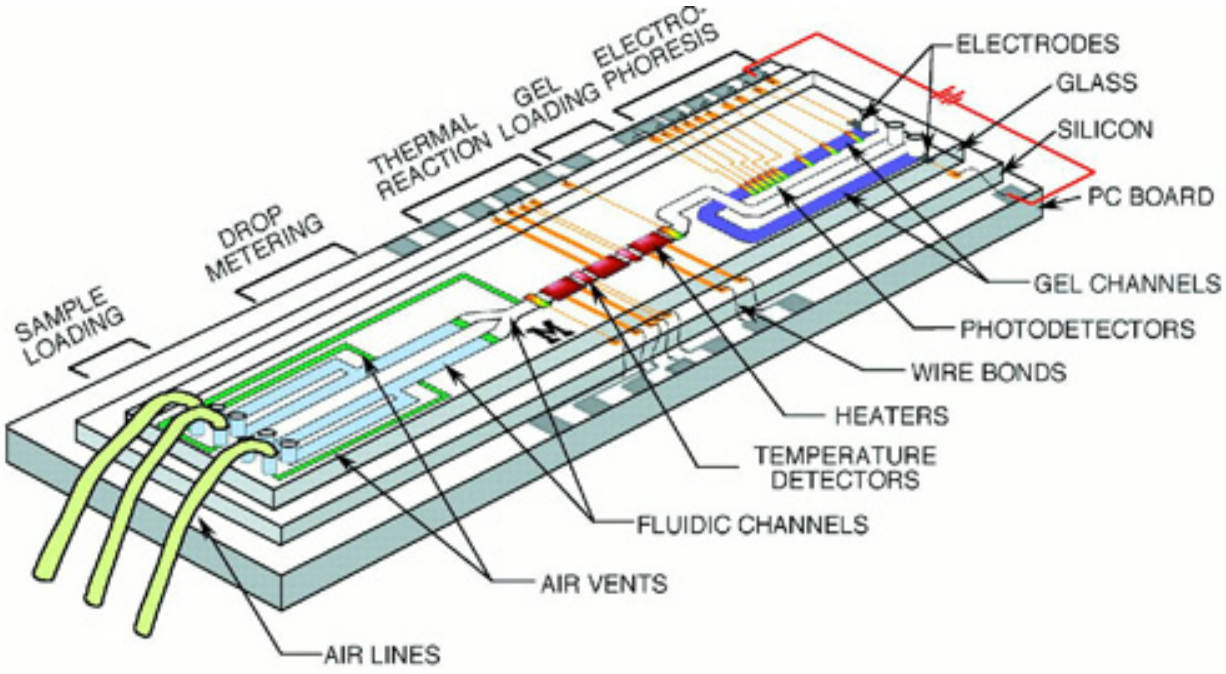

Figure 1-1: Lab-on-a-chip (LOC) illustration [9]

1.3 FLUIDIC CHANNELS FABRICATION PROCESS

Since the emergence of the reliable, reconfigurable, and scalable microsystems, the needs of innovative procedure for creating nano-fluidic channels have accelerated significantly. Fluidic channels are the fundamental building block for any fluidic device fabrication. Applications of fluidic channels include: DNA sequencing [10-12], protein separation [13-15], drug delivery [16, 17], and single molecule detection [18-20]. The fluidic channels fabrication

processes can be categorized by the microfluidic device materials: inorganic materials and polymeric materials.

1.3.1 FABRICATION OF FLUIDIC CHANNELS IN INORGANIC MATERIALS

Due to the rapid developments in the semiconductor industry, photolithography and fabrication of glass, quartz and silicon have been investigated intensively. Inorganic substrates were the first-generation materials used in making μTAS platforms. Earlier biochips were fabricated in either silicon or glass using technologies developed extensively in the microelectronics industry. The first microfluidic devices were made in silicon [7] and glass [8]. Currently, a broad range of inorganic materials are used in μTAS, including glass, silicon, quartz [21-23] and CaF_2 [24].

1.3.1.1 Lithography fabrication

The processes developed for microelectronics, such as standard photolithographic methods, can be applied to silicon, glass or quartz substrates producing channel networks in two dimensions for sample transport, mixing, separation, and detection systems on a microchip. The fabrication in inorganic materials involves the conventional steps such as, photolithography followed by wet or dry etching, and substrate bonding. The microfluidic channels fabrication process in silicon and glass is schematically illustrated in Figure 1-2. The etching process depends on the morphology of the channels needed for the final application. Wet etching of silicon and glass results in trapezoidal and semicircular channels, respectively. Dry etching of silicon or glass using specialized RIE systems is performed to fabricate microfluidic channels

with high aspect ratio and vertical walls. The etched wafers are then bonded to silicon or glass by fusion [25-27], anodic [27], or adhesive bonding techniques [28].

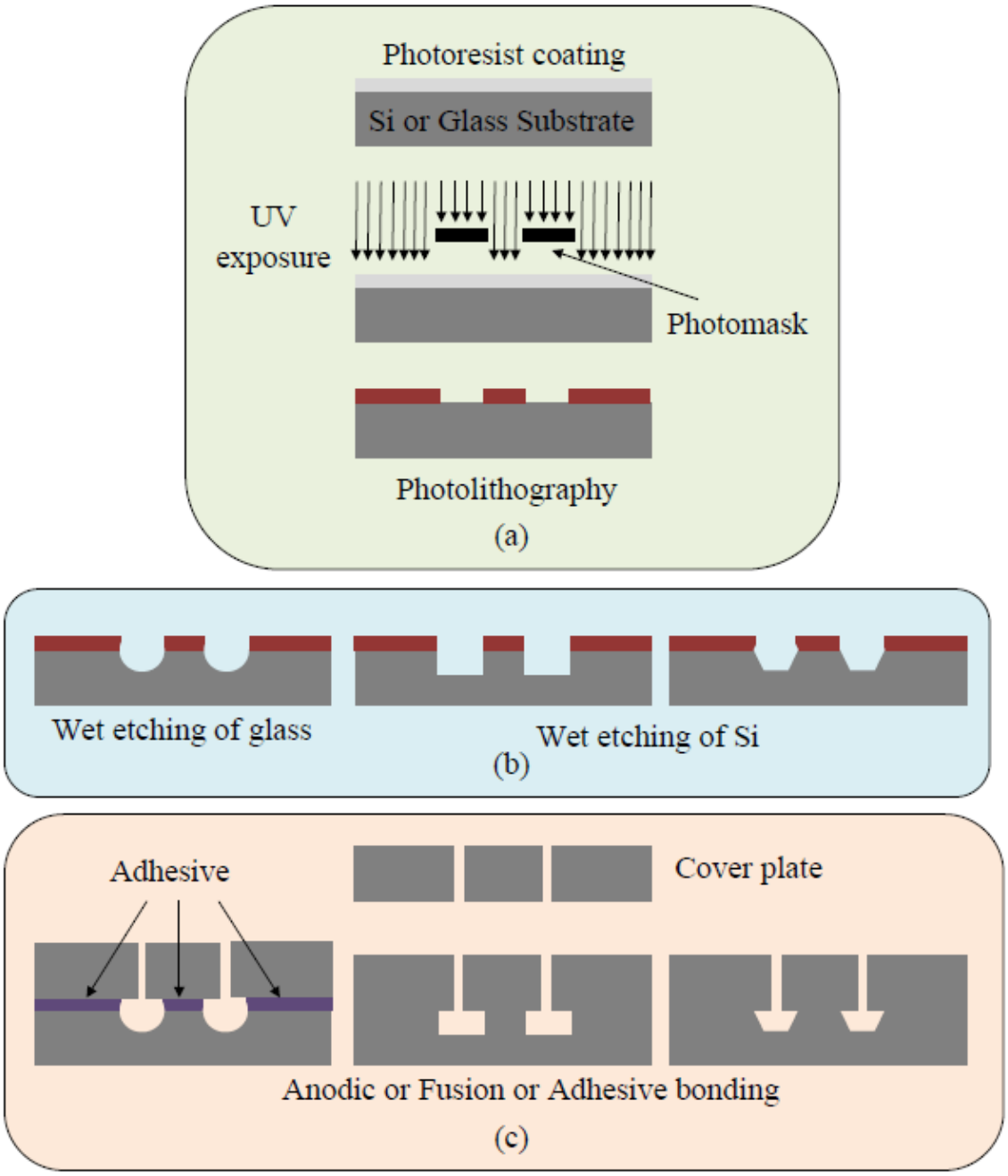

Figure 1-2: Schematic diagram illustrating fabrication of microfluidic channels in silicon and glass (a) step one: photolithography (b) step two: etching (c) step three: bonding

Lithography is very popular in micro-fabrication because of its capability of transferring complex nano patterns to the substrate with high aspect ratios. Also, it has been researched and improved vastly since the era of IC fabrication. With one common goal of reducing the feature size, many researchers over the years have proposed different versions of lithography techniques that can be used to fabricate fluidic channels. Such techniques include soft X-ray lithography [29], extreme UV (EUV) lithography [30], electron beam lithography (EBL) [31, 32], focused ion beam (FIB) [33] and Nano-imprinting lithography (NIL) [34-36]. A brief compression of these techniques used in microfabrication is presented in Table 1-1. The fundamental difference between these techniques is the light source used to polymerize the photoresist. As a general rule, the selection of a fabrication method is determined by several factors, including the available technologies and equipment, cost, speed, fabrication capabilities, and the preferred materials for resists and substrates. Because of the nature of the lithography process, these processes greatly rely on a mask or mold fabrication processes, which are very expensive, time consuming and not feasible for rapid prototyping; therefore alternative patterning techniques are required. In addition, they have complicated fabrication stages, requirements of various special equipments, and the limitation of materials.

Table 1-1: Comparison of lithography techniques used in microfabrication [37]

Technique	Description	Advantages	Disadvantages
DUV and Vacuum-UV Lithography	• Exposure Area: DUV 250 nm, Vac-UV 90 nm • Large complex structures transferred in the size of a chip • Requires High Optical Precision, Homogenous Illumination & Sensitive and Transparent Resists • Improve Resolution by Polarized Light, High Numerical Apertures & use of chemically amplification UV resists	• Cost-Efficient & Highly Productive compared to other lithography techniques	• Light Diffraction Issues • Multi-Million Dollar Equipment & Mask • No Rapid Prototyping since mask required • Multistep
EUV and X-ray Lithography (XRL)	• EUV useful for Medium Nanometric Devices (20-50 nm) as of 2009 • XRL for Nanometer and Sub-Nanometer range • EUV based on reflection optics • X-ray can be used for direct writing into X-ray sensitive resist	• No light diffraction issues • Optical projection easy to control	• Multi-Million Dollar Equipment & Mask • No Rapid Prototyping since mask required • High Resolution Optics difficult to fabricate • Multistep
Electron Beam Lithography	• Sub 10-nm level structures have been realized • Fast electrons applied to knock electrons out of inner shells leading to material ionization • Resolution limited by excitation pear which is caused by proximity effect • Excitation pear dependent on target material and beam parameters especially acceleration voltage • Application in generation of photolithography masks	• Not limited by diffraction • Submicron features can be generated • Maskless process	• Proximity Effect • Expensive resists • Multi-Million Dollar Equipment • No Rapid Prototyping since very slow and expensive
Ion Beam Lithography	• 2-3 nm width cuts in GaAs with Focused Ion Beam (FIB) has been achieved • Similar to electron beam lithography except ions are used • Ions generated and accelerated by electrodes and guided by electronic optics • Applications Can achieve highest resolution, hence used to repair the masks	• High Resolution • Higher Productivity than EBL • Maskless process	• Vacuum environment required • Proximity Effect still present • Multi-Million Dollar Equipment • No Rapid Prototyping since very slow and expensive

1.3.1.2 Thin-film fabrication

A new approach called thin-film fabrication is shown in Figure 1-3 [38]. First, a ~500 nm thick layer of aluminum is deposited on a clean quartz substrate by thermal evaporation, and a ~3 μm thick layer of photoresist is spin coated afterwards. The aluminum and photoresist form a sacrificial layer for the microchannel. Photolithography techniques are used to pattern the sacrificial layer in desired patterns. The channel features are thus defined by the sacrificial layer. A SiO_2 layer is then deposited on the substrate to form a channel and enclose the sacrificial features. Last, the sacrificial layer is removed to form a hollow channel.

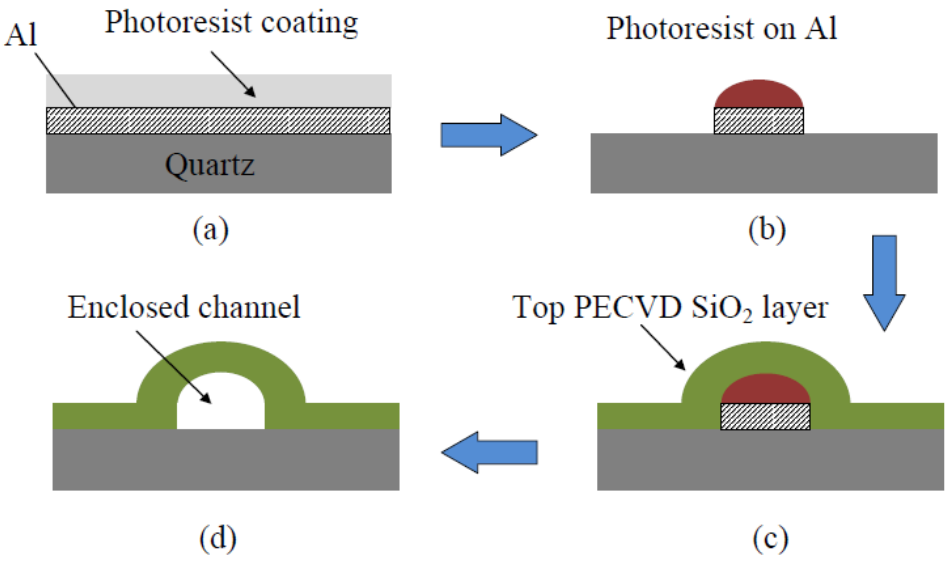

Figure 1-3: Fabrication of microfluidic devices using thin-film methods (a) a quartz substrate is coated with aluminum and photoresist (b) the photoresist and aluminum are patterned via photolithography (c) plasma enhanced chemical vapour deposition (PECVD) is used to deposit SiO_2 over the sacrificial layer (d) etching of the sacrificial layer forms an enclosed channel.

In this process, polymer material is exposed to a pulsed UV source, and the absorption of the light induces bond-breakage in the polymers backbone due to either photodegradation or thermal degradation, or combination of the two. The local temperature of the polymer surface

can be very high where particles are ejected from the substrate creating a channel. Effective ablation largely depends on the absorption rate of the polymer at the source wavelength. Because of such interdependence, the selection of the polymer and the laser source plays an important role to have an efficient fabrication process. The advantage of this method is that a mask is not required since the design path can be written directly. Also, the post process of substrate bonding is unnecessary. Finally, since the microchannels are fabricated using plasma enhanced chemical vapour deposition (PECVD), physical and chemical properties of the channels can be varied by selecting different materials for vapor deposition. The disadvantage is that the parts are made in a sequential manner, which in turns limits the mass production of devices for commercial applications.

1.3.2 FABRICATION OF FLUIDIC CHANNELS IN POLYMERIC MATERIALS

Although microfluidic devices made using inorganic materials have had great success, the disadvantages of inorganic substrates (such as cost, fragility, and fabrication techniques) have limited their applications. Thus, scientists have been investigating the possibility of fabricating microfluidic devices in polymeric materials. The most commonly used polymeric materials are polydimethylsiloxane (PDMS), poly(methyl methacrylate) (PMMA) and polycarbonate (PC). The two major ways of fabricating polymeric features are replication from a master and direct machining. Replication methods often produce a microstructure by allowing a polymer workpiece to form an inverse copy of a mold. The three different existing mass replication technologies evolved from the macro fabrication processes are hot embossing and injection molding and casting. Direct writing method such as laser machining removes the small amount of polymer in places where microstructures, such as fluidic channels, should be located.

1.3.2.1 Hot embossing

Hot embossing has been one of the most widely applied replication processes for microchannel fabrication. The process is rapid, inexpensive, simple and straightforward. After fabrication of the master mold template, a hard plastic substrate is placed in contact with the mold and the stack is then placed in a hydraulic press (Figure 1-4). The polymer substrate is heated to just above its transition temperature (T_g) and pressure is maintained while the temperature is cooled to below T_g. The thermal expansion coefficient of a material determines the extent of change in length or volume resulting from a change in temperature. To minimize thermally induced stresses in the material and the replication errors due to the difference in thermal expansion coefficients of the master mold and the substrates, the thermal cycle should be as small as possible.

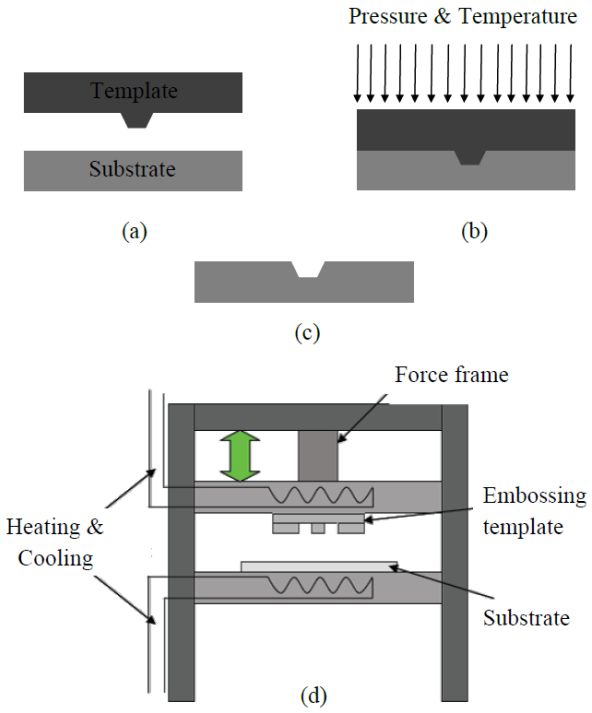

Figure 1-4: Hot embossing ((a)-(c)) process steps (d) schematics of hot embossing press [5]

The replication capability of the embossing method is limited by the process used for the fabrication of the master. Hence, most embossed channel systems are single layer planar structures. Fabrication of the template can be a time consuming process, making it unsuitable for prototyping a few devices for testing.

1.3.2.2 Injection molding

Injection molding is a widespread standard process in the macroscopic world, and can be used to form almost any geometry in thermoplastic materials with dimensions in the range of few millimeters. Injection molding differs from hot embossing mainly in the fact that molten polymer material is injected into the mold. First, a raw, granular, polymer material is fed into the cylinder, where a screw heated to or above the melting temperature of the polymer pushes the melted polymer toward an evacuated cavity that holds the mold insert as the master structure (Figure 1-5). The molten material is then injected under high pressure into the master mold.

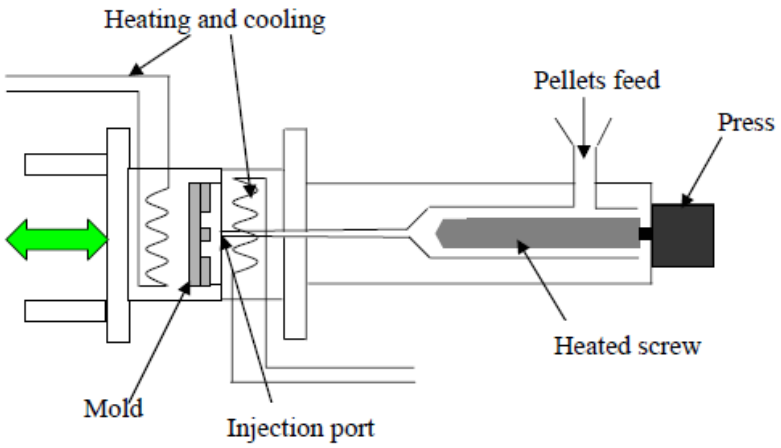

Figure 1-5: Schematics of injection molding apparatus [38]

An advantage of injection molding over hot embossing is that pre-formed elements can be embedded into ensuing components during the molding process. In addition, the cycle time is

shorter, which is preferred in mass production. Nonetheless, since high temperature and pressure are used, high-quality metal templates are usually required, which is an added cost.

1.3.2.3 Casting

Unlike hot embossing and injection molding, which require special fabrication facilities and careful control of conditions, casting is a relatively simple and versatile technique. Casting offers low cost access to planar microchannel structures. Hot embossing and injection molding use a heating and cooling cycle to soften and structure the polymer on a mold, something they both have in common. In contrast, casting uses chemical processes to harden the polymer. The most commonly used material of manufacture is PDMS which offers reasonably useful optical properties. For a typical casting process, liquid PDMS is mixed with cross-linking agent and poured into a cartridge with a template on the bottom (Figure 1-6 (c)). Then, the PDMS liquid is cured at room temperature or at high temperature (to reduce curing time), during which the pattern on the template is transferred to the PDMS surface (Figure 1-6 (d), (e)). After curing, the soft elastomer can simply be peeled off the mold and placed on a planar surface, i.e. plastic or glass slide to form a microchannel by conformal sealing.

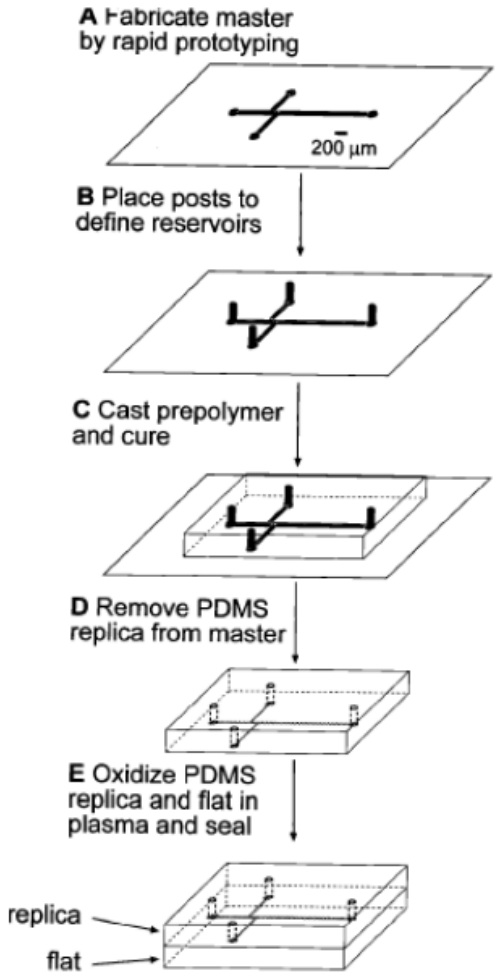

Figure 1-6: Schematic of microfluidic devices casting using PDMS (A) master is fabricated by rapid prototyping (B) posts are positioned on the master to define reservoirs (C) prepolymer is casted on the master and cured. (D) PDMS replica is removed from the master (E) exposing the replica and an appropriate material to air plasma to form an irreversible seal. [39]

Common restrictions among hot embossing, injection molding and casting techniques include: (1) the interface chemistry between the mold and the polymer must minimize any physical or chemical interaction between the two, (2) minimal surface roughness of the mold is needed for the primary success, the lifetime of the mold tool, and the achievable aspect ratio, and (3) undercut structures (i.e., those with overhanging edges) are not possible since the polymer structure has to be removed from the mold.

1.3.2.4 Laser ablation

In contrast to the aforementioned replication methods, laser machining through ablation is a direct machining method. It is based on the removal of polymer material by using intense UV or infrared radiation provided by laser. In this process (Figure 1-7), a pulsed laser is exposed to a polymer material resulting in polymer ablation to create channels. Excimer lasers with emission of 193 nm (ArF) and 248 nm (KrF) are more effective than UV source in polymer ablation.

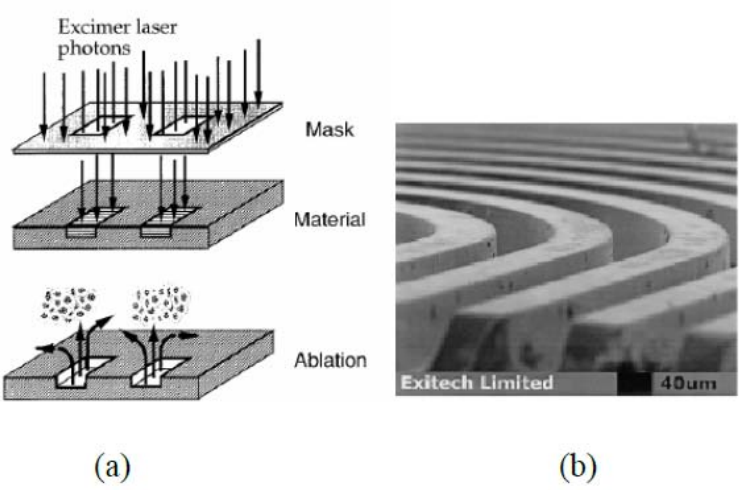

Figure 1-7: (a) UV laser micromachining process. UV excimer laser pulse rapidly breaks chemical bonds and ejection of ablated material (b) laser ablated microchannels [2, 38]

The channels generated using lasers ablation always have greater surface roughness than those fabricated using hot embossing, injection molding, and casting. Finally, it should be mentioned that the ejected polymer residues or decomposed compounds produced during laser ablation may re-deposit on the surface of polymeric substrates and, hence, it may require post process. A comparison of fabrication characteristics of the aforementioned techniques for polymeric material is given in Table 1-2.

Table 1-2: Fabrication techniques comparison for polymeric material

Process	Cost	Cycle time	Force & Temperature	Automation	Geometry	Master mold/mask
Hot embossing	Low-medium	Medium-long	High (kN) & (100-200 °C)	Little	Planer	Yes
Injection molding	High	Short-medium	High (kN) & (150-400 °C)	Yes	Bulk, spherical	Yes
Casting	Low	Long	No force & (room temp-80 °C)	Little	Planer	Yes
Laser ablation	High	Short-medium	No force & (200-500 °C)	Yes	Planer	Yes

1.4 RESEARCH OBJECTIVES

Unlike microelectronics, where the current emphasis is on reducing the size of transistors and the fabrication processes are very well establish, microfluidics is relatively new. The current focus is on making more complex systems of channels with more sophisticated fluid-handling capabilities with innovative fabrication techniques that are feasible for rapid prototyping, rather than just reducing the size of the channels. The need for innovative fabrication methods to integrate higher levels of functionality into microfluidic and LOC devices is growing almost as rapidly as the number of potential applications for these miniature devices. Previously established microelectronics fabrication methods have served greatly in fabricating, miniaturizing, and improving the functionality of devices created in the IC industry. These methods can be utilized in microfluidic channels fabrication. Nonetheless, the alternatives fabrication methods are continually being sought to improve following desirables: (1) Flexibility and versatility in design. (2) Ability to integrate multiple components such as microfluidic valves, pumps and MEMS. (3) Fast processing, reduced cost and ease of fabrication.

Even though the feasibility of using femtosecond lasers has been predicted for over a decade now, its applications in fabricating fluidic components for μTAS is still awaited due to

the challenges faced in terms of laser parameters and inadequate experimental studies in this area. The main aim of this thesis is to discover and investigate novel fabrication techniques for fabricating fluidic channels utilizing the high repetition rate femtosecond laser system.

In order to exercise the TPA polymerization for fabricating fluidic channels, the fundamentals of TPA polymerization must be well understood. One of the major factors influencing the TPA polymerization is the photoinitiation threshold fluence mechanism for a photoresist which greatly depends upon the repetition rate, pulse energy and pulse width. Hence, the outline of the research objectives of this thesis can be summarized as:

1. Study the fundamentals of TPA polymerization and verify the capabilities of the high repetition rate, high average power femtosecond laser system for inducing TPA polymerization.
2. Investigate the photoinitiation threshold fluence mechanisms and its dependency on critical laser parameters such as repetition rate, pulse energy and pulse width.
3. Propose and analyze novel fabrications processes for fluidic channels utilizing TPA polymerization.
4. Evaluate the influence of laser parameters on channel size and quality.

1.5 OVERVIEW OF THESIS

The thesis discusses three novel fabrication techniques developed via TPA polymerization with high repetition rate femtosecond laser. In Chapter 2, the theory of TPA and the polymerization process is discussed in general. Existing mechanism and theories describing

laser-polymer interaction during the short pulse irradiation and the resulting polymeric evolution of a photoresist to polymerized feature are summarized.

The important laser beam characteristics, the selection of substrates and polymers are presented in Chapter 3. This chapter also highlights the details of the experimental setup, the critical laser beam parameters and the overall fabrication process.

The three novel and distinctive fluidic channel fabrication processes are presented in Chapter 4, 5 and 6. Systematic experimental studies of the influence of various laser parameters and process parameters were conducted for each of these processes and the results were reported. In Chapter 4 a very simple yet effective approach to create open fluidic channel is presented, where the spacing between two adjacent TPA polymerized ribs are controlled to form nanofluidic channel in between. The fundamentals of the photoinitiation threshold fluence and average threshold power are studied with respect to the repetition rates. Finally, the effects of repetition rate on the controllability and the reduction in the fluidic channel width are discussed.

In Chapter 5, for the first time, the capability of TPA polymerization assisted ablation is reported. By ablating the pre-polymerized ribs in the center, the microfluidic channels are fabricated. The benefits of utilizing the polymerization assisted ablation instead of direct ablation are discussed here. Also, the fundamental of polymerization assisted ablation threshold are studied.

In Chapter 4 and 5 two different fabrication processes are suggested to create open fluidic channels. Unlike those, a new technique to create self-enclosed fluidic channels is reported in Chapter 6. A model of sub-sequent polymerization is presented to understand the linking of two

polymerized ribs on the top to create hollow fluidic channels. A systematic experimental study of the influence of repetition rate, pulse width and scan speed on the effectiveness of enclosing channels is investigated and the results are discussed.

Chapter 7 summarizes the results obtained from this research work. Also, the mechanisms and achievements of the proposed fabrication processes for rapid prototyping of microfluidic channels via TPA polymerization are summarized. Finally, the chapter also includes suggestions for further research that can be carried out to enhance the proposed processes.

CHAPTER 2

TWO PHOTON ABSORPTION (TPA) POLYMERIZATION

2.1 INTRODUCTION

The possibility of very high localization of laser energy has led to more and more advanced laser applications. Now that the ultrashort lasers are widely available, TPA polymerization, in particular, has been gaining a vast interest in the research community. TPA polymerization is a direct write technique in which the source such as laser focal point moves in three dimensions with respect to the substrate to generate a true three dimensions (3D) pattern. The reason for its increasing popularity is because of its advantages over conventional microfabrication techniques. Some of the most appealing advantages for microfabrication industries are listed below.

- It has intrinsic ability to produce true 3D structures.
- Ultrashort pulses can start intense nonlinear processes at relatively low average power, without thermally damaging the samples.
- No mask, mold, or stamp is needed for fabrication. It directly converts computer-designed patterns into matter structure.
- The rapid turnaround time for fabrication allows one to quickly iterate and modify design.

Despite the fact that the TPA polymerization technique is considered to be a very young technology, it has impacted many fields in a significant manner. The photonics, MEMS, Biomedical and florescent imaging of biological molecules have benefited tremendously with TPA polymerization. Fabrication of 3D photonic crystals [40] (see Figure 2-1 (a)) by the TPA polymerization technique was first proposed and demonstrated by Maruo et al. and now it is recognized by different research groups around the world. They were also able to expand its applications for many other 3D features. For example, Doraiswamy et al. were able to fabricated microneedles [41], shown in Figure 2-1 (b), for transdermal drug delivery. Fabricating 3D MEMS devices are one of the most attractive applications TPA. Nanotweezers [42](see Figure 2-1 (c)) and microgears [43](see Figure 2-1 (d)) were also fabricated by Maruo et al.

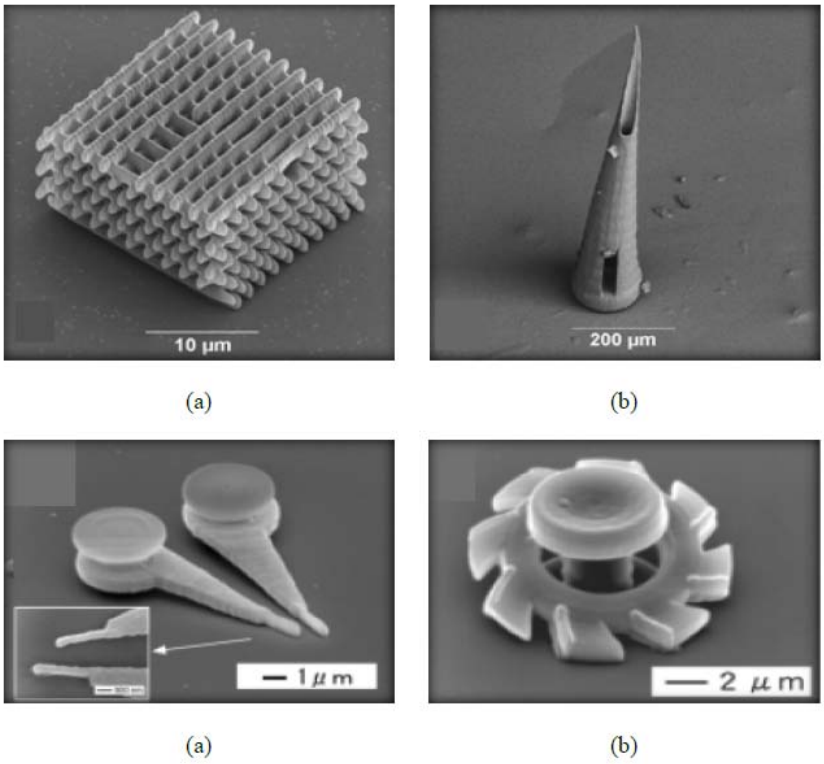

Figure 2-1: Features fabricated using TPA polymerization (a) a woodpile structure 3D photonic crystals (PhCs) [40] ***(b) microneedle*** [41] ***(c) nanotweezers*** [42] ***(d) microgear*** [43]

2.2 CONCEPT OF TWO PHOTON ABSORPTION (TPA)

In 1931, Maria Göppert-Mayer first predicted multi photon absorption (MPA), in which, an atom or a molecule could interact with multiple photons simultaneously in the same quantum event [44]. MPA requires a very high density of photon, therefore it was not until 1961 when it first achieved the experimental proof of MPA using continuous-wave laser source [45]. Assuming that we have a media with an energy bandgap E_g, a single photon with energy $h\nu > E_g$ is able to generate a single electron-hole pair giving rise to linear absorption in such a material, as shown in Figure 2-2 (a). But now let suppose that the energy of the photons is lower such that $E_g/2 < h\nu' < E_g$. In this situation, one photon is not able to excite an electron from the lower edge to the upper edge of the bandgap, but a single electron-hole pair may be produced by the instantaneous absorption of two photons. In TPA, as light passes through a molecule, a virtual energy state is formed by absorption of the first photon, as shown in Figure 2-2 (b). According to Heisenberg's Uncertainty Principle, it persists for a very short duration (for several femtoseconds). TPA can result if the second photon arrives, before the decay of the virtual state. Consecutively, an electron of the molecule is transferred to excited state molecular orbital. If the energies of the two photons are identical, the process is referred to as degenerated TPA, otherwise, the process is a non-degenerated TPA.

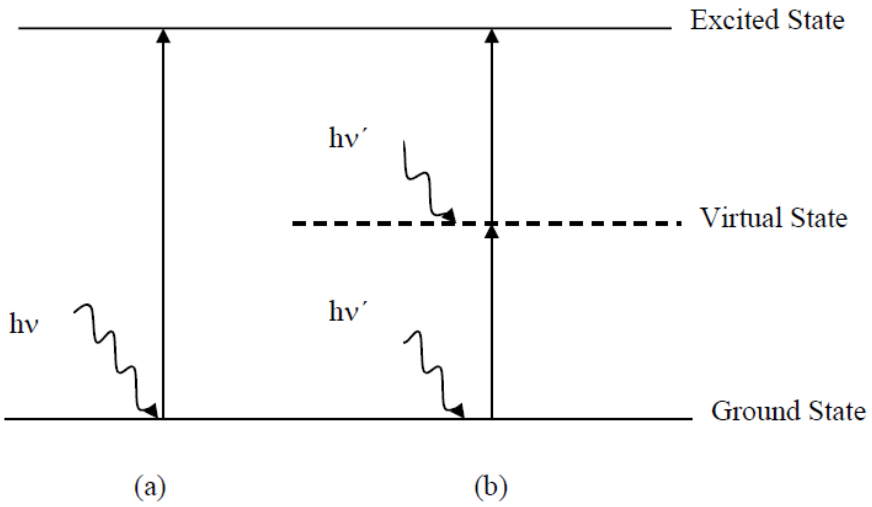

Figure 2-2: Electron excitation via photon absorption (a) Single photon absorption (b) Two photon absorption

2.3 PHOTOPOLYMERIZATION PROCESS

Photopolymerization is a process in which light is used as an energy source to excite unsaturated molecules in a photoresist and convert them from liquid to solid state by polymerization reactions. The excitation light can be anywhere in the UV to IR spectrum.

Once the basic components of any photoresist, the monomers or oligomers, are excited they are solidified by polymerization. The important feature of polymerization is the chain reaction of macromolecules, as shown in Eqn. (2.1) [46].

$$M \xrightarrow{M} M_2 \xrightarrow{M} M_3 \ldots M_{n-1} \xrightarrow{M} M_n \tag{2.1}$$

Here M is the monomer or oligomer unit, and M_n, the macromolecule containing n monomer units. The overall process of photopolymerization can be sub-divided into three stages: initiation, propagation and termination and can be shown as in Eqns. (2.2) to (2.6) [46].

2.3.1 INITIATION

In a commercial resist, more components, such as photoinitiators and photosensitizers, are added to initiate and enhance the photopolymerization. The quantum yield of general monomers and oligomers is very low. In order to increase the initiating efficiency, one or several low-weight molecules that are more sensitive to light irradiation are added. They form initiating species of radicals or cations by absorbing photons. Such small molecules are called photoinitiators. The production of active species that attack monomers or oligomers is called photoinitiation, the most important step in photopolymerization. The initiation phase begins with the formation of the free radicals, *R*, due to the absorption of photons by the photoinitiators, *I*.

$$I + 2hv \xrightarrow{k_{i1}} 2R \tag{2.2}$$

Here, *h* is Plank's constant, *v* is the frequency of the photon, and k_{i1} is the reaction rate constant for the first initiation reaction. The primary radicals *R* is then attach to monomer molecule, *M*, to complete the initiation phase.

$$R + M \xrightarrow{k_{i2}} P_1 \tag{2.3}$$

Here, P_1 is the active, growing free-radical polymer and k_{i2} is the second initiation reaction rate constant. The photoinitiation can be expressed by a photosensitizer molecule, *S*, which absorbs light and then transfers the energy to a photoinitiator.

$$S + 2hv \rightarrow S^* \ldots \rightarrow I \rightarrow 2R \tag{2.4}$$

2.3.2 PROPAGATION

In the propagation phase, monomer molecules attach to the growing, free-radical polymer to form macroradicals, P_N (N=1,2,. . .), which combine with new monomers, and so on; so the macro-radicals expand in a chain reaction. As long as the polymer chain remains reactive, more monomer molecules continue to adhere to the chain. Here, k_p is the propagation rate constant.

$$M + P_{N-1} \overset{k_p}{\rightarrow} P_N \tag{2.5}$$

2.3.3 TERMINATION

Polymer chain termination occurs either through radical combination, which is when a primary radical attaches to the growing, free-radical polymer or two active polymer radicals attach together to form dead polymer P, or through the trapping of active radicals between immobile crosslinked polymer. Here, k_t is the termination rate constant.

$$P_N + P_M \overset{k_t}{\rightarrow} P \tag{2.6}$$

2.4 NON-LINEAR NATURE OF TWO PHOTON ABSORPTION (TPA)

The most important characteristic of TPA that enables the true 3D features with excellent spatial resolution is its non-linear nature of absorption. The probability of a molecule absorbing one photon is proportional to the intensity of the excitation beam [47]:

$$n^{(1)} = \sigma(\nu) N_g \frac{I}{h\nu} \tag{2.7}$$

Here $n^{(1)}$ is the number of molecules excited by SPA per unit time and unit volume in the material, σ is the cross section of the absorption process at frequency ν, N_g is the density of

molecules in the ground state *g*, *I* is the intensity of the excitation source (in energy per unit time and area), and *hv* is the photon energy. In contrast, the probability of a molecule absorbing two photons simultaneously is proportional to the square of the intensity of the excitation beam [47]:

$$n^{(2)} = \frac{1}{2}\delta(\nu)N_g\left(\frac{I}{h\nu}\right)^2 \tag{2.8}$$

Here $n^{(2)}$ is now the number of molecules excited by TPA in the unit volume per unit time and $\delta(\nu)$ is the TPA cross section for a photon of energy *hv*. The pre-factor of 1/2 reflects the fact that two photons are needed to excite one molecule. Figure 2-3 is an illustration of the dependence of the intensity and of the square of the intensity for a laser beam with a Gaussian profile is graphed as a function of *z*, the distance from the focal plane.

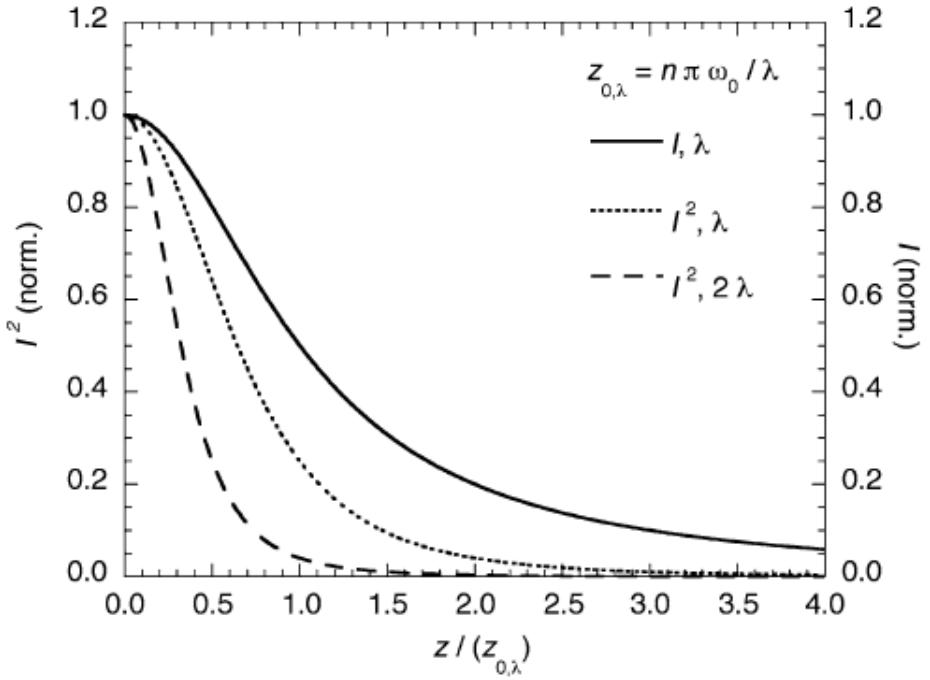

Figure 2-3: Relative excitation rates for the SPA and TPA process along the beam propagation direction. (Solid line, SPA): On-axis intensity for a Gaussian beam with waist ω_0 and wavelength λ; (dotted line, TPA): on-axis square of the intensity a Gaussian beam with waist ω_0 and wavelength λ; (dashed line, TPA): on-axis square of the intensity a Gaussian beam with waist ω_0 and wavelength 2λ. In all cases, the ordinate is normalized to the value at the focus [47]

As a result of this intensity dependence, TPA provides a mechanism by which chemical or physical processes can be activated with high spatial resolution in three dimensions, with excitation being confined to widths down to few nanometers. The ability of TPA to excite molecules with this 3D spatial resolution results from the fact that the intensity of a focused laser beam decreases approximately as the square of the distance, z, from the focal plane. Thus, since TPA scales quadratically with light intensity (see Eqn. 2.8), the number of excited states formed by TPA is proportional to z^{-4}, whereas the number of excited states formed by one-photon absorption is proportional to z^{-2}.

The TPA transition requires photons with approximately half the energy (or twice the wavelength) of the photons needed for SPA into the lowest excited state of a molecule. If the beams at wavelengths λ and 2λ have the same waist at the focus, ω_0, the excitation rate follows the trend of the solid line in the figure for the SPA case and the dashed line in the TPA case. It can be seen that the width of the peak is narrower in the latter situation. Thus, the excited region of volume is significantly confined for TPA in comparison to SPA, as illustrated in Figure 2-4.

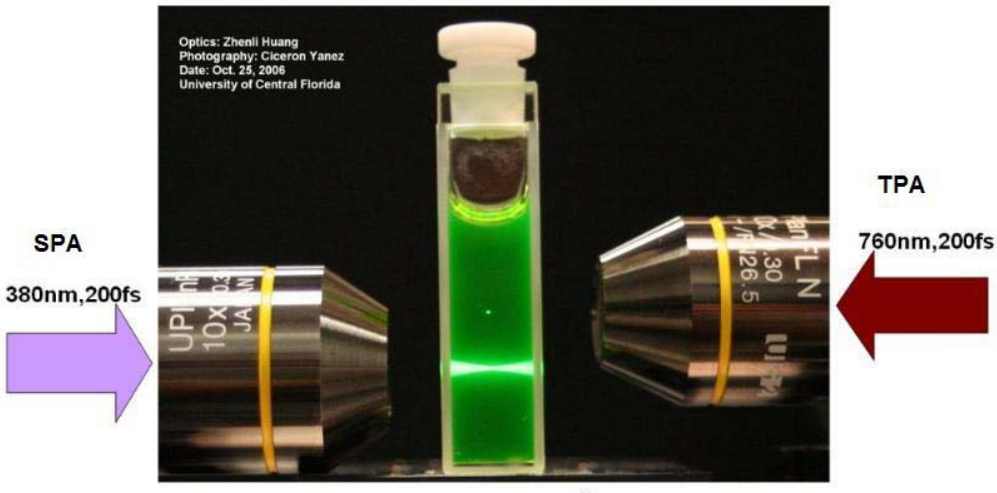

Figure 2-4: Linear and non-linear absorption demonstration in fluorescein dye [48]

Finally, the TPA process is very weak relative to one-photon excitation, in the sense that the ratio $n^{(2)}/n^{(1)}$ (from Eqs. (2.7) and (2.8)) is typically small for low intensity and small absorption cross section. Therefore, usually a pulsed laser with high peak power or resist with large absorption cross section is required to induce TPA in materials.

2.5 TWO PHOTON ABSORPTION (TPA) POLYMERIZATION

The fabrication process of TPA polymerization is very similar to photolithography. The major differences between the two are that in TPA polymerization a laser beam is applied instead of UV light and TPA polymerization does not require any mask. Stereolithograpy, which utilize a laser beam, is another fabrication process similar to TPA polymerization. Much like photolithography, stereolithography is a planner process and cannot generate true 3D features. To generate 3D features in stereolithography, layers of 2D geometric features are created on different layers and stacked to provide the third dimension. On the other hand, in TPA polymerization the laser can be maneuvered three dimensionally inside a volume of photoresist, thereby it is a volumetric process.

2.5.1 FABRICATION STEPS

The overall process of generating 3D features by TPA polymerization with negative tone photoresist is depicted in Figure 2-5 [49]. The laser beam scans in a two dimensional XY planer motion and the substrate moves along Z axis to achieve three dimensional movement of laser focal spot. Alternative approach would be to have laser focusing mechanism capable of changing focal depth along the Z axis in addition to moving the laser in XY plane. After the

exposure, the substrate is immersed into a developing solution where the unexposed resist dissolves.

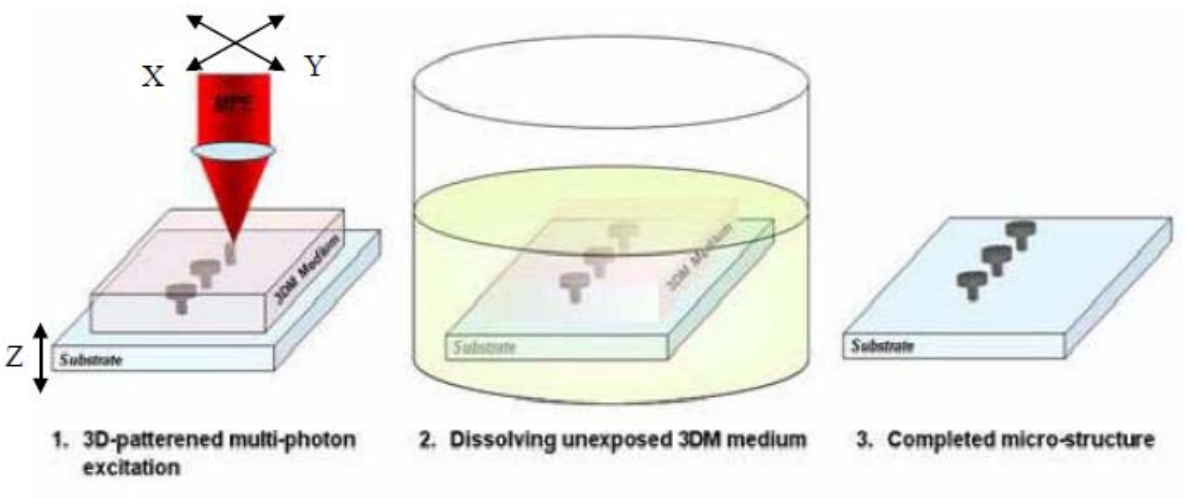

Figure 2-5: Steps of generating 3D features by TPA polymerization with a negative tone photoresist [49]

2.5.2 TWO PHOTON ABSROPTION (TPA) POLYMERIZATION THRESHOLD

The photoresist that is capable of TPA at particular wavelength behaves as transparent media. As a result, laser can be tightly focused in the volume of resist, illustrated in Figure 2-6 (b). In the case of TPA, the rate of absorption in a transverse cross section of a laser beam is proportional to the intensity squared times the number of molecules in the cross section [50]. Therefore, both photon flux and photon flux density are critical for TPA polymerization. Essentially, the highest absorption rate at the focal point, as can be seen in Figure 2-6 (a), results in the greatest fluence to exceed the polymerization threshold. The minimum fluence required for the initiation of the irreversible photochemical reaction, whether it is by single pulse or multiple pulses in short timeframe, is called photoinitiation threshold fluence. Thus, femtosecond lasers are favorable for TPA polymerization because of its very high peak

intensities, yet controllable moderate average laser power. Also, the ultra-short pulses in femtosecond time scale greatly reduce heat diffusion in the resist; therefore it provides greater controllability over feature size. Only the exposed area of the laser beam, where the laser fluence exceeds the photoinitiation threshold fluence polymerizes. This is illustrated in Figure 2-6 (c), where only at the focal plane the laser fluence exceeds the photoinitiation threshold and results in polymerization. Since the energy distribution of machining spot follows a Gaussian profile, the photoinitiation threshold can be precisely determined and controlled by manipulating the laser pulse energy, the number of applied pulses and the irradiation time. By varying the laser power as well as the irradiation time, one can measure the dependence of the polymerization process and the voxel size on these parameters.

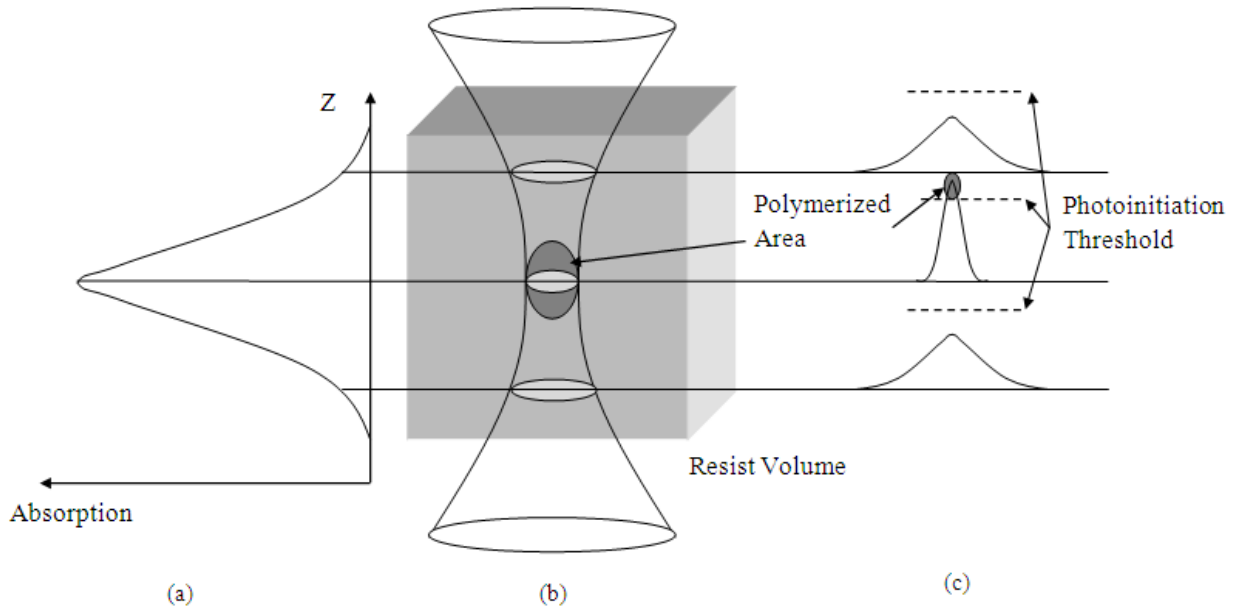

Figure 2-6: TPA polymerization by focused laser beam (a) energy absorption relative to the depth-of-focus (b) laser focused inside volume of resist (c) photoinitiation threshold presentation to Gaussian beam

2.5.3 VOXEL SIZE

If the femtosecond laser pulses are focused into the volume of the resist without scanning the laser beam and moving the sample, the solidified volume represents a 3D image of the laser focus, where the intensity reaches the threshold. If the laser focus is located slightly above the substrate, the solidified volume (voxel) will stick on it and can be used for measurements (see Figure 2-7). These voxels can be tailored by moving the laser to create any 3D features, as shown in Figure 2-8 [51].

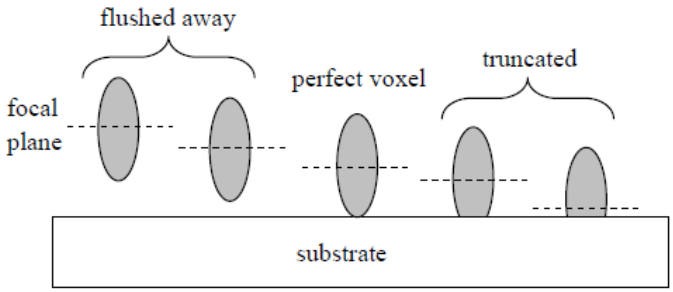

Figure 2-7: Voxel generation depending on focal plane

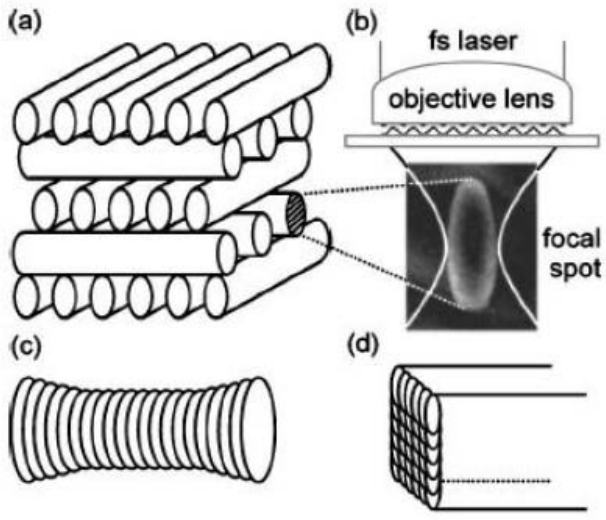

Figure 2-8: Voxel tailoring of logpile photonic crystals (PhCs). (a) Schematic logpile PhC structures. (b) SEM image of a two-photon polymerized individual 3D voxel, which reflects the cross-sectional shape of line-scanned rods. (c) Schematic conventional single-line scanning approach and (d) illustration of finely quantified pixel writing [51]

In order to start the chemical reaction, the locally generated density of radicals, $\rho = \rho(r, t)$, must exceed a certain minimum concentration ρ_{th} to start the polymerization. Serbin et al. proposed the model for calculating the density of radicals, $\rho(r, t)$, produced by intense laser pulses by solution of a simple rate Eqn. (2.9) [52]:

$$\frac{\partial \rho(r,t)}{\partial t} = \big(\rho_0 - \rho(r,t)\big)\sigma_2 N^2(r,t), \tag{2.9}$$

where $N = N(r, t)$ is the photon flux, and ρ_0 is the primary initiator particle density. The effective two photon cross section for the generation of radicals σ_2 [cm^{4}s] is defined by $\sigma_2 = \eta\sigma^a{}_2$, representing the product of the ordinary two photon absorption cross section, $\sigma^a{}_2$ and the efficiency of the initiation process, $\eta < 1$. They approximated the light distribution at the focal plane ($z = 0$) by a Gaussian distribution assuming that the photon flux N_0 is constant during the laser pulse:

$$N(r,t) = N_0 e^{-\frac{2r^2}{r_0^2}} \tag{2.10}$$

They were able to estimate the diameter of the voxel, d, generated by TPA polymerization as the region where $\rho \geq \rho_{th}$. The voxel diameter can be given by:

$$d(N_0,t) = r_0\sqrt{\ln\left(\frac{\sigma_2 N_0^2 n\,\tau_L}{C}\right)},$$
$$C = \ln\left(\frac{\rho_0}{(\rho_0 - \rho_{th})}\right), \tag{2.11}$$

where n is the number of pulses, t is the total irradiation time, and τ_L is the laser pulse width. Using the same expression the voxel length, l, for the Gaussian beam can be determined by:

$$l(N_0, t) = 2z_R \sqrt{\sqrt{\frac{\sigma_2 N_0^2 n \tau_L}{C}} - 1}, \tag{2.12}$$

where z_R is the Rayleigh length.

Serbin et al. were able to relate their theoretical model of predicting voxel size in Ormocer with the experiment data as shown in Figure 2-9 [52]. Ormocer is a negative type resist, which polymerizes upon laser irradiation. The polymerization process in negative type resist is explained in detail in Chapter 3.

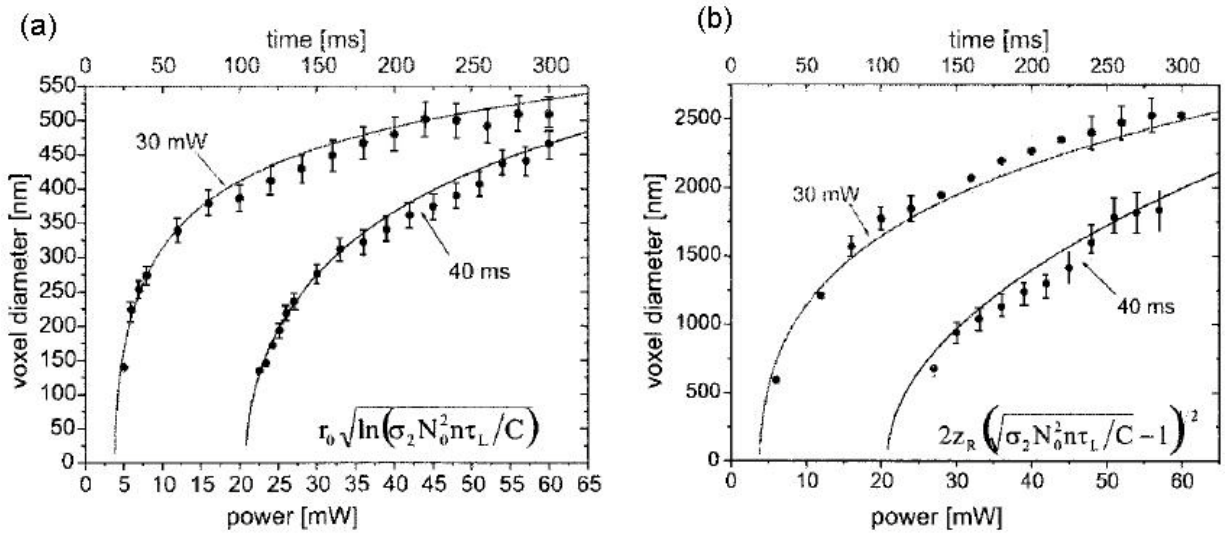

Figure 2-9: Theoretical and experimental results of voxel sizes in Ormocer (a) voxel diameter dependence on irradiation time and average laser power (b) voxel length dependence on irradiation time and average laser power [52]

A voxel size can be modified by keeping the energy constant and varying the irradiation time. This gives the size dependence on the irradiation time. Alternatively, the irradiation time can be kept constant while changing the energy to identify the voxel size dependence on the laser energy. To achieve a nearly spherical voxel ($l/d \approx 1$), it is important to work at low laser energy and short irradiation time, i.e. close to the polymerization threshold. This provides not only the best resolution, but also the best (closest to spherical) shape of the polymerized voxel. The

spherical shape voxels are preferred because they are easy to tailor and manage three dimensionally to produce 3D features.

2.6 SUMMARY

In summary, the TPA polymerization is a micro-/nanofabrication technique, in which, ultra short laser pulses are induced to polymerized photoresist. In contrary to lithography techniques based on SPA, the TPA is initiated by absorbing two simultaneous photons. Instead of a linear dependency on laser intensity, TPA exhibits a quadratic relationship with the laser intensity. Such nonlinear characteristic of TPA enables ultrashort pulse lasers to focus inside the volume of resist and polymerize the area in the vicinity of the focal point. As a result of this, TPA provides a mechanism by which chemical or physical processes can be activated with high spatial resolution in three dimensions, with excitation being confined to widths down to few nanometers. The three dimension polymerized zone is identified as the voxel and its size can be determined with the irradiation time and average laser power. With the understanding of TPA polymerization mechanism and its dependency on the laser parameters, microfeatures such as fluidic channel can easily be fabricated.

CHAPTER 3

LASER AND EXPERIMENTAL DETAILS

3.1 INTRODUCTION

Even though the concept of TPA was first realized in 1931, it could not be shown experimentally until 1961, when the continuous-wave laser with high energy became available to provide the required photon flux density. Selection of laser system and understanding of the laser beam characteristics are most essential for understanding the TPA phenomena. In the first part of the chapter, a laser background and laser beam characteristics are presented. The substrate materials and the characteristics of the photoresists are also discussed here. In the later part, detailed experimental setup used for this study is discussed. All the experiments for this study were conducted using a high power, high repetition rate femtosecond laser in the Micro and Nano Fabrication research lab at Ryerson University, Toronto, Canada.

3.2 LASER BACKGROUND

The word “laser” is an acronym for Light Amplification by Stimulated Emission of Radiation. Through the supply of energy, the electron of an atom, molecule or crystal can change into an excited state. An electron absorbs a light particle (photon) and makes temporary transition to higher-energy state. Subsequently, it jumps back from a higher-energy to a lower-energy state as it emits a photon, which is seen as light. With conventional light sources, this transition occurs by spontaneous emission, that is, the timing and the direction in which the photon is emitted are random. In contrast, with a laser this transition occurs through stimulated

emission. This means a photon stimulates the energy transition within an active medium and thus a second photon emerges whose properties such as frequency, phase, polarization and direction are identical or proportional with the first photon. The emitted light is reflected back and forth between two mirrors through the active medium in the resonator. One of the two mirrors is semi-transparent (in the range of one percent), in order to release light from the laser.

Soon after the invention of the first laser, several different types of lasers were invented. These lasers can be divided into different sub-groups according to the principal type of operation and construction. The solid-state lasers, like the Nd:YAG and gas lasers, like the helium-neon (HeNe), the argonion laser, the XeCL excimer laser, and the high-power CO_2 lasers are the most important types in material processing. The rest of the types, semiconductor lasers, liquid lasers, chemical lasers, and X-ray lasers, have more importance in research rather than in practical applications.

Laser applications in material processing has a very significant impact in mechanical engineering processes such as drilling, cutting, welding, and surface treatments. In electrical engineering and material science, processes such as photolithography, thin film deposition, doping, annealing, and defect scanning are also witnessing the importance of lasers. Most importantly, advancements in laser systems have opened doors for faster, efficient and inexpensive fabrication techniques in micro- and nano-fabrication industries. Laser processing is an ideal technique for these industries, because of its flexibility and ability to create high resolution features with great throughput.

3.3 LASER BEAM CHARACTERISTICS

The laser light is characterized by a number of interesting properties. Various applications of lasers exploit specific combinations of the laser properties. This section briefly explains the most important properties of laser light.

3.3.1 MONOCHROMATICITY

In addition to high power, lasers have many other characteristics suitable for material processing. Monochromaticity is one of the unique characteristics of laser light. It is the most important property of a laser beam and is measured in terms of spectral line width. It is nearly impossible to achieve a perfectly monochromatic light, but the laser light is many times more monochromatic than any other light. This is an important property because material processing is wavelength dependent. Hence, choosing a proper wavelength laser allows greater control in laser focus without compromising its depth.

3.3.2 COHERENCY

The laser light is coherent, in which waves travels in the same direction (spatial coherence) at the same frequency and in phase (temporal coherence). Spatial coherence describes the ability for two points in space, in the extent of a wave to interfere, when averaged over time. Temporal coherence is the measure of the average correlation between the values of a wave at any pair of times, separated by delay. It is a measure of how monochromatic a source is. The spatial coherence allows the laser beam to be focused tightly down to the micron level with a very high energy density necessary for extremely small features.

3.3.3 COLLIMINATION

Collimation of the laser radiation is related with the directional nature of the beam. Highly directional beams are highly collimated beams, which can be focused on a very small area even at longer distances. Hence, energy can be efficiently collected on a small area without much loss in the beam intensity over the longer distance of laser beam travel. The laser light is naturally collimated because it forms in optical resonator. The degree of collimation is directly related and measured with the beam divergence angles. The collimated light has divergence in the order of less than a milliradian. This characteristic of a laser is very important to achieve desired constant spot size at different focal lengths.

3.3.4 GAUSSIAN BEAM

In most laser applications, it is necessary to focus, modify, or shape the laser beam by using lenses and other optical elements. In general, laser-beam propagation can be approximated by assuming that the laser beam has an ideal Gaussian intensity profile, corresponding to the theoretical TEM_{00} mode. In order to select the best optics for a particular laser application, it is important to understand the basic properties of Gaussian beams.

In TEM_{00} mode, the beam emitted from a laser is a perfect plane wave with a Gaussian transverse irradiance profile as shown in Figure 3-1. The Gaussian shape is truncated at some diameter either by the internal dimensions of the laser or by some limiting aperture in the optical system. The Gaussian has no obvious boundaries to give it a characteristic dimension like the diameter of the circular aperture, so the definition of the size of a Gaussian is somewhat

arbitrary. The commonly adopted definition is the diameter at which the beam irradiance (intensity) has fallen to $1/e^2$ (13.5%) of its peak value.

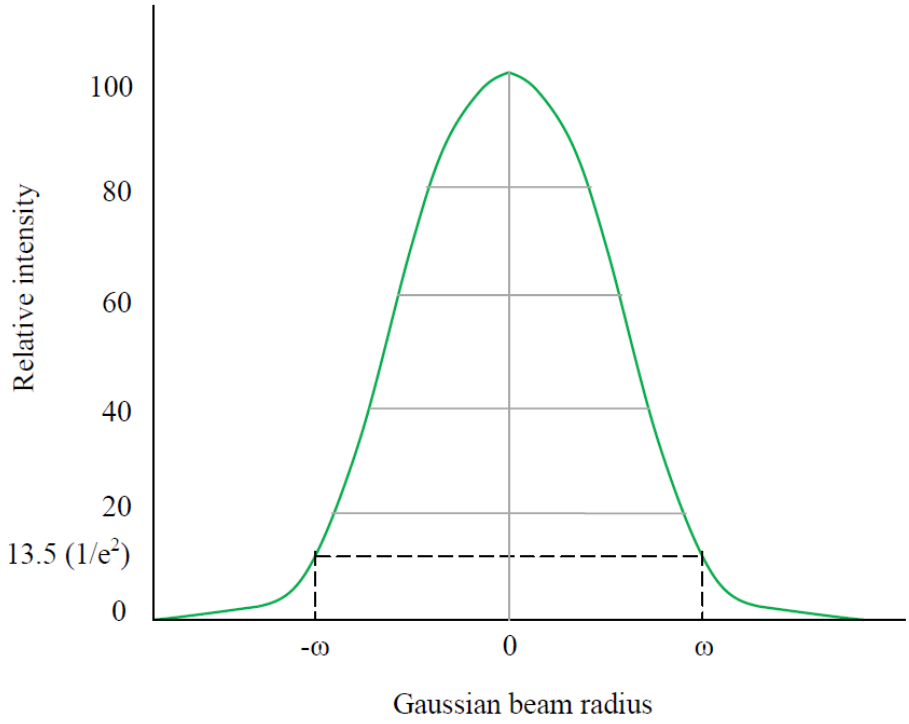

Figure 3-1: Intensity profile of Gaussian TEM_{00} mode

3.4 SUBSTRATE MATERIALS

Almost all early designs and fabrications of fluidic channels were on silicon, glass, quartz, or plastic. This is unsurprising since standard photography and wet-etching techniques perfected in the microelectronics and semiconductor industries could be used to efficiently structure all these materials to produce microchannels networks. In terms of fabrication methods, several considerations must be made for selecting suitable substrate material.

3.4.1 SILICON

Silicon is the most widely accepted substrate and leverages commercially available equipment for fabrication from the well-established semiconductor and microelectronics fields. Advanced fabrication techniques with anisotropic etching can yield high aspect ratio silicon microstructures. However, silicon is seldom used for cellular analysis due to a lack of surface modification, low breakdown voltage, and most importantly its optical opacity. While silicon can be modified with a thermal oxide, the passivated surface has been shown to degrade rather rapidly due to protein absorption, limiting its long-term utility in cell-based assays. Since silicon is a semiconductor, applications employing high voltage such as capillary electrophoresis and dielectrophoresis are challenging. Although oxide modification can minimize this problem to permit microgel electrophoresis on chip, separation field strengths have been limited to ~25 V/cm, resulting in longer analysis time and low resolution separations [53]. To enable optical detection, the opaque silicon substrate can be anodically bonded to a glass wafer to form silicon–glass microchannels. The major disadvantage of silicon substrate is relatively high cost and limitations in mass production, which is important for medical and clinical diagnostic applications that require disposable tools to eliminate cross contamination.

3.4.2 PLASTIC

The limitations and challenges of fabricating silicon-based microfluidic devices encouraged researchers to turn to alternative substrates, such as ceramics, plastics, and polymer-based materials. A vast range of plastic and polymeric materials are commercially available with diverse mechanical, chemical, electrical and optical properties. Plastic and elastomer have the key advantage of simple and rapid fabrication using either injection molding or soft lithography

techniques. Soft lithography is the technique most often employed for creating microfluidic systems. Devices are cast from a mold, so high aspect ratio features can be easily generated. Advantages of microfabrication in thermoplastics and elastomer include the expanding availability and relative low cost of fabrication. In addition, thermoplastics and elastomers are used with simple sealing methods that do not require a clean room. Elastomer can either bond to another elastomer to form all-elastomer microchannels or bond to glass forming hybrid elastomer–glass microchannels. The primary drawbacks of using a polymer-based substrate are the native fluorescence and porosity. Additionally, elastomeric compounds do not readily permit surface modification. Also, another disadvantage is widely unknown surface chemistries, in comparison to largely researched and documented surface morphologies for silicon-based materials. Therefore, it is difficult to predict surface interactions with chemical and biological sample.

3.4.3 GLASS

Glass is a useful platform because it offers chemical surface modification for compatibility with many different assays, including capillary electrophoresis. It also has high mechanical strength, high chemical resistance, and low conductivity. Advantages of glass microsystems include fabrication with conventional wet etching techniques, high dielectric strength, low background fluorescence, and optical transparency in the visible wavelengths. Since the wet etching of the glass is isotropic, the critical dimension attained is larger than silicon substrates. Another disadvantage of glass substrates is their lack of disposability due to its high unit cost.

3.5 PHOTORESISTS

Photoresist is the generalized term for all photon sensitive macromolecule polymers. They are photon sensitive, therefore, can be optically solidified into pattern structure. When a femtosecond laser is tightly focused into the volume of photoresist, it initiates TPA polymerization. There are two classes of photoresists which can be structured by TPA polymerization: positive and negative type photoresist. Figure 3-2 illustrates the difference between positive and negative photoresists.

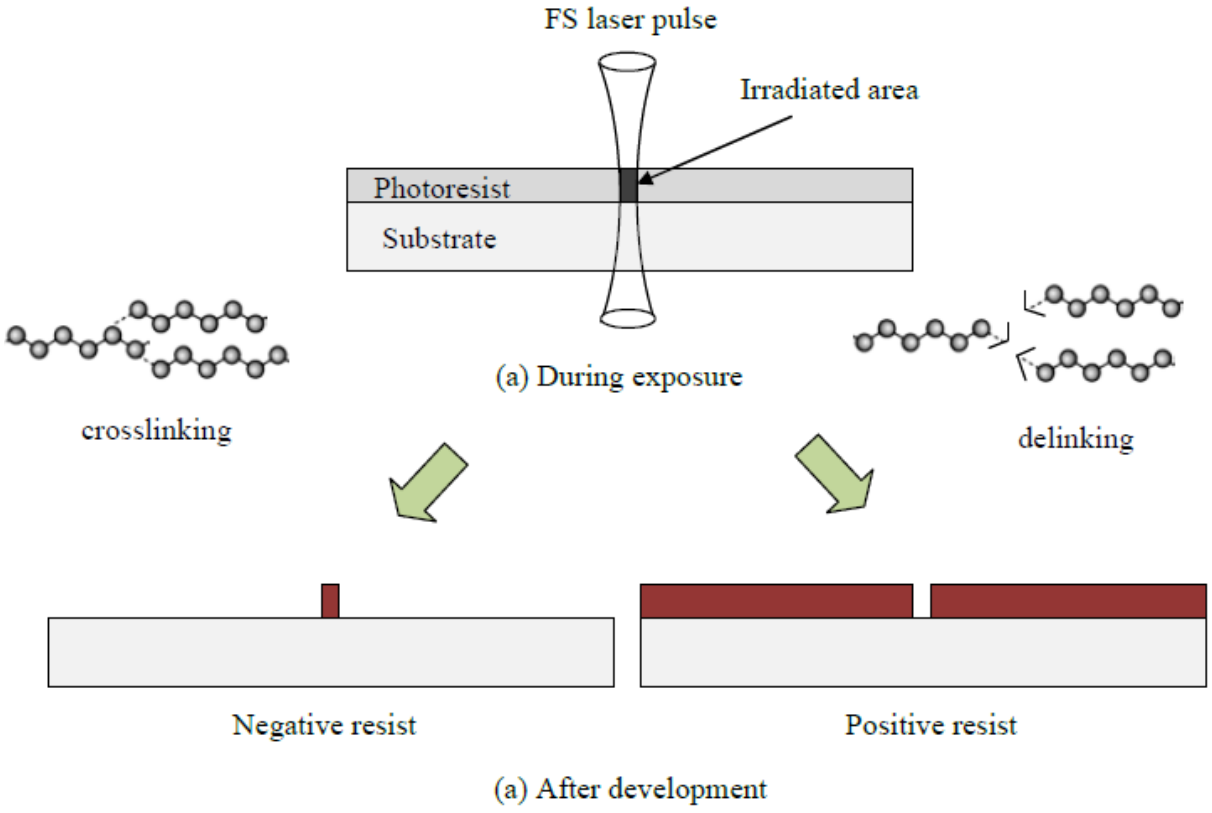

Figure 3-2: Difference in positive and negative resist polymerization

The main difference between positive and negative types of photoresist is photochemical reactions responsible for linking or delinking of monomers. A positive photoresist that has long chain molecules can be broken by photon energy into short chains by the delinking process,

while for negative photoresist, initially short chain molecules can join together to form long chains after absorbing photon energy. The macromolecule polymers with long chains are insoluble in the developer where polymers with short chain molecules are soluble in the developer. Hence, the exposed part is removed by developer for a positive resist, while the unexposed part is removed for negative photoresist.

Apart from the photochemical reaction, positive and negative photoresists are different in many other properties (see Table 3-1). These properties present general guidelines for choosing a suitable photoresist for a given application.

Table 3-1: Comparison of general properties of positive and negative photoresists

Photoresist properties	**Positive resist**	**Negative resist**
Adhesion	Average	Good
Sensitivity	Fairly low	High
Cost	Fairly expensive	Fairly low
Developer	Aqueous based	Solvent
Etch selectivity	High	Low
Swelling	No	Yes
Thermal stability	Good	Average

Only negative resists were considered for this study. Furthermore, negative resists can be sub-divided into solid and liquid phases due to its appearance during the TPA polymerization process. The solid phase resists are epoxy based and polymerized due to the cationic polymerization process. In solid phase resists, an acid is generated in the illuminated region, but the reflective index stays unchanged. Hence, the scan patterns cannot be seen during exposure. Actual crosslinking happens during the post-baking process, and only after that the scan pattern becomes visible. In contrast, liquid phase resists are acrylate based materials, which are polymerized via free-radical polymerization and are visible during exposure.

3.5.1 SU-8

SU-8 is a solid phase, an epoxy-based near UV, a negative tone resist which was developed at IBM in the mid-1990s [54]. It contains EPON® SU-8 epoxy resin synthesized with photoinitiator dissolved in an organic solvent gamma-butyrolacton (GBL). Its viscosity is primarily determined by the amount of solvent and thus, its thickness can be achieved anywhere from few nanometers to millimeters. The one of the most important characteristics of SU-8 is its ability to create near vertical and very high aspect ratio (AR) side-walls. AR is defined as the ratio of the polymerized structure height to its width and it plays a significant role in device design. Figure 3-3 (a) [54] shows the molecule structure of SU-8 with eight epoxy sites and 16 epoxy functional side groups per monomer providing a dense 3D network of crosslinks. As a result, high AR and vertical sidewalls can be achieved and high epoxy functionality provides high chemical and thermal resistance. Figure 3-2 (b) and (c) [54], respectively, illustrate initiation of polymerization via the opening of epoxy groups, and chain propagation of the crosslinking process. It is an ideal photoresist for TPA because of its advantageous properties, such as low-cost, low optical absorption in near UV, thermal and chemical stability, good resolution, and controllable spin coating thickness. For this study, SU-8 2000.5 (Microchem Technology GmbH) was used.

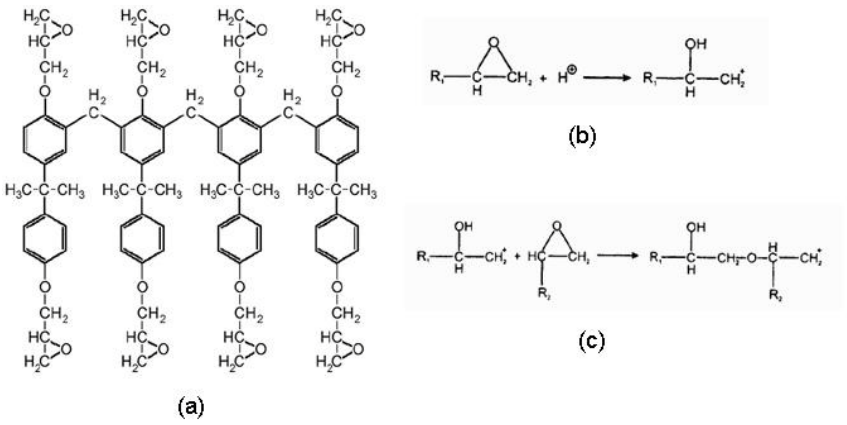

Figure 3-3: (a) SU-8 molecule structure (b) initiation of polymerization via opening of epoxy group (c) chain propagation of crosslinking process [54]

3.5.2 ORMOCER®

ORMOCER represents the family of originally modified ceramic materials. It is a liquid phase, arcylate based negative photoresist. ORMOCER is also classified as inorganic-organic hybrid polymers. The most important attribute of ORMOCER is that its physical and chemical properties can be tailored. Hence, they can be used for a wide verity of applications. Also, its chemical, mechanical and thermal stability along with good processing ability is an upgrade over organic polymers in most applications. ORMOCER combines properties of organic polymers, such as, toughness and low processing temperature requirements, with inorganic materials, such as, harness, chemical and thermal stability. A type of ORMOCER used for this study was low viscosity ORMOCOMP (Micro Resist Technology). It has outstanding stability in humid atmospheres, high electrical resistance, good adhesion on most substrates and fast curing. It contains 1% of Ciba® Darocur TPO two photon initiator (see Figure 3-4).

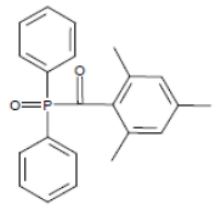

2,4,6-Trimethylbenzoyl-diphenyl-phosphineoxide

Figure 3-4: Darocur TPO structure

3.6 EXPERIMENT DETAILS

The fabrication processes proposed in this thesis is very similar to any lithography process, which is briefly explained here. The overall process flow is depicted in Figure 3-5. The four major stages are substrate preparation, exposure, post-exposure bake and development.

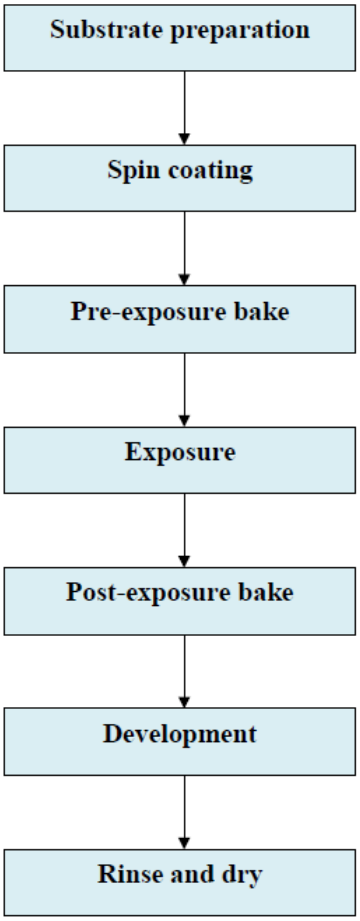

Figure 3-5: Process flow

3.6.1 SUBSTRATE PREPARATION

Borosilicate glass of two inches in diameter were used as a support substrate because of its mechanical strength, non-conductivity, optical transparency, compatibility with chemical analysis, and its preference over other substrate material in microfluidic devices designs.

3.6.1.1 Spin coating

To obtain maximum process reliability, substrates should be clean and dry prior to applying the photoresist. Figure 3-6 is a schematic drawing, illustrating the spin coating process. Two step spin coating was carried out to achieve desired coating thickness of 0.5 µm.

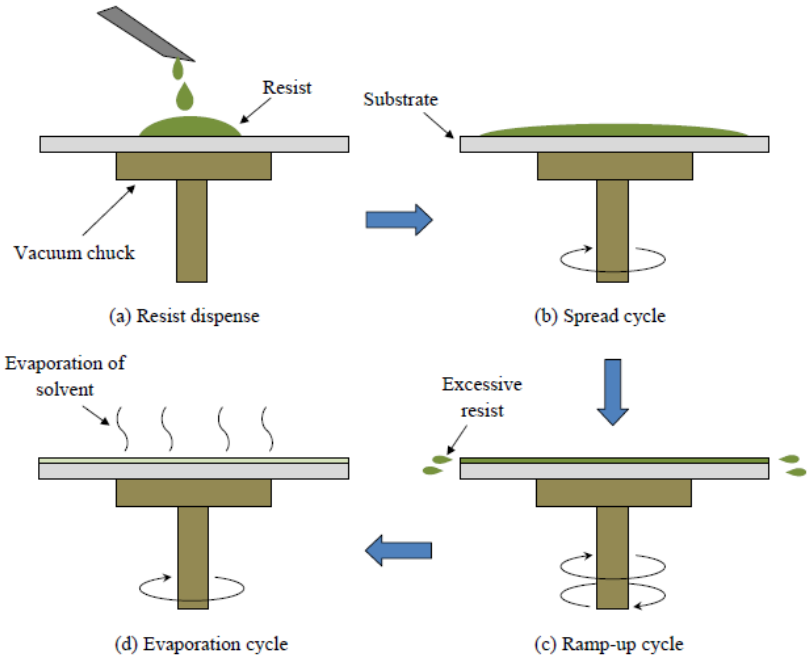

Figure 3-6: Spin coating of resist on substrate (a) resist is dispensed on substrate (b) resist is spread evenly by spinning at low speed, low acceleration (c) high speed, high acceleration to develop a uniform coating thickness and expelling excess resist (d) evaporating of solvent at final speed to obtain desired final coating thickness

First, five ml of resist was carefully dispensed in the center of the substrate (see Figure 3-6 (a)) and spun for five seconds at the speed of 500 rpm with an acceleration of 100

rpm/second (see Figure 3-6 (b)). Immediately after, the sample was spun again with higher acceleration and higher speed for a few seconds (see Figure 3-6 (c)). The first step allows the resist to spread evenly using the centrifugal force. The second step was to disperse off excessive resist and to evaporate the solvent to achieve desired coating thickness.

Figure 3-7 and Figure 3-8 illustrate the required spin speed of the second step for any desired film thickness of photoresists SU-8 and ORMOCOMP, respectively.

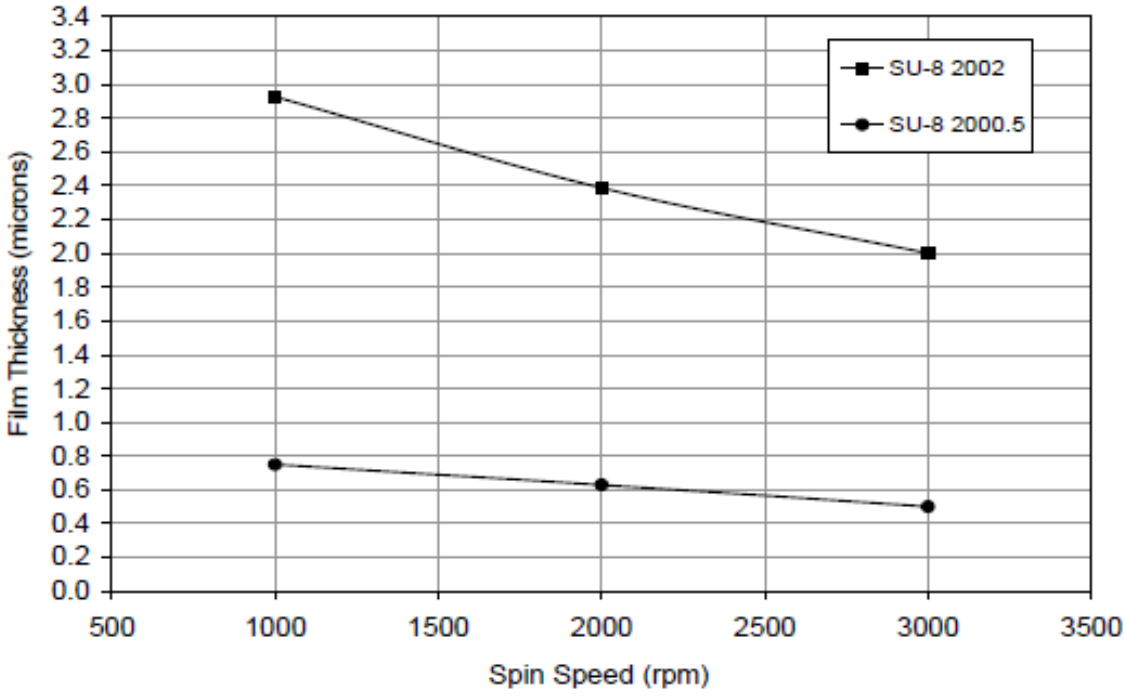

Figure 3-7: Film thickness achievable for SU-8[1]

[1] Source: SU-8 technical data sheet.

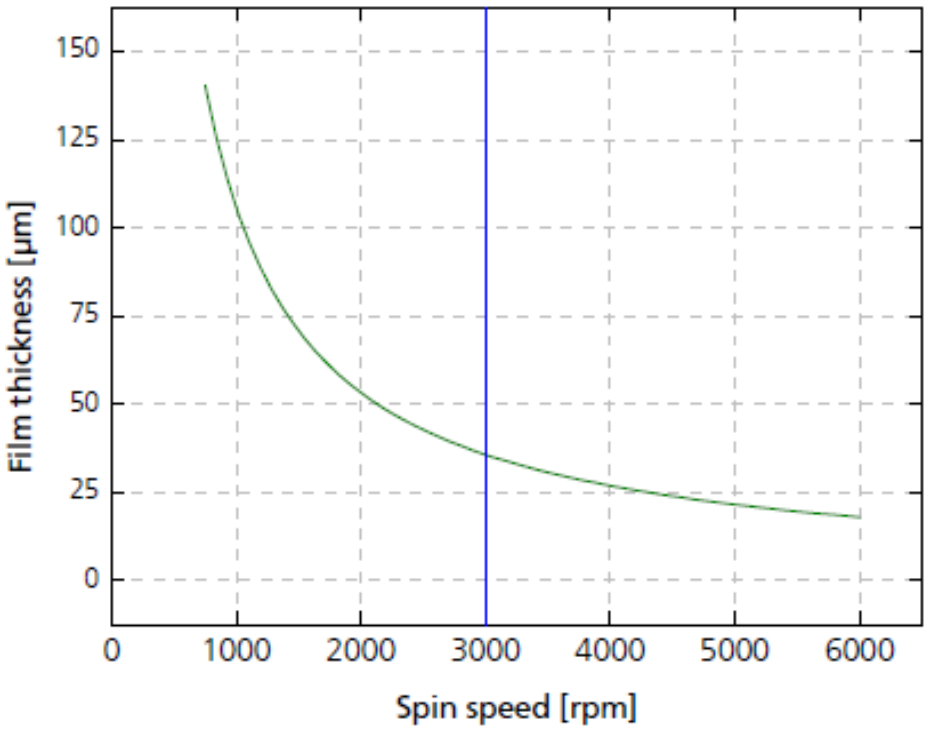

Figure 3-8: Film thickness achievable for ORMOCOMP[2]

3.6.1.2 Pre-exposure bake

After coating photoresist, the substrate should be softbaked before exposing it with laser source. The purpose of pre-exposure bake is to dry out all the solvent present in the photoresist. The time and temperature for baking are specified by photoresist manufacturers. The baking can be done either in an oven or on a hot plate. Using oven may form a skin on the surface, which may inhibit in incomplete drying and may extend the baking time.

For the experiments performed using SU-8, the substrate was softbaked on a hot-plate at a constant temperature of 95°C for one minute with the coated surface on top. The substrate coated with ORMOCOMP was softbaked on a hot-plate for two minutes at a constant

[2] Source: ORMOCOMP technical data sheet.

temperature of 90°C. The glass substrate coated with the resist then exposed under the controlled laser beam for specific geometries created by AutoCAD®.

3.6.2 EXPOSURE

A thin layer of resist was exposed by focusing the laser beam at the resist/glass interface. Laser parameters such as pulse energies and repetition rates, are varied to study their effects on the polymerization process. Thinner coating eliminates the need of precise control over actual position of the focal point at the resist/glass interface plane. This is critical to have good adhesion to the glass substrate. If the focal plane is inside the volume of resist, the polymerized structure does not have any base to adhere, and subsequently it will be washed-out during the development. When resist is exposed, it may go through thermal expansion and swelling depending on the pulse energy, number of pulses, and the absorption time.

3.6.2.1 Laser system and laser beam delivery

All the experiments were carried out using a diode-pumped Yb-doped fiber oscillator/amplifier system capable of producing variable repetition rates from 200 kHz to 26 MHz with a central wavelength of 1030 nm and a maximum output power of 15 W at a repetition rate of 26 MHz. However, as an exposing light source, a second harmonic (515 nm) central wavelength with variable major laser parameters such as repetition rate, pulse width and average beam power was used.

Figure 3-9 is a schematic presentation of the machine setup used to expose spin coated SU-8 sample with a controlled laser beam. A plano-convex lens of 500 mm focal length and a plano-concave lens of 150 mm focal length were used to reduce the laser beam diameter and a

λ/2 wave-plate is used in between these lenses to control the polarization of the beam. A harmonic generator was used to convert the laser beam to the second harmonic (515 nm) central wavelength. Previous work has demonstrated that second harmonic increases the efficiency and the ease with which the micromachining of the features were carried out due to the reduction in the order of MPA [55]. Another study of the ultrafast lasers ablation mechanism concluded that since the smallest diffraction-limited focus spot (given as the intensity diameter of the laser focus spot) is proportional to the laser wavelength, a smaller wavelength will result in better machining resolution [56]. The 515 nm mirrors were used to dump the 1030 nm wavelength out of the beam. Afterwards, a plano-concave lens of 75 mm focal length and a plano-convex lens of 300 mm focal length were utilized to expand the beam diameter by 4 times to 10 mm. A quarter waveplate was used to rotate the polarization state of the laser beam to circular. In addition, a diaphragm is used to improve the beam profile. Finally, the 214 fs laser beam was scanned onto the substrate surface with SU-8 coating through a piezo tip/tilt mirror.

1. 1030 nm Mirror
2. F = 500 mm Convex Lens
3. 1030 nm λ/2 Waveplate
4. F= -150 mm Concave Lens
5. 515 nm Harmonic Generator
6. 515 nm Mirror
7. 515 nm Mirror
8. F= -75 mm Concave Lens
9. 515 nm λ/4 Waveplate
10. F = 300 mm Convex Lens
11. 515 nm Mirror
12. Diaphragm
13. Piezo Scanner
14. EFL = 12.478 mm Telecentric Lens
15. Sample and Sample Holder
16. Computer controller

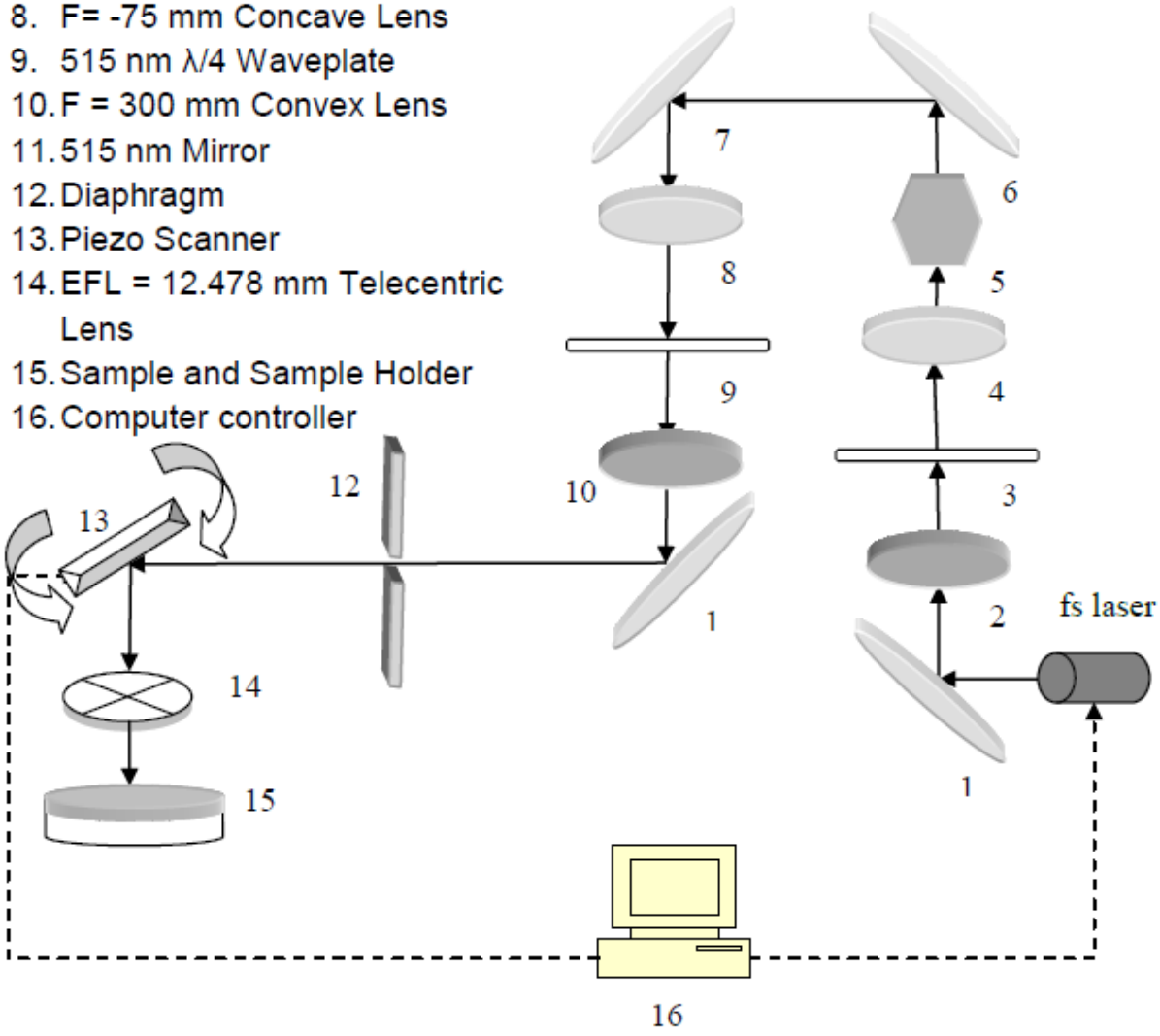

Figure 3-9: Experimental setup

3.6.2.2 Laser spot size and depth of focus

The spot size, also known as the beam waist, is the minimum diameter of the Gaussian beam travelling in a free space. Figure 3-10 shows a schematic diagram of the laser spot size and depth of focus for a laser beam converged by a telecentric lens.

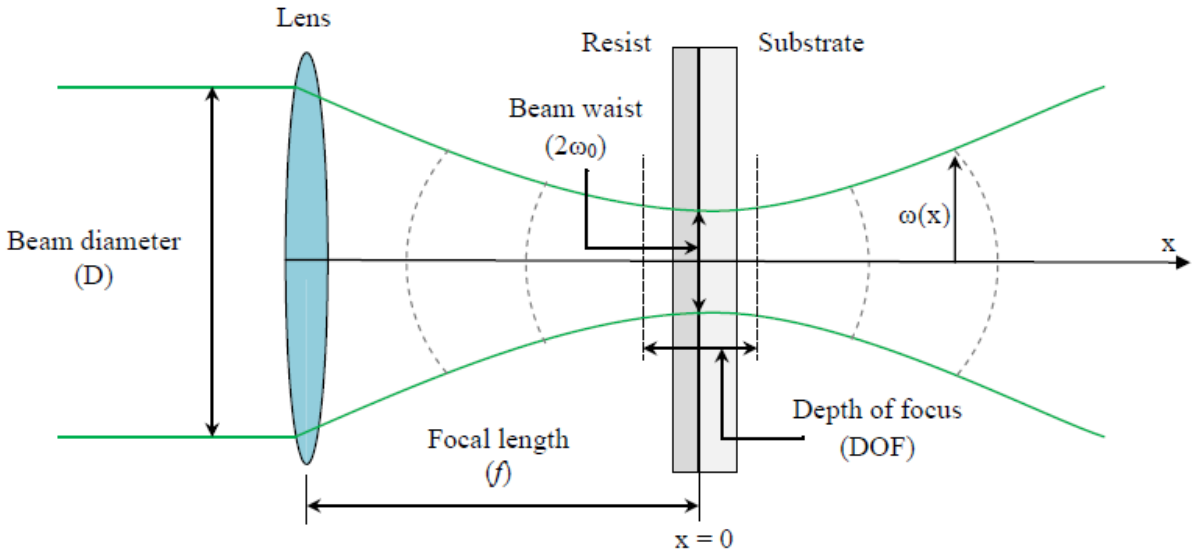

Figure 3-10: Laser spot size and depth of focus for converging laser beam using a telecentric lens

Telecentric scanning lenses are specially designed to make the focused beam always perpendicular to the flat focal plane regardless of the beam's position in the scan lens (see Figure 3-11). They also offer greater depth of focus and smaller spot sizes when used for laser material processing. Therefore, it is possible to focus the beam on a very thin film of resist without any precision positioning stage. Telecentric scanning lens, by the very nature of their design, maintains a near normal incidence angle of the beam to the work piece. This ensures that position errors and image distortions are minimized over the entire scan field. Having a greater depth of field and smaller spot size are important for precision laser micro-machining processes

where there is a need to produce fine spot sizes while maintaining precise placement over a relatively large field.

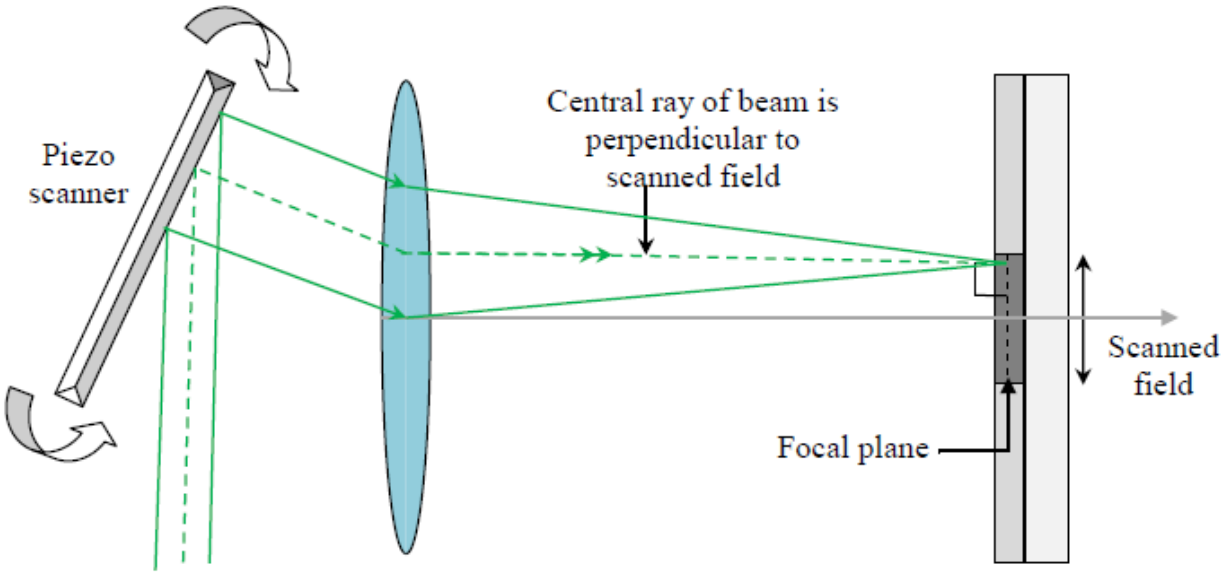

Figure 3-11: Telecentric scanning lens

For this study, a telecentric lens with a 12.5 mm focal length was used to focus the laser beam. In order to find the size of the focused beam spot, a single spot can be machined on a thin metal film, with pulse energy just above the material threshold. The size of the machined spot, measured using a Scanning Electron Microscope (SEM), gives the size of the focused beam spot. The theoretical laser spot size ($2\omega_0$) can be calculated using [57]:

$$2\omega_0 \approx 1.27\frac{\lambda_0 f}{D} \tag{3.1}$$

Here, f is the effective focal length of the telecentric lens, λ_o is the wavelength of the laser and D is the laser beam diameter. Values for these parameters are 12.5 mm, 515 nm and 8 mm, respectively. Hence, the theoretical spot size diameter was calculated to be 1.02 µm.

Generally, smaller spot size results in higher photon flux, as a result, TPA probability increases with smaller spot size. The depth of focus (*DOF*) is calculated to be 3.19 μm using:

$$DOF = \left(\frac{8\lambda_0}{\pi}\right)\left(\frac{f}{D}\right)^2 \tag{3.2}$$

3.6.3 POST-EXPOSURE BAKE

After exposure, the substrate was hard-baked on a hot-plate at the constant temperature. of 95°C for two minutes. SU-8 crosslinking occurs during this step in the regions that contain the acid catalysts generated during exposure [54]. On the other hand, the polymerized ORMOCOMP cure and harden during the post-exposure bake. SU-8 and ORMOCOMP were post-baked for two minutes at 95°C and for 30 minutes at 90°C, respectively.

3.6.4 DEVELOPMENT

Once the substrate was cooled, it was immersed in developer solution for approximately two minutes at room temperature to remove unpolymerized and unhardened resist. The developer solutions used for SU-8 and ORMOCOMP were SU-8 developer (Microchem Technology GmbH) and ORMODEV (Micro Resist Technology), respectively.

Finally, the parallel fluidic channels formed by TPA polymerization were observed under Scanning Electron Microscope (SEM). Since the sample is nonconductive, it had to be gold sputtered before observation.

Most of results that can be obtained in atmospheric conditions can be further improved by using clean-room facilities. However due to the associated cost and setup requirements, all experiments were carried out in ambient atmosphere settings.

3.7 SUMMARY

The knowledge of laser systems and characteristics of laser beam is necessary in order to verify the capability of the system for TPA polymerization. This also determines the proper selection of the substrate material and the photoresist. Finally, the experimental parameters must be defined. In using femtosecond lasers as an alternative for polymerizing a photoresist to fabricate fluidic channels, laser parameters including wavelength, repetition rate, pulse width, pulse energy, and scan speed must be analyzed to satisfy the requirements of specific tasks, stabilize the process and to maximize the efficiency of laser power usage. Table 3-2 and Table 3-3 summarize the selected parameters and their effect on the feature and the process.

Table 3-2: Laser parameters effects

Laser parameters		**Effects**
Power output	(40mW – 1W)	Throughput
Wavelength	(515 nm)	Feature size
Pulse energy	(5 – 50 nJ/pulse)	Feature quality
Pulse width	(214 fs – 3.57 ps)	Feature quality
Repetition rate	(4 – 26 MHz)	Feature controllability
Spot diameter	(1.02 μm)	Feature size & shape

Table 3-3: Process parameters effects

Process parameters	**Effects**
Prebake	Adhesion to substrate
Spin coating thickness	Feature size, aspect ratio
Postbake	Shrinkage, resolution
Scan speed	Feature quality, linearity, throughput

For each exposure (i.e. constant pulse energy, repetition rate and scan speed) an array of fluidic channels were created. The dimension of each of the channels within the array was measured and the mean values are reported in each of the studies.

CHAPTER 4

A DIRECT WRITING OF OPEN NANOFLUIDIC CHANNELS

4.1 INTRODUCTION

In the last decade, the micromachining process has been employed to advance the development of microfluidic channels. The advancement of scaling the fluidic channels to nanometer dimensions could open a new world for the fundamental and applied research of nanofluidics. Nanofluidic channels defined as channels with at least one cross section dimension on the nanometer scale are of great interest for one major reason. The nanometer scale of channels allows the discovery of a new field, because the channel dimensions are in the order of the size of the atoms or molecules comprising the fluid, and physical surface phenomena in nanochannels will dominate over bulk phenomena, more than in microchannels [58]. Therefore, fluid transport and molecular behavior at extremely small dimensions are desirable for investigation.

Nanofabrication of fluidic structures is a powerful tool for the product of nanochannels which are essential components in the nanofluidic system. However, previous fabrication techniques based on lithography, thin-film method, hot embossing, injection molding, casting and laser ablation, are all expansive and not suitable for rapid prototyping. Also, many of these methods rely on mold or mask fabrication and require controlled pressure and/or temperature environment.

In this chapter, an alternative approach to create nanochannels is presented, where the spacing between two adjacent TPA polymerized ribs are controlled to form nanofluidic channels in between. The presented method is extremely cost effective as it is a direct write method, because it eliminates the requirement of any kind of mask or mold. In addition, the entire process is carried out in atmospheric conditions and does not demand any specific equipment except of the femtosecond laser source and laser scanning arrangements.

4.2 FABRICATING FLUIDIC CHANNELS BETWEEN TWO ADJECENT POLYMERISED RIBS

To create the open nanofluidic channels, the femtosecond laser is tightly focused onto the SU-8 resist coated substrate in the pattern of parallel lines with fixed pitch, as shown in Figure 4-1 (a). The laser pulses initiate the photochemical process via two-photon absorption and subsequently the expose area polymerizes. After the development process, as shown in Figure 4-1 (b), the exposed pattern of lines converts into polymerized parallel ribs and the spacing between two consecutive lines into the fluidic channels. Figure 4-1 (c) is an SEM image of the two adjacent, parallel polymerized ribs after development and the Figure 4-1 (d) is the magnified view of the fluidic channel between the ribs.

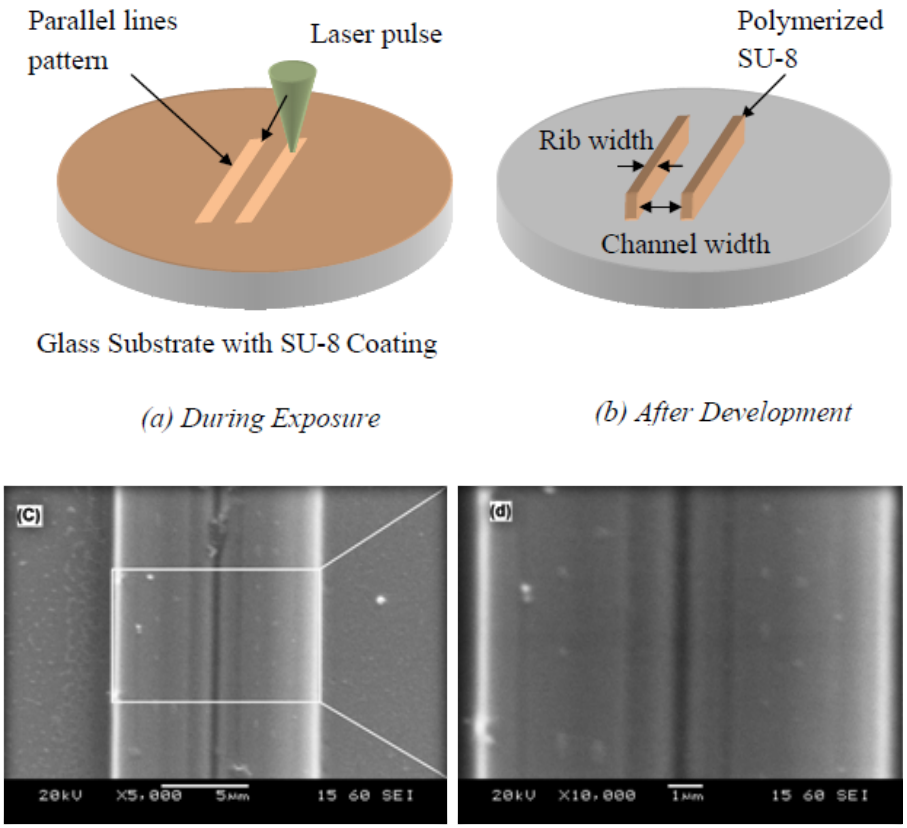

Figure 4-1: TPA process for fabricating fluidic channels. (a) During exposure, femtosecond laser is focused inside SU-8 resist. (b) After development, exposed resist turns into parallel ribs. (c) SEM image of two parallel ribs. (d) Magnification of channel between

Unlike any lithography technique, which is governed by single-photon absorption (SPA), femtosecond laser irradiation via TPA has threshold and nonlinear behavior, because the absorbed energy is proportional to the square of the intensity of light [59]. In addition, the photoinitiation threshold is precisely confined in TPA polymerization for SU-8 resist. In other words, since the energy distribution of machining spot follows a Gaussian profile, the photoinitiation threshold can be precisely determined. Thus, by controlling the focal point, the laser pulse energy, and the number of applied pulses, one can control two ribs close to each other creating a nanofluidic channel between them. Finally, ultra-short pulses in femtosecond time scale greatly reduce heat diffusion in resist; therefore it provides greater controllability over feature size.

4.3 PURPOSE OF THE STUDY

The fabrication of nanofluidic channels on glass substrate using TPA technique is fairly simple and repeatable. The purpose of this study was to create multiple fluidic channels parallel to each other with various laser parameters to achieve the smallest channel width with the highest controllability. Figure 4-2 is an SEM image of parallel fluidic-channels formed between two successive ribs. Channels of around 1 μm width were formed in between ribs with 5 μm in width. The goal here was to bring two ribs as close as possible, by increasing the width of the ribs precisely, to reduce the channel width to nano-scale.

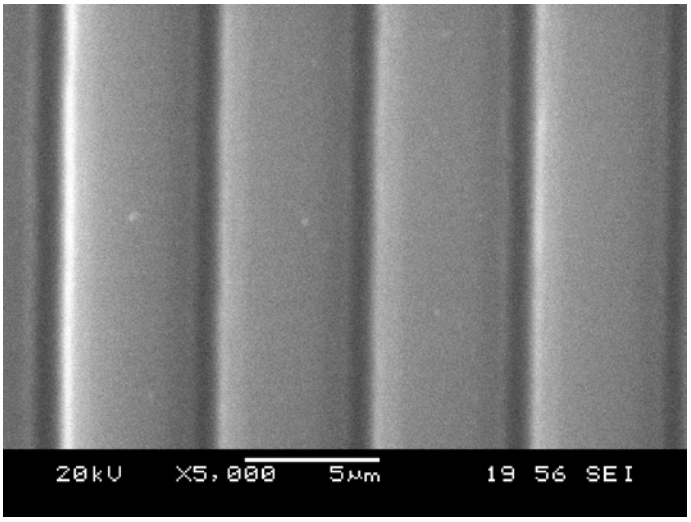

Figure 4-2: Parallel fluidic channels

4.4 THE PHTOINITIATION THRESHOLD FLUENCE

Generally, every photoresist has a photoinitiation threshold. The cross linking occurs only if the energy absorbed by the resist reaches a certain value that is called photoinitiation threshold fluence, expressed by laser energy per unit area [50]. This photoinitiation threshold fluence, Φ_{th}, depends essentially on the material pulse energy and number of laser pulses, applied

at each scanning point. For laser pulses with Gaussian intensity profile, the feature size obtained is related to the maximum laser fluence Φ_0 on the sample surface by [60].

$$D^2 = 2\omega_0^2 ln\sqrt{\frac{\Phi_0}{\Phi_{th}}} \tag{4.1}$$

where ω_0 is the beam radius, Φ_0 is the maximum laser fluence and Φ_{th} is the threshold fluence. The maximum laser fluence is related to the measured pulse energy E_{pulse} by:

$$\Phi_0 = \frac{2E_{pulse}}{\pi\omega_0^2} \tag{4.2}$$

According to Eqn. (4.1), the threshold fluence Φ_{th}, is the laser fluence Φ_0 at which the diameter of the polymerized pit equals to zero. Thus, the Φ_{th} can be determined by extrapolating the linear plot of squared diameter D^2 of polymerized circular pit versus the laser fluence to $D^2=0$ [61]. However from the experiment, it is determined that the photoinitiation threshold of SU-8 resist are 8.08 nJ/pulse, 7.61 nJ/pulse, 6.08 nJ/pulse and 1.962 nJ/pulse for repetition rates of 4.33 MHz, 8.67 MHz, 13 MHz, and 26 MHz, respectively. For a given time period, increasing the repetition rate will increase the number of irradiating pulses. Thus, it can be said that each pulse carries less energy for high repetition rate lasers.

The photoinitiation threshold fluence and threshold power were plotted in Figure 4-3 for their respective repetition rates. From Figure 4-3, it is evident that photoinitiation threshold fluence for SU-8 decreases linearly, and average threshold power increases, as the repetition rate increases. This agrees with the results obtained in similar process of thin film ablation by femtosecond laser [61]. Hence, the threshold fluence and threshold power are said to be inversely related. The inset of Figure 4-3 shows that, opposite to threshold fluency, the average

threshold power increases with the increase of repetition rates and reaches to saturation after 13 MHz. This can be explained by the combined effect of the effective number of pulses and threshold fluence. The threshold pulse energy required to initiate the polymerization reduces with the decrease of pulse repetition rate, thus the threshold fluence reduces with repetition rate. The increase in average power can be explained by change in the pulses energy for each repetition rates and time duration between two successive pulses. In essence, high repetition rate laser has low pulse energy, therefore require more power to overcome the threshold power.

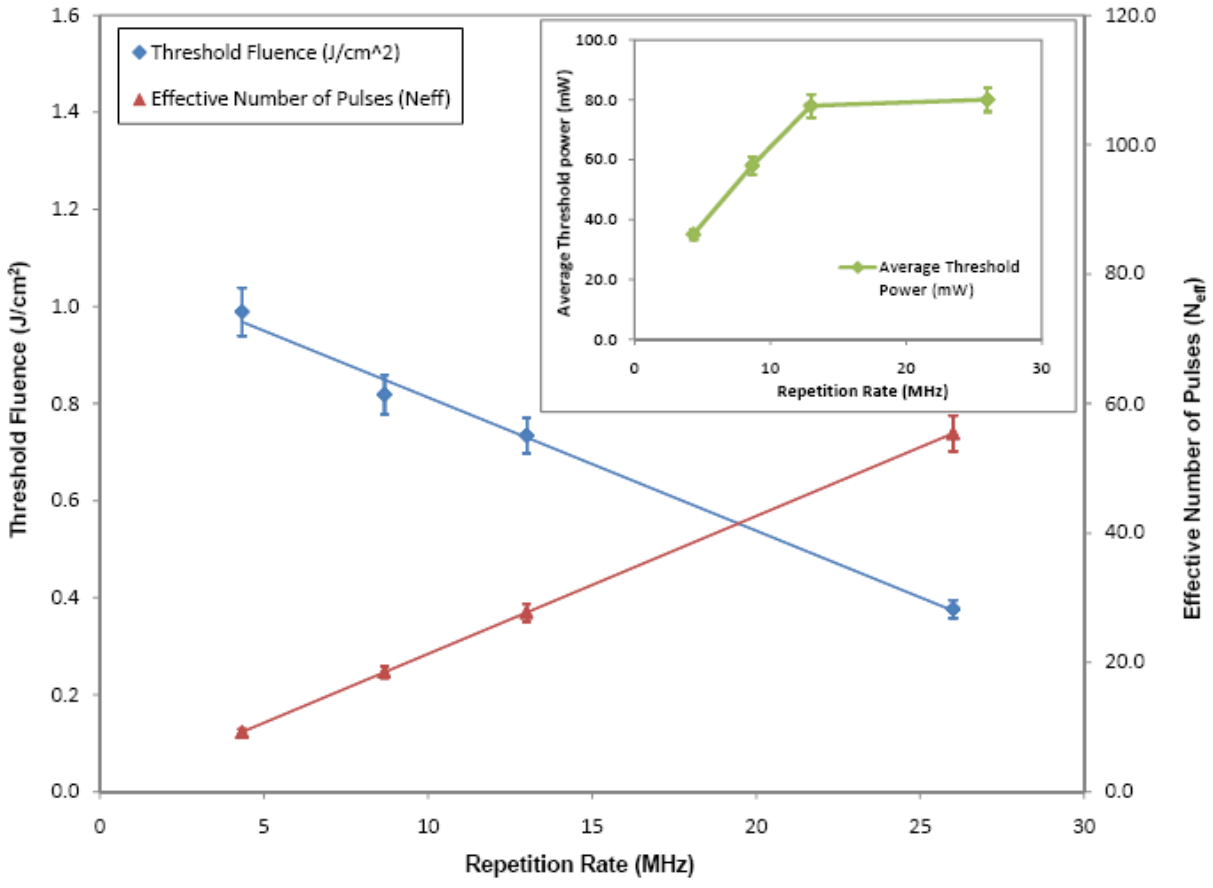

Figure 4-3: Threshold fluence and number of effective pulse for a for various repetition rates; inset figure represents average threshold power for given repetition rates

Furthermore, by increasing the repetition rate, the effective number of pulses can be increased. The effective number of pulses, N_{eff} is a convenient measure of the feed rate in order to compare the results to stationary process of polymerization by multiple pulses. N_{eff} can be calculated from [59, 62]:

$$N_{eff} = \sqrt{\frac{\pi}{2}}\left(\frac{\omega_0 f}{v}\right) \tag{4.3}$$

Here, ω_0 is the machining spot radius which is 0.51 µm, f is the laser repetition rate and v is the piezo scanning speed, which is kept constant at 300 mm/s. The expression relates accumulated fluence of multiple pulses with a Gaussian intensity profile, and subsequent spots separated by v/f. The N_{eff} for 26 MHz, 13 MHz, 8.67 MHz and 4.33 MHz was calculated to be 56 pulses, 28 pulses, 19 pulses, and 10 pulses, respectively. The resist is likely to polymerize even with low laser fluence, if the N_{eff} is high enough to provide sufficient energy required to start photoinitiation. This agrees with the linear decrease in the photoinitiation threshold observed in Figure 4-3. As a result, high repetition rate laser with low fluence, but high N_{eff} provides enough energy to overcome the photoinitiation threshold relative to low repetition rate laser.

4.5 MINITURIZATION OF FLUIDIC CHANNEL

To study the effect of fluence and repetition rates on the feature size, particularly on the channel width, the fluence and channel width were plotted in Figure 4-4 for various repetition rates. It is observed that high fluence and high repetition rates are preferred to minimize the channel width. At high repetition rate, the increment of fluence is small, which provides better

control on the line width. This phenomenon can be explained by the Gaussian energy distribution of laser pulse.

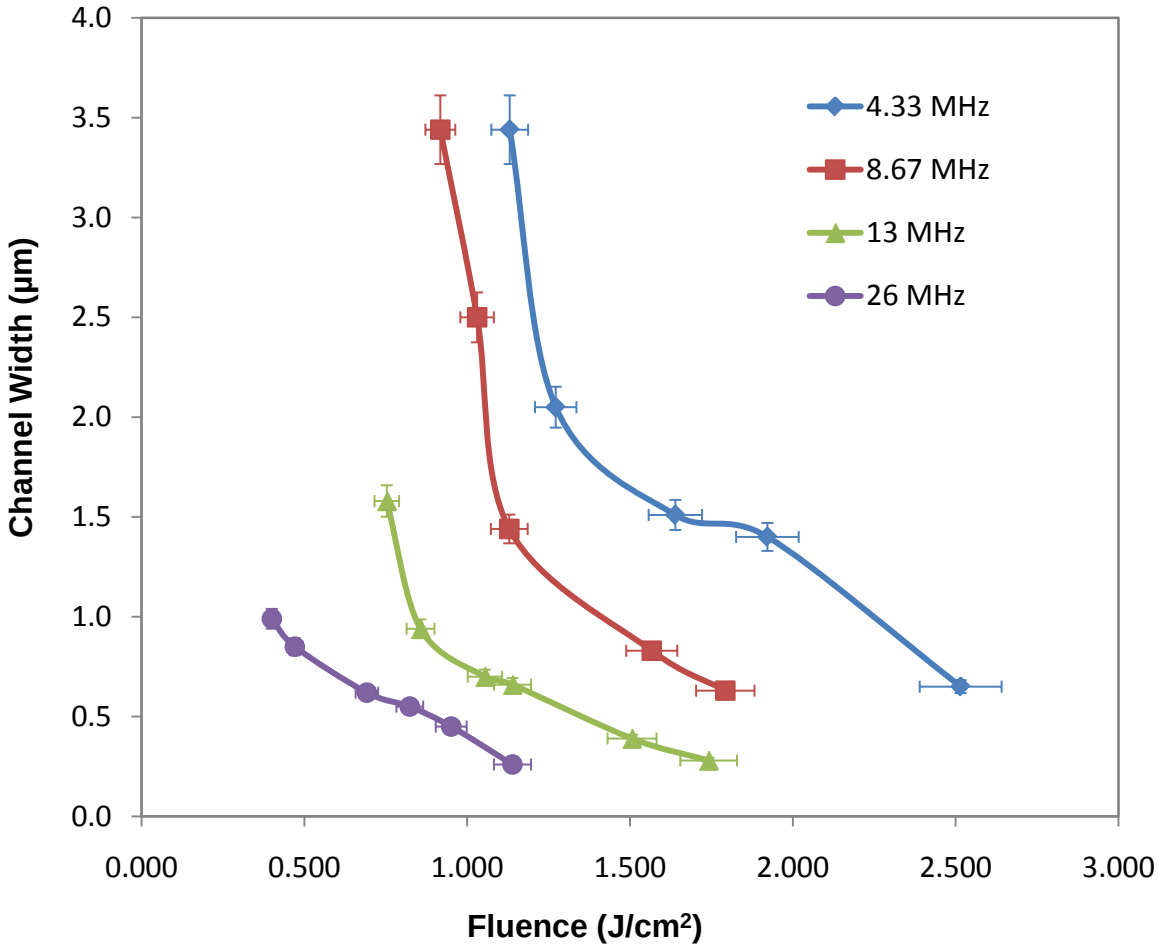

Figure 4-4: Channel width for respective fluence for various rates

Figure 4-5 shows the Gaussian shaped intensity profile for effective machining spot [63]. The lower intensity outer edges of the beam do not polymerize at 10 effective pulses, but they do polymerize at 56 effective pulses, due to the heat accumulation effect. Thus, at a given laser fluence, the machine spot diameter for 56 pulses, $\Phi(56)$, is greater than the effective machining spot for 10 pulses, $\Phi(10)$ resulting in the wider area of exposure of SU-8. As shown in Figure

4-3, the threshold fluence reduces with the increase of N_{eff}. Since the spacing between two laser paths is constant, the ribs width increases as the energy increases, thus the channel width decreases.

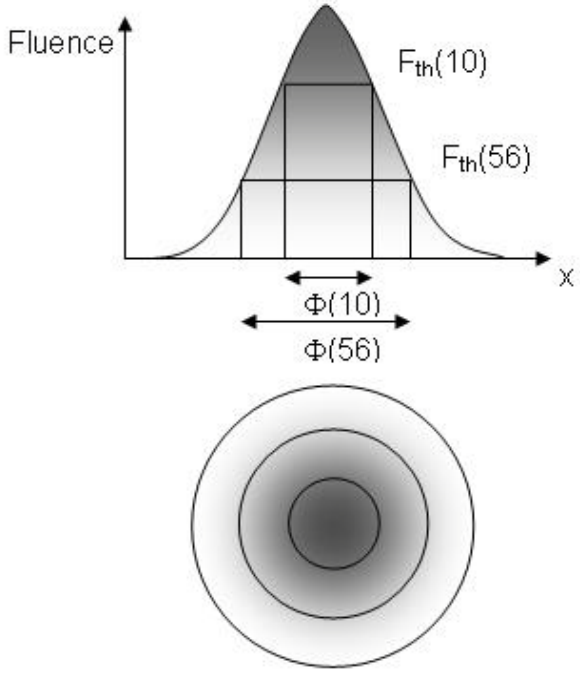

Figure 4-5: For a given fluence, the effective machining spot diameter increases with increasing Neff

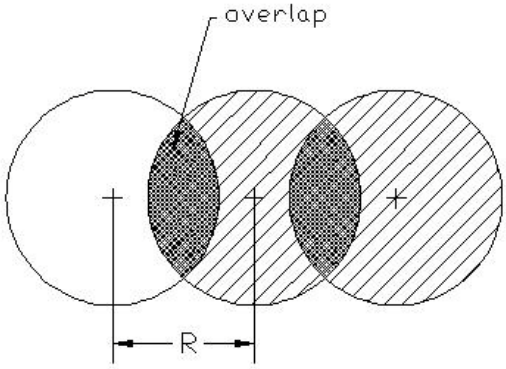

Figure 4-6: Scanning pattern

Scanning resolution, R, is given by the distance between two consecutive scan points, as shown in Figure 4-6. Similar to N_{eff}, scanning resolution also has an effect on size of the polymerized area, which can be determined from:

$$R = \frac{v}{f} \tag{4.4}$$

Where the scanning speed is constant at 300 mm/s. Here, *R* is inversely proportional to the repetition rate *f*. Thus, higher the repetition rate, smaller the value of *R* will be. If the value of R is smaller than the spot diameter, there will be an overlap. The length of intersection of adjacent focus spots is $2\omega_0$-*R*, so the spot-overlap as a percentage of focal spot diameter can be given by:

$$\%\, Overlap = \left(1 - \frac{R}{2\omega_0}\right) \times 100 \tag{4.5}$$

The percent overlap for 26 MHz, 13 MHz, 8.67 MHz, and 4.33 MHz are calculated to be 99.43%, 98.87%, 98.30% and 96.60%, respectively. Higher repetition rates with tighter resolution and greater overlap results in higher degree of polymerization. Also, the linearity of the scan line significantly improves with high percent overlap, which is necessary in order to have smooth sidewalls in fluidic channels.

Low pulse energy in high repetition rate laser provides the flexibility and controllability in fluence increments required to gradually increase the width of ribs. Hence, for both 26 MHz and 13 MHz the channel width decrease gradually as the fluence increases. In contrast, a minor increment of fluence for low repetition rate laser results in a sudden decrease in channel width, because of high pulse energy associated low repetition rate. In addition, it is very difficult to control the channel width at low fluence, just above the threshold fluence; a minor increment in

fluence above threshold fluence results in the significant reduction in channel width. Nevertheless, it is evident from the results that the width of the polymerized ribs can be well controlled at high repetition rates and fluence well above the threshold.

Figure 4-7 shows the fluidic channels created by the 26 MHz repetition rate. However, this time the pulse energy is not the same for each line. From left to right the pulse energy for each of the lines were 4.86 nJ/pulse, 7.35 nJ/pulse, 8.90 nJ/pulse, 9.30 nJ/pulse, 7.70 nJ/pulse, and 5.63 nJ/pulse respectively, and the channel created between them are 1.23 µm, 0.62 µm, 0.42 µm, 0.69 µm and 0.93 µm, respectively. It is evident that the smallest channel is between the two lines with the highest pulse energy.

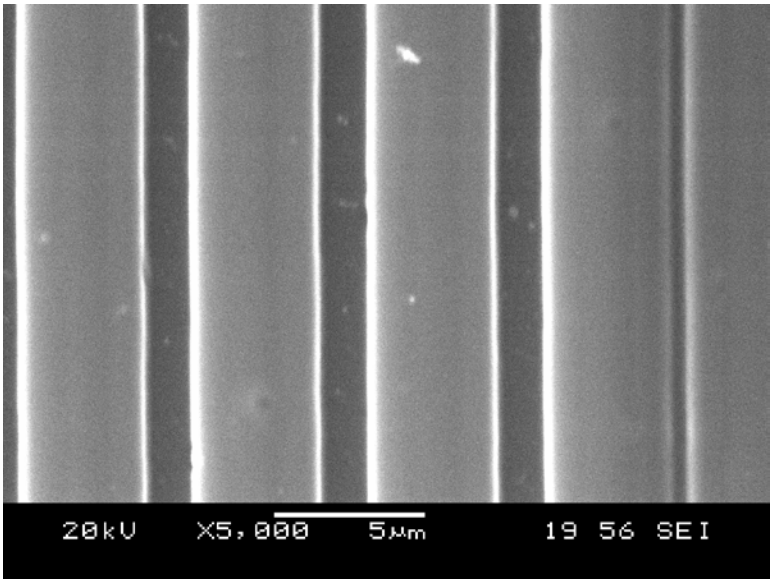

Figure 4-7: Fluidic channels obtained for 26 MHz; change in channels width due to change of pulse energy of 26 MHz from left to right: 1.23 µm, 0.62 µm, 0.42 µm, 0.69 µm and 0.93 µm

Figure 4-8 shows the smallest channel width of 110 nm achieved with the pulse energy of 9.30 nJ/pulse, and the repetition rate of 26 MHz.

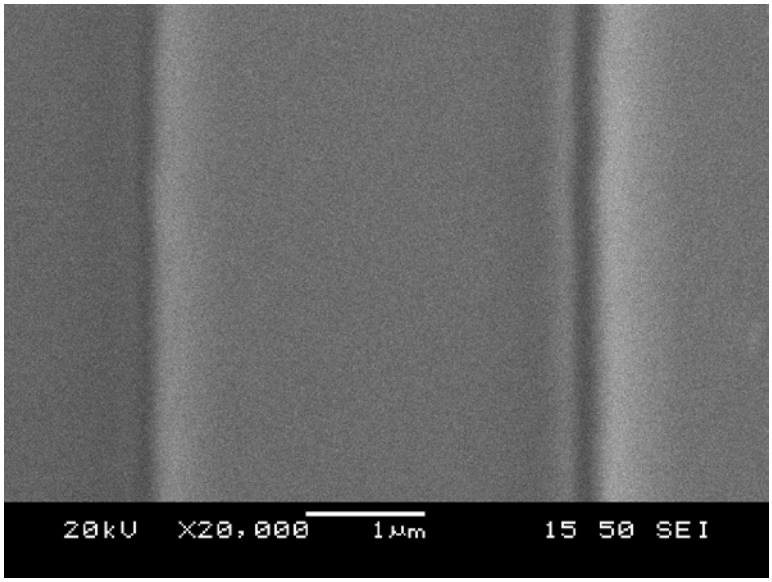

Figure 4-8: Smallest fluidic channels obtained left to right: 110 nm, 150 nm

4.6 SUMMARY

This study has demonstrated a simple, fast and inexpensive process for fabricating open nanofluidic channels using TPA polymerization in SU-8 by femtosecond laser. Unlike other lithography processes, this process does not require a mask and it is configurable to design requirements. By controlling the polymerization of parallel ribs close to each other, the fluidic channel as small as 110 nm in width was successfully achieved. It is also demonstrated that SU-8 has a threshold pronounced behavior, and it does not polymerize until the laser fluence is above the photoinitiation threshold. The photoinitiation threshold fluence for SU-8 decreases linearly as the repetition rate increases. Femtosecond laser with the repetition rates of 4.33 MHz, 8.67 MHz, 13 MHz and 26 MHz found to have the photoinitiation threshold of 0.989 J/cm^2, 0.819 J/cm^2, 0.734 J/cm^2, and 0.400 J/cm^2, respectively. Experimental results showed that high repetition rate is preferred to obtain minimum channel width due to the controllability. Other than the mechanical positioning, the channel width can be controlled by selecting optimum

effective number of pulses and scanning resolution. Among many repetition rates investigated, 26 MHz is the most capable of creating nano-channels with maximum flexibility and controllability because it has the lowest threshold fluence. Moreover, it has high number of effective pulses N_{eff} with low pulse energy impacting the resist resulting in high controllability in applied energy dosages. Hence, this technique is very well capable of creating fluidic channels close to few nanometers. However, there are some challenges in creating 2D channels, because it is extremely difficult to manage the offset and polymerization of two ribs in both X and Y directions.

CHAPTER 5

FLUIDIC CHANNELS VIA TWO PHOTON ABSORPTION (TPA) POLYMERIZATION ASSISTED ABLATION

5.1 INTRODUCTION

In the previous chapter, fabrication technique is developed based on the concept of controlling the spacing between two polymerized ribs parallel to each other. The smallest channel (i.e. the spacing) successfully achieved is about 110 nm. However, it was noted that controlling the spacing can be extremely difficult for two dimensional channels, especially with a sharp bend. Therefore, the effective alternative technique is required for creating two dimensional networks of channels.

In this chapter, a new fabrication process is proposed based on a well-known ablation phenomenon in any laser processing. The process of laser ablation can be briefly summarized as the following. Upon irradiation of the laser beam on the surface, the heat waves penetrate into the bulk of the substrate, generating vapor and melt. As more heat is supplied, due to the rapid heating and heating-induced instability, evaporated particles are explosively ejected from the surface. Also, the surface plasma is formed by the incident laser beam. The surface plasma is a large population of loosely bound electrons and ions which absorb and reflect laser energy. The expansion of plasma on the surface and the rapid ejection of removed material create

shockwaves. Because of the propagation of the large shock-waves, and pressure-induced and thermal-induced stresses, micro-cracks and fractures may result.

5.2 FABRICATING FLUIDIC CHANNELS VIA POLYMERIZATION ASSISTED ABLATION

To create the channels, the femtosecond laser is tightly focused onto the ORMOCER resist in a linear pattern, as shown in Figure 5-1 (a). The laser pulses initiate the photochemical process via TPA and subsequently the exposed area is polymerized. The laser is scanned for the second time on the same path, as shown in Figure 5-1 (b). However, this time the laser energy is consumed to ablate the polymerized rib.

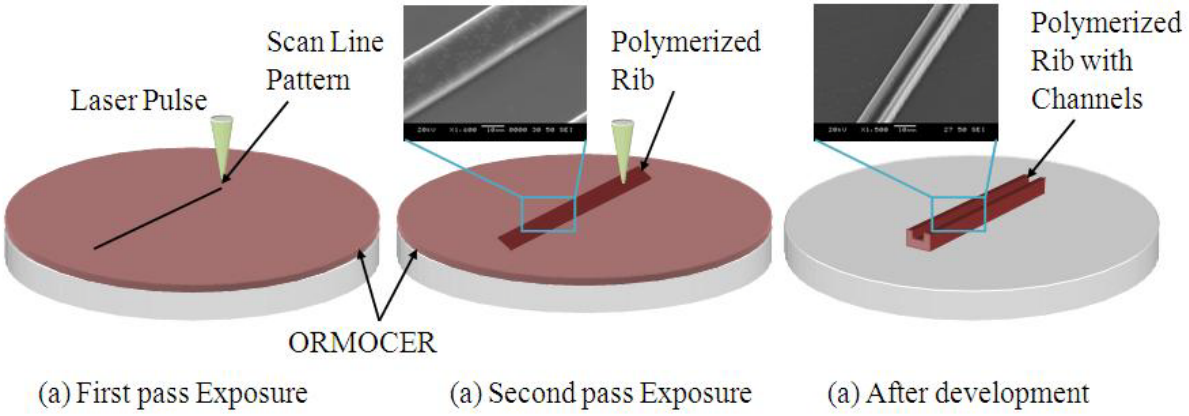

Figure 5-1: Fluidic channel fabrication via TPA polymerization assisted ablation (a) laser is focused in lines for the first time (b) polymerized ribs are exposed for the second time; SEM image of polymerized rib shown in inset (c) parallel ribs with channels in between are achieved after development; SEM image of fluidic channel created through ablation shown in inset

It is observed that without changing any parameters for the second pass (i.e. same amount of laser energy is supplied), the polymer starts to ablate, which indicates that the ablation threshold of resist successively reduces after the initial TPA polymerization. This is due to the

reason that the exposed and unexposed resist reacts differently during further processing depending on the absorbed energy per unit volume. TPA assisted ablation presents greater opportunity in ablating resist with low laser power as explained in later sections. In comparison to direct ablation of resist, TPA assisted ablation also presents superior controls on desirable feature size and spatial resolution. After the development, as shown in Figure 5-1 (c), the exposed pattern of line converts into polymerized parallel ribs with microchannels engraved in the center.

The width of the ribs and the microchannel can be controlled by manipulating the laser average power and the scan speed as a measure of the laser fluence and the exposure time, respectively. Arrays of fluidic channels with various laser parameters are created to achieve the smallest channel width with highest controllability. The sample is exposed for average laser powers ranging from 80 mW to 700 mW and four scan speeds of 10 μm/s, 50 μm/s, 100 μm/s, and 500 μm/s. However, the speed and power for the second pass are kept same as the first pass. Figure 5-2 is a SEM image of a micro-fluidic channel created by proposed method with the repetition rate of 26 MHz, the scanning speed of 50 μm/s, and the average power of 390 mW. In addition, high precision nano positioning stages or laser beam steering mechanisms can be used to precisely position the focal point on the rib to achieve desired rib thickness, channel width and channel depth and further improve the resolution and quality of the channels.

Since the proposed method is a direct write method, microchannels with any two-dimensional geometry can be fabricated in a single step. In addition, particular channel width and depth in an array of channels can easily be controlled by manipulating laser power and scan speed.

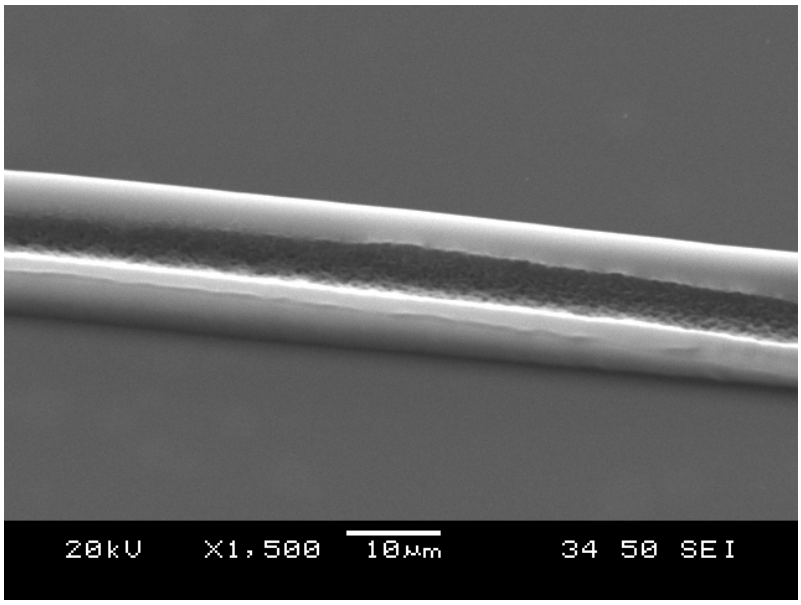

Figure 5-2: Fluidic channel with high aspect ratio

Figure 5-3 shows the SEM images of fluidic channels fabricated using different CAD drawings. Figure 5-3 (a) is a result of polymerization of a rib with ablation at the end point to create the reservoir for buffer fluid. This is achieved by single pass laser irradiation, but only the end of the rib was exposed for the second time to create the well. If the entire rib is scanned for the second time, the reservoir in connection with the channel can be fabricated, as shown in Figure 5-3 (b). A channel with a bend and a T-junction of fluidic channels, shown in Figure 5-3 (c) and (d), respectively, are also fabricated with the proposed technique. Therefore, any type of two dimensional network of fluidic channels can easily created by TPA assisted ablation by simply steering the laser on the path generated by the CAD program.

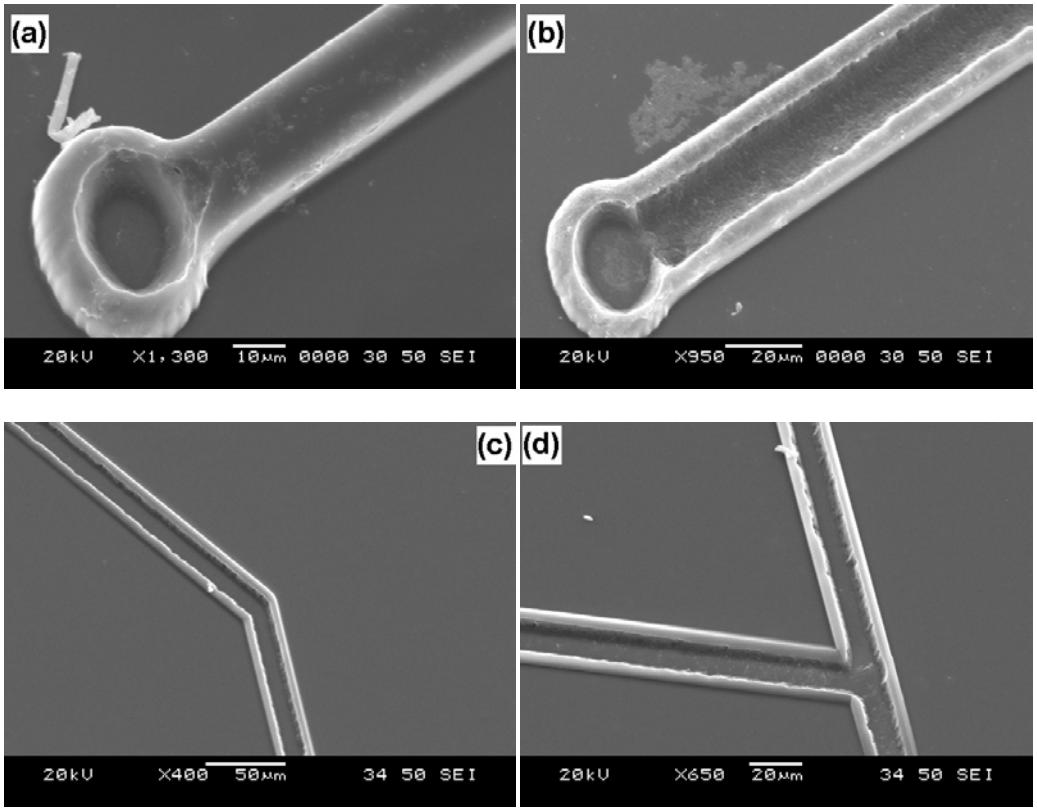

Figure 5-3: Features fabricated via TPA polymerization assisted ablation (a) reservoir well (b) reservoir connected with fluidic channel (c) fluidic channel with a bend (d) T-junction of fluidic channels

5.3 ABSORPTION AFTER POLYMERIZATION

It is observed that the resist reacted differently to the laser during the first pass than the second pass. The laser-resist interaction can be summarized as the following. If the pulse energy is sufficient enough to induce the photoinitiation process during the first pass, the resist undergoes polymerization. Once the resist is polymerized, during the subsequent pass it starts to ablate. If the pulse energy is less than the photoinitiation threshold, the resist does not polymerize. In contrast, if the pulse energy is considerably higher than the photoinitiation threshold for the initial pass, the resist starts to breakdown and boil/evaporate. The laser induced breakdown is shown in the Figure 5-4 for the repetition rate of 26 MHz, the scanning speed of 50 µm/s, and the average power of 1.2 W.

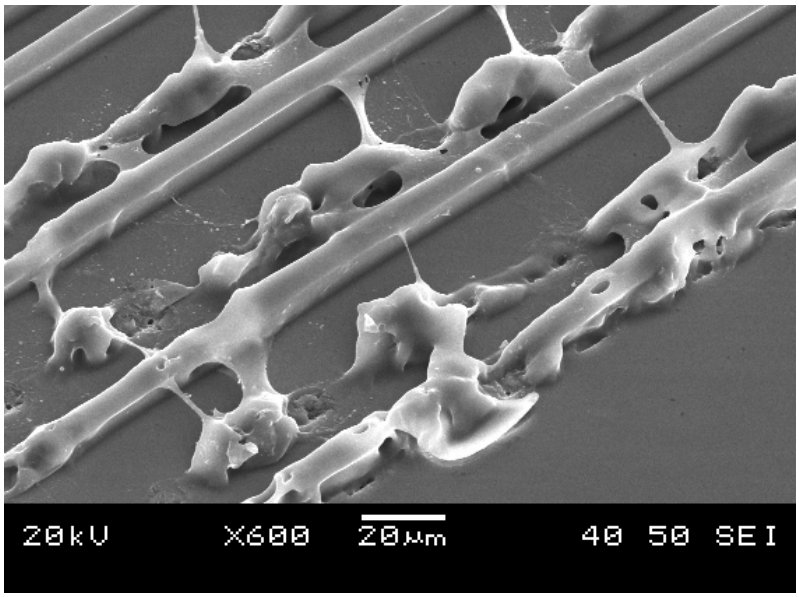

Figure 5-4: Laser induced breakdown for high energy

The ratio between photoinitiation threshold and laser induced breakdown threshold for the same conditions is experimentally determined to be 3.2. Thus, the window between the photoinitiation threshold and the laser induced breakdown threshold [64] is quite smaller than (several times) the polymerization threshold [55, 65], leaving very little room for power tuning. The polymerization with the energy beyond the boiling threshold is extremely difficult to control and the resulting structures have significant broken features. Hence, it is very difficult to control direct ablation of the photoresist. Nevertheless, once the resist is polymerized, it can be easily ablated with considerable less energy to achieve desirable features with exceptional spatial resolution. This phenomenon can be explained by the absorption taken place in polymerized resist. Figure 5-5 illustrates that the absorption before and after the TPA polymerization increases linearly as the intensity increases. The total uncertainty in measuring the average absorption is approximately ±5%.

During the second scan, approximately 40% of the energy is absorbed and consumed for ablation. Before the polymerization, the absorption is approximately 5% or less. The significant

increase in the absorption justifies the reduction of the ablation threshold for the second pass. The linear nature of the absorption, after initial TPA polymerization, presents excellent opportunity to control and predict the ablating area. Additionally, the TPA polymerization assisted ablation threshold is significantly lower than the direct ablation and reduces the effects of boiling, evaporation and structural damage on the features. It is also noted that the absorption is wavelength dependent, as it can be seen in Figure 5-6. ORMOCER absorbs energy for wavelengths starting from 500 nm to 1050 nm; nonetheless, it is most receptive for the wavelengths between 650 nm to 850 nm. The maximum absorption is at approximately 735 nm which is almost twice the wavelength at which Darocur TPO exhibits the maximum UV absorption. Hence, it can be concluded that ORMOCER has experienced TPA polymerization.

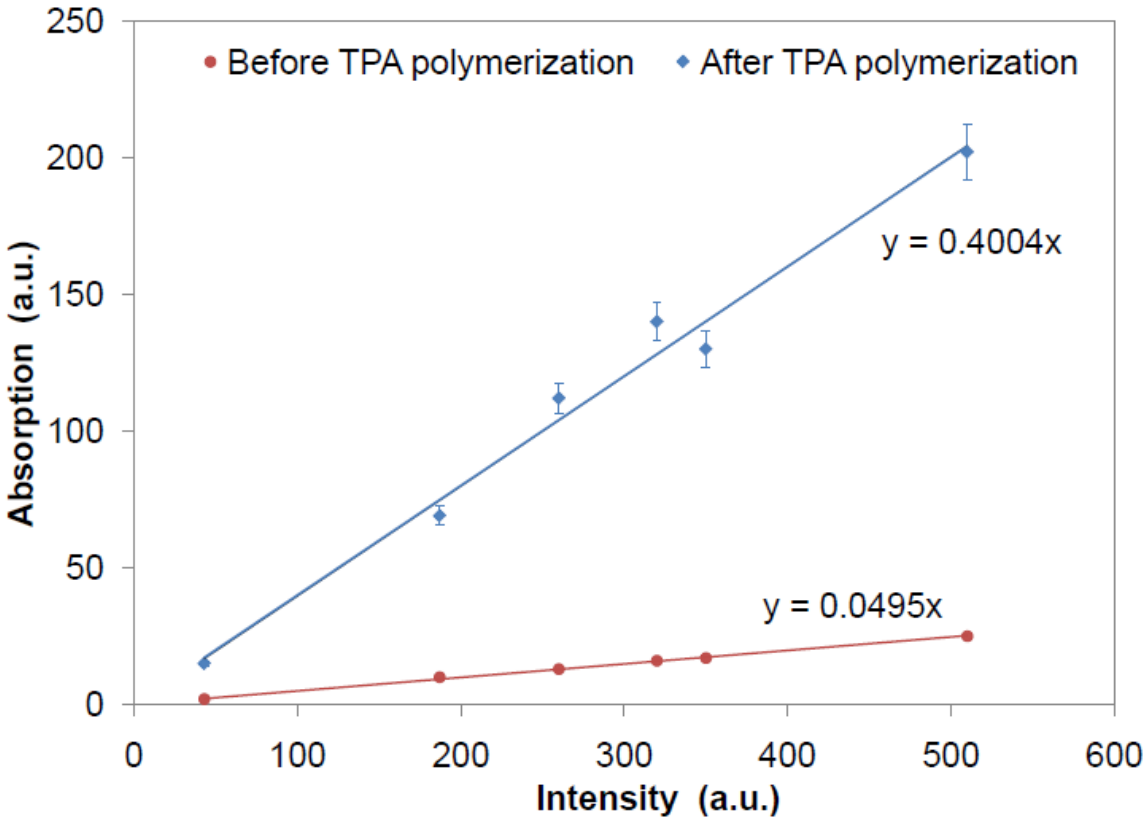

Figure 5-5: Absorption before and after TPA polymerization at 515 nm

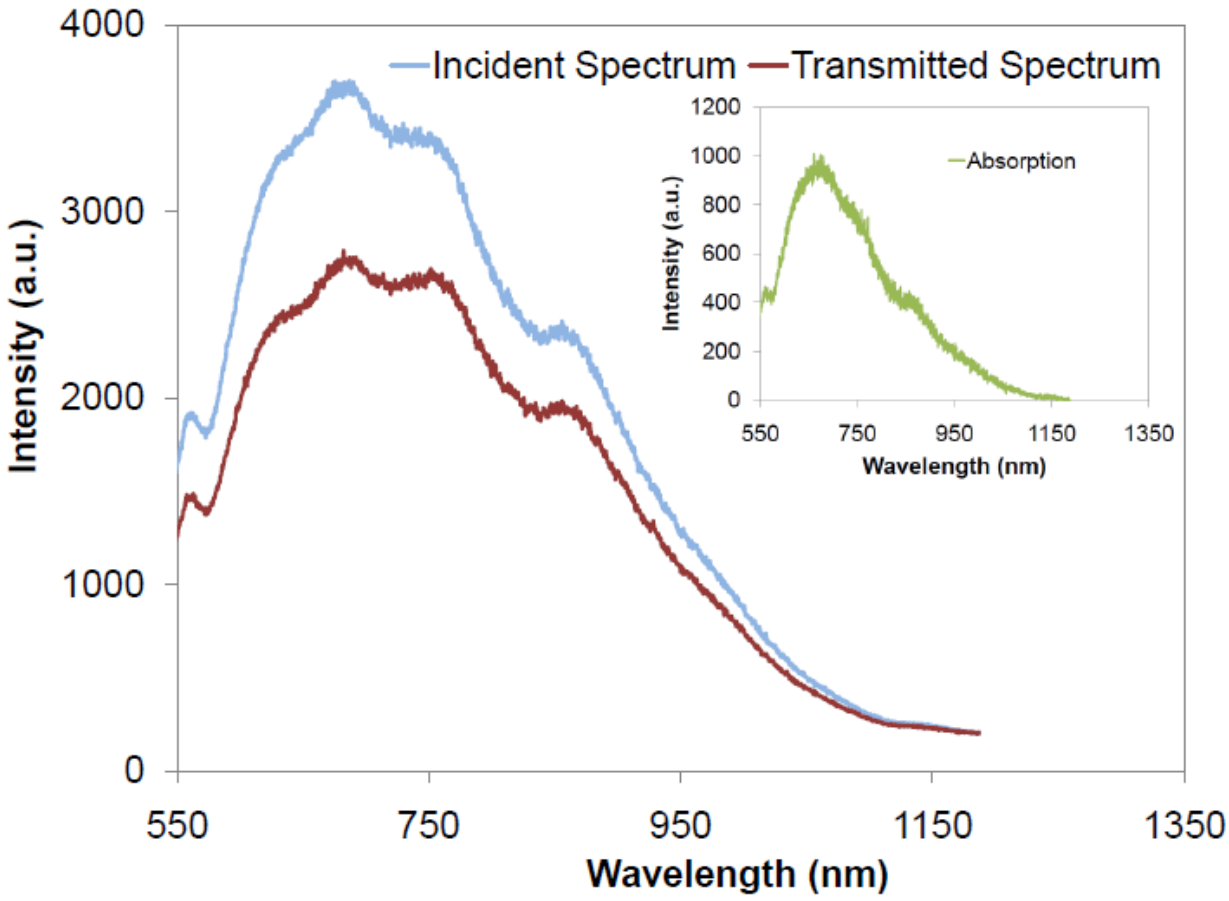

Figure 5-6: Incident and transmitted spectrum for relative wavelengths; inset figure represents an absorption spectrum for TPA polymerized resist

5.4 TWO PHOTON POLYMERIZATION (TPA) POLYMERIZAITON ASSISTED ABLATION THRESHOLD

As explained in the Chapter 4, the ablation threshold of ORMOCER after polymerization for repetition rates of 13 MHz and 26 MHz for different scan speeds can be determined. Previously, it has also been shown that the photoinitiation threshold fluence decreases and controllability of the polymerized area improves for high repetition rates. The same trend is observed here for the ablation threshold after TPA polymerization. The reason for such tendency is explained in depth in Chapter 4 and also reported in [66].

Table 5-1: Threshold fluences and effective number of pulses for different scan speeds

Speed (μm/s)	13 MHz		26 MHz	
	Φ_{th} (mJ/cm^2)	N_{eff} (10^3)	Φ_{th} (mJ/cm^2)	N_{eff} (10^3)
10	753.11	830.947	696.62	1661.895
50	988.45	166.189	941.38	332.379
100	1317.94	83.095	1190.85	166.189
500	2259.32	16.619	1873.35	33.238

Table 5-1 summarizes the threshold fluence and the effective number of pulses, calculated using Eqn. (4.3), for their respective scan speeds and repetition rates. A high repetition rate with slower scan speed results in a higher degree of polymerization and ablation. Also, the linearity of the scan line significantly improves with high percent overlap of the two consecutive spots, which is necessary in order to have good sidewalls in fluidic channels.

The threshold fluences as a function of the effective number of pulses are plotted in Figure 5-7. Total uncertainty in the average threshold power measurement causes an uncertainty in the threshold fluence calculation of approximately ±5%. Empirically, the threshold fluence has been found to roughly obey the equation

$$\Phi_{th} = A\left(N_{eff}\right)^{-b}, \tag{5.1}$$

where A and b are fit parameters and depend on the resist's chemical properties. The experimental values of these constants are listed in Table 5-2.

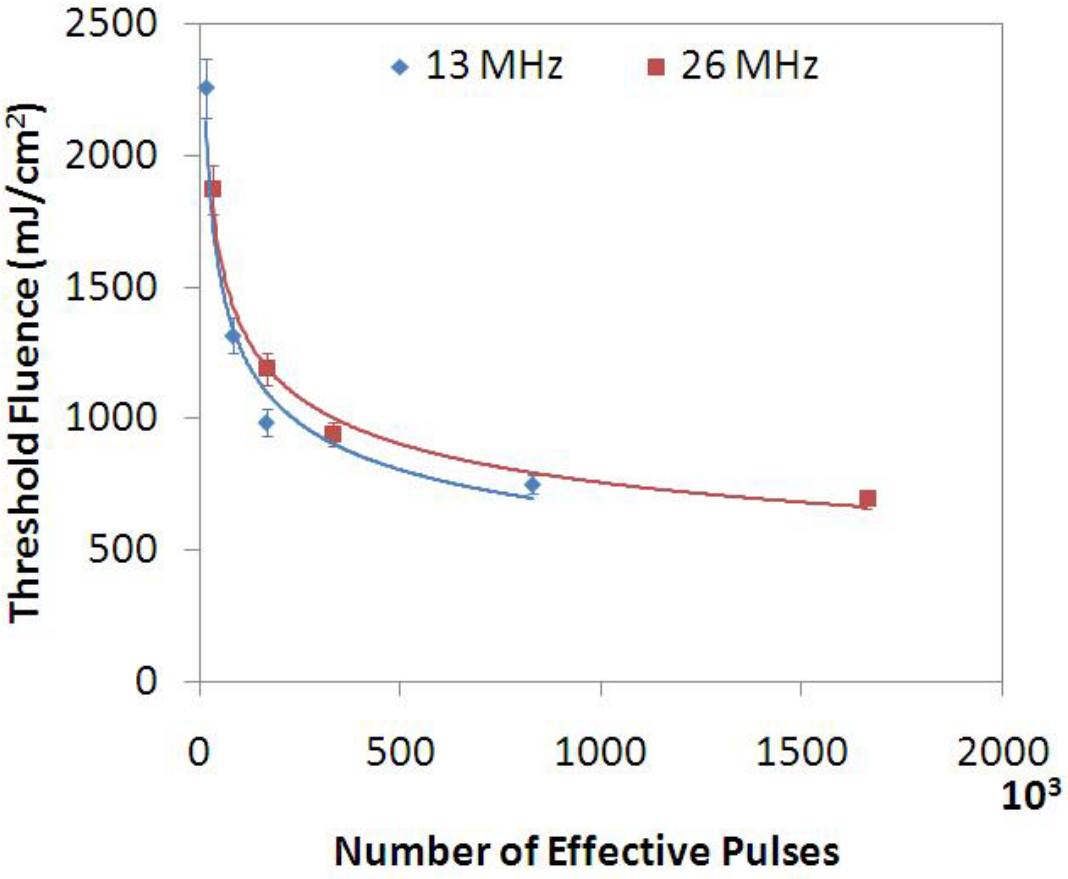

Figure 5-7: Threshold fluence for number of effective pulses

By substituting N_{eff} from Eqn. (4.3) into Eqn. (5.1), one can relate the threshold fluence directly to the laser parameters spot radius, repetition rate and scan speed by the following:

$$\Phi_{th} = C\left(\frac{\omega_0 f}{v}\right)^{-b}, \tag{5.2}$$

where C is a product of constant A and $(\pi/2)^{-b/2}$ and can be defined as another constant that depends on resist properties. The Eqn. (5.2), directly relates the threshold fluence with process parameters such as scan speed and the spot size for the given condition. In addition, the threshold fluence is also related to the repetition rate. By increasing the repetition rate, spot size and decreasing the scan speed, the amount of polymerization can be increased. As explained

previously, the absorption is significantly more for polymerized resist thereby the ablation threshold value decrease. For any photoresist, the values of the contestants *C* and *b* can be determined experimentally. The values of these constants for ORMOCER for the repetition rates of 13 MHz and 26 MHz are summarized in Table 5-2. Knowing the values of these constants, the TPA polymerization assisted ablation and the feature size can be predicted. The in-depth analysis on relations of the constants to the photoinitiators is out of scope for this thesis, but it would be considered for future investigation.

Table 5-2: Fit parameters for ORMOCER for respective repetition rates

Repetition rates (MHz)	**A (mJ/cm^2)/pulse**	**b**	**$C = A(\pi/2)^{-b/2}$ (mJ/cm^2)/pulse**
13	33960	0.28	29926
26	25919	0.25	23151

5.5 SUMMARY

The proposed fabrication process in here is a simple, fast and inexpensive process for creating fluidic channels via TPA polymerization assisted ablation. This process can be seen as an alternative to the one suggested in Chapter 4. Unlike the previous method, where the channel is formed between two ribs, this time the channel is inscribed on the rib by ablation. In the previous method, it is very difficult to control the spacing between two ribs for the two dimensional channels with the sharp angle. However, in the ablation method, it is very easy to steer the laser in XY plane to generate any two dimensional channels because the laser follows the same path as the previous one used to polymerize the rib. It is also demonstrated that ORMOCER has an ablation threshold behavior. The ablation threshold significantly reduces after initial polymerization. The reason for such tendency is a result of enormous increase in the energy absorption after the TPA polymerization. The polymerization as well as the ablation can

be controlled with the laser repetition rate, spot size and scan speed. This presents the outstanding opportunity of ablating resist at significantly less pulse energy, which allows superior spatial resolution and greater control on the desired feature size in comparison to direct ablation.

CHAPTER 6

SELF-ENCLOSED FLUIDIC CHANNELS VIA SUB-SEQUENT POLYMERIZATION

6.1 INTRODUCTION

Many versions of lithography techniques have been developed to fabricate enclosed fluidic channels. Nonetheless, to a great extent these lithography techniques rely on a mask or mold fabrication, which is very expensive, time consuming and not feasible for rapid prototyping. In addition, they have complicated fabrication steps, and require multiple sacrificial layers. A laser direct write method is a good alternative to lithography, but it still requires substrate bonding to enclose the channels. In Chapter 4 and 5, the techniques of fabricated open fluidic channels are introduced. The first technique is for creating the fluidic channels down to the nanometer scale. The second technique is to effectively create two dimensional fluidic channels to be easily integrated in a fluidic network with other fluidic components. Nonetheless, both require additional post-processing to enclose or seal the channels on top. It is very critical to have enclosed channels to avoid evaporation of sample and chemical reagents. It is a major challenge for polymer-based microfluidic devices to bond parts together or layering-up.

6.2 BONDING TECHNIQES

Various techniques have been reported for sealing fluidic channels. After channel fabrication, the microchannels (which are normally open on top), must be sealed to form a complete channel; the challenge here is to achieve this seal without clogging or altering the

dimensions of the channel pattern during the sealing process. This step often is the limitation for high volume fabrication methods. Several bonding methods have been reported and are reviewed here.

6.2.1 THERMAL BONDING

Thermal bonding or thermal fusion is the most widely-used approach for sealing microfluidic patterns made in thermoplastics [67-69]. A patterned substrate is bonded to a blank substrate on top using this method; a clamp or hydraulic press is used to hold the two pieces together. Then the assembly is heated to elevate the temperature around the glass transition temperature (T_g) of the substrate. After a period of time, the temperature is lowered and the bonded microdevice is released from the clamp. It should be mentioned that since bonding depends on the intermolecular interactions between the contact polymer layers, this bonding method cannot provide high bonding strength for polymeric substrates, and de-lamination often occurs. Moreover, since thermal bonding is performed at a temperature close to T_g, channel deformation is very common, which makes this technique unsuitable for sealing microstructures with very low aspect-ratios and small dimensions.

6.2.2 SOLVENT BONDING

Alternatively, organic solvents that dissolve the polymeric substrates can be used in microdevice bonding [70, 71]. A thin layer of solvent is spin-coated on a blank substrate, and, then, a patterned substrate is quickly brought into tight contact with the blank. After a period of time, the solvent partially dissolves the polymer at the contact surface, and the flexible polymer

chains in both substrates are bonded when external pressure is applied. As a result, strong intermolecular interactions are established between the two substrates [70].

Unlike the thermal bonding, solvent bonding is performed at room temperature and can provide very high bonding strength; however, the organic solvents used should have moderate solubility in the polymer substrates, and their volatilities should not be high. In addition, the amount of solvent coated on the substrate surface should be very carefully controlled; otherwise, excessive polymers may dissolve and flow into the channels, which can block the channels.

6.2.3 ADHESIVE BONDING

The procedure for adhesive bonding is the same as the one for solvent bonding. However, unlike solvents, which can be absorbed inside the polymer matrix, adhesives will stay on the substrate surface after bonding and, thus, the thickness of the adhesive layer must be small enough to prevent the adhesive from flowing into and blocking the channels. The top surface of the enclosed channel will be coated with adhesive. Therefore, adhesives with similar surface properties to the substrate must be selected [72].

6.2.4 CHEMICAL BONDING

In chemical bonding or permanent bonding, polymeric substrates are bonded through chemical bonds formed at the contact surface. Because various polymeric materials are used in microfabrication, specific chemistries must be used in the chemical bonding process. PDMS not only bonds to glass, silicon, and itself through intermolecular interactions, but it can also bond to these substrates covalently. To chemically bond PDMS to other substrates, low power O_2 plasma is used to treat both the PDMS and the blank substrates for one min. Following O_2 plasma

treatment, the PDMS is quickly pressed onto the blank, and the substrates become bonded chemically after several minutes [73, 74]. During O_2 plasma treatment, siloxane bonds in the substrates are cleared by the plasma. If the substrates are brought into contact in less than 30 s, covalent bonds will form between the broken bonds in both substrates. To bond a patterned SU-8 substrate, uncured SU-8 is spin-coated on a piece of glass and the glass is then attached to the patterned substrate. Permanent bonding forms when the temporarily attached substrates are subjected to UV exposure and high temperature baking. During this process, epoxy groups in the polymer side-chains are activated by a photo-generated acid ($HSbF_6$), which form covalent bonds with other epoxy rings nearby at elevated temperature. This cationic polymerization happens not only in bulk, but also at the contact surface, thereby forming covalent bonds between the SU-8 surfaces.

Various other channels enclosing methods have been studied, including sealing with soft elastomers [75], fusion bonding [76], and depositing materials over sacrificial layers followed by thermal decomposition [77] etc. All the aforementioned methods have their own advantages and disadvantages. Soft elastomers (e.g. PDMS) provide a uniform sealing over a large area but the channels might be clogged as soft materials can be easily pressed into the channels [78]. The most commonly used thermal bonding requires stringent cleaning and high temperatures, often resulting in channel morphing and weak bonds [79]. The residuals stuck to the channel walls after removal of sacrificial layers may hinder the flow inside the channels [80]. Finally, these enclosing methods required multiple steps and significantly increase the complexity.

6.3 FABRICATION OF ENCLOSED FLUIDIC CHANNELS VIA SUB-SEQUENT TWO PHOTON ABSORPTION (TPA) POLYMERIZATION

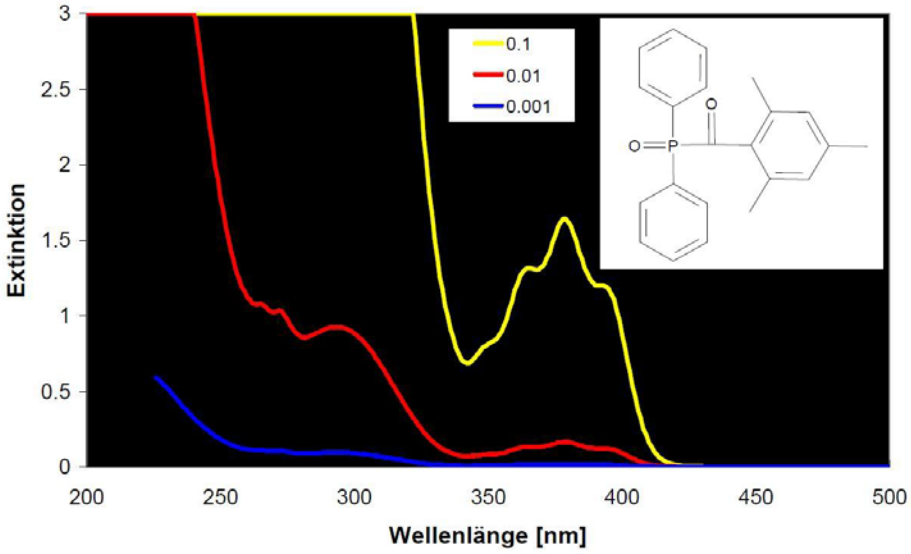

Figure 6-1: Photoinitiator Darocur TPO UV absorption spectrum; inset is a structural representation of Darocur TPO as 2,4,6-Trimethylbenzoyl-diphenyl-phosphineoxide photoinitiator[3]

The resin used for this experiment is Ormocomp Low Viscosity, with 1%(w/w) concentration of Darocur 4265. Darocur 4265 has three absorption peaks: 240 nm, 272 nm and 380 nm for different concentrations (see Figure 6-1). Laser repetition rates of 13 MHz and 26 MHz with pulse duration of 214 fs , 1.45 ps and 3.14 ps were used in this experiment. The second harmonic (515 nm) central wavelength is used to expose the resist instead of 1030 nm. There are several motivating factors to use the second harmonic light frequency. Firstly, with 1030 nm MPA is more likely to occur. In comparison, 515 nm will result in TPA. With reduction in the order of MPA, it is easier to achieve a better polymerization efficiency and

---

[3] Ciba® Darocur® Material Data sheet

Source: "DAROCUR TPO." *Welcome to Ciba*. Web. 07 Aug. 2009. <http://cibasc.com/darocur_tpo-3.htm>

smaller special resolution [55]. Secondly, absorbance of the photoinitiator, Darocur 4265, at 240 nm and 274 nm is much higher than that at 380 nm. Therefore, photoinitiation threshold at 515 nm will be much lower than that at 1030, which in turn further improves spatial resolution [81]. Finally, the shorter wavelength proportionally reduces the diffraction limit of the focal spot and results in smaller feature size. A glass substrate is spin-coated with Ormocomp (Microchem Technology GmbH) to achieve desired thin film thickness and then exposed under laser beam.

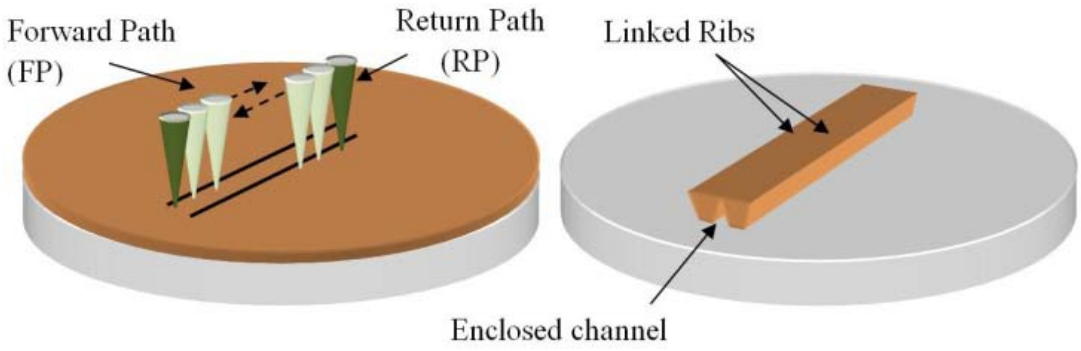

Figure 6-2: Schematic drawing of fabrication process

In order to investigate the formation of the enclosed channels, a systematic series of experiments were carried out. The focus of the experiment was the formation of an adjacent pair of ribs and cross-link on the top surface creating a hollow channel between them. The typical exposure steps used are shown in Figure 6-2 (a). First the laser is scanned in a forward path (FP), and then with a defined offset it is scanned in a parallel return path (RP). If the return path is placed close enough to the forward path, the two parallel polymerized ribs link at the top. Figure 6-2 (b) illustrates a channel formed by linking two adjacent ribs at the top. Experimental trails showed that the linking was greatly affected by pulse energy, scanning speed, line offset, pulse width and repetition rate. With correct combination of the laser parameters, arrays of self-enclosed channels by scanning laser beam in parallel lines were created. The sample was

exposed for average laser power ranging from 80 mW to 700 mW, repetition rates of 13 MHz and 26 MHz, various scans speeds and offsets.

After the exposure, the resist was hard-baked on a hot-plate at the constant temperature of 95°C for two minutes. Once the substrate was cooled, it was immersed in Ormocomp developer solution (Microchem Technology GmbH) for two minutes at room temperature. Finally, the parallel fluidic channels formed by TPA polymerization were observed under a Scanning Electron Microscope (SEM). Since the sample was nonconductive, it had to be gold-sputtered before imagining.

6.4 SUB-SEQUENT POLYMERIZATION MODEL

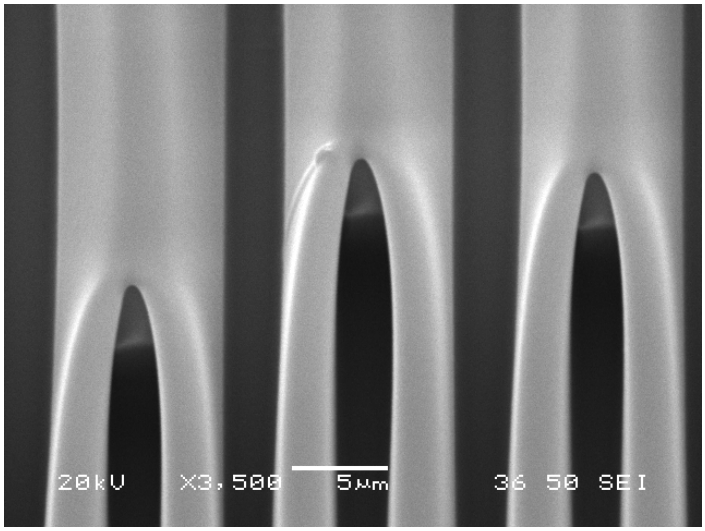

Figure 6-3: SEM image of enclosed channels

Figure 6-3 is a SEM image of a micro-fluidic channel created by the proposed method with a repetition rate of 26 MHz, average power of 828 mW, pulse width of 428 fs, and scanning speed of 300 mm/s. The wall thickness of the two ribs is 2.62 µm, the width of the enclosed

channel is about 2.44 μm. The total height of the enclosed channel is around 10 μm. The offset between the two parallel adjacent walls is measured (center to center) as 6 μm.

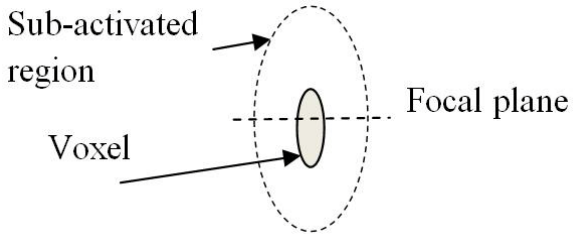

Figure 6-4: Voxel and surrounding sub-activated region

TPA is a nonlinear process; thereby, it has well-defined threshold type behavior. The volumetric region that has the fluence greater than photoinitiation threshold generates highly active radical concentration, which causes the solidification of resin. According to the scaling laws of TPA polymerization [82], polymerized region forms in an ellipsoid shape with center plane at the focal plane. It is named voxel (volumetric pixel) and depicted as solid voxel in Figure 6-4. However, its surrounding is not a clear-cut division of solid and liquid phases. The intermediate region resulting from the concentration gradient of the active radicals is a sub-activated region, where radicals are initiated but the concentration is below the threshold. According to Nitin Uppal [83], with a 1-μm laser spot this region is about 10 μm in radial direction and about 150 μm from the focal plane in the axial direction. The voxel was calculated to be 2-4 μm in radial direction [83], which agrees well with the wall thickness.

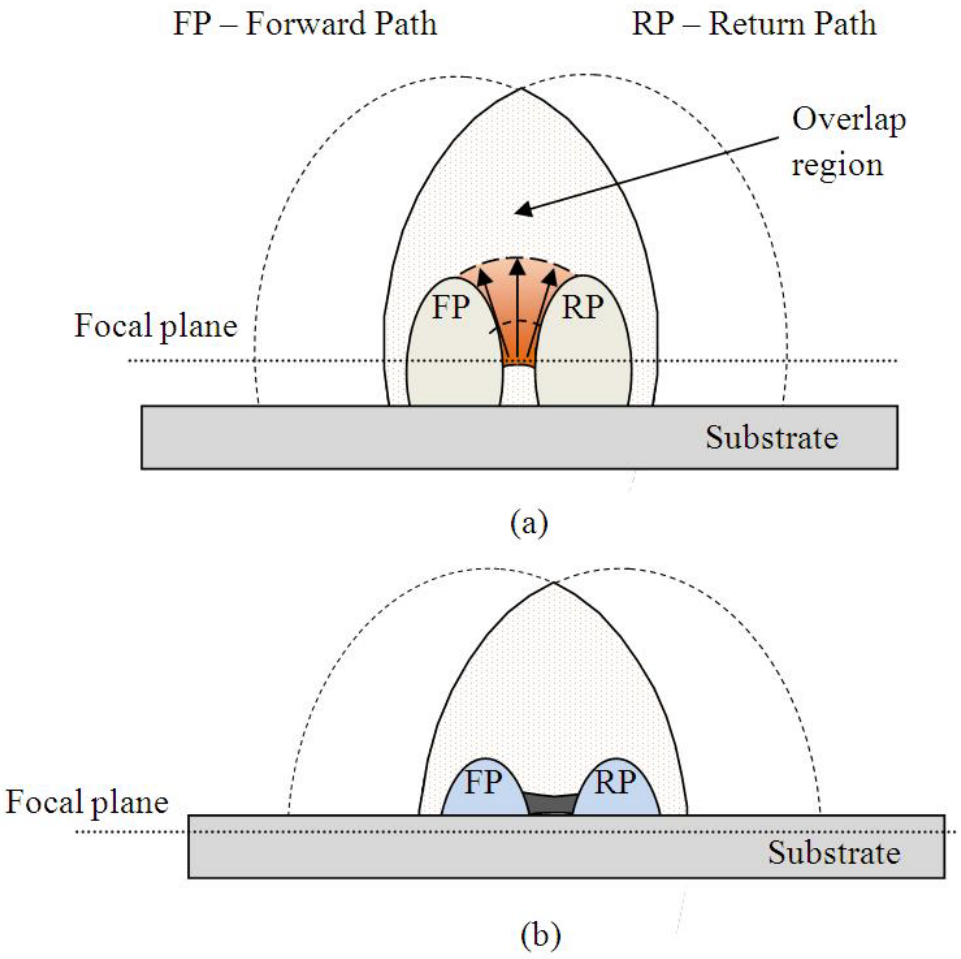

Figure 6-5: Linking by sub-sequent polymerization (a) when the focal plane is above the substrate (b) when the focal plane is below the substrate

Figure 6-5 illustrates the polymerization mechanism resulting of sub-sequent polymerization phenomena. In the first step, the laser is scanned in a forward path (FP) with specific pulse energy, repetition rate, and scan speed. In a following step, the laser is scanned in a parallel return path (RP) with the same parameters. The exposure dosage determines the actual size of the solidified ribs. If FP and RP are close enough, there will be an overlap of the sub-activated region. In this case, the offset between the two adjacent walls (6 μm as measured) is comparable to the radius of the sub-activated region, which is calculated to be 5 μm in radius [83]. Therefore, it can be concluded that this overlap did occur. The overlap would increase the

concentration of the active radicals in the sub-activated region, thus increases the probability of the completion in the polymerization process by combining with oligomer molecules. The remainder of the sub-activated region, with low concentration of radicals, diffuses; and then finally it is dissolved and removed by the post-exposure development. Only those at the vicinity of the solid walls are attached with the oligomer molecules and form a roof on top of the walls. Figure 6-6 (a) shows a linking is created along two adjacent walls. However, since the two walls are far away, 15 µm offset, the linking is scarce and random. When parallel walls are placed close enough, as shown in Figure 6-6 (b) where the offset is 6 µm, the substantial linking occurred and the enclosed channels formed. However, since the array of walls are evenly spaced, interweaved linking took place. This can be avoided by placing pairs of walls with wider spacing.

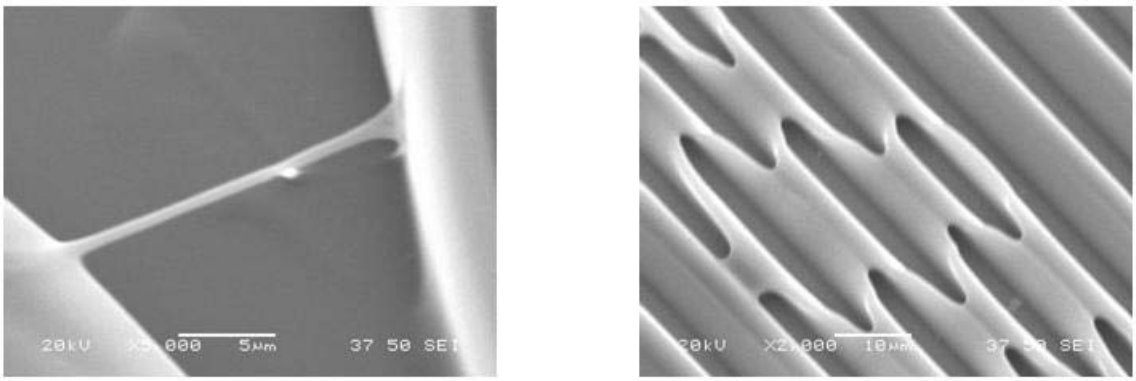

Figure 6-6: SEM images of roofing between two adjacent ribs (a) 2.48 ps, 13 MHZ, 15 µm offset, 260 mW, 150 mm/s (b) 2.48ps, 26 MHz, 6 µm offset, 296 mw, 150 mm/s

For a Gaussian beam, the highest absorption rate occurs at the focal point. Because of the greatest availability of high density photons at the focal plane, the concentration of active radicals would be highest here. Therefore, when the focal plane is above the substrate, depicted

in Figure 6-5 (a), the linking is most likely to initiate at the focal plane and continue along the axial direction because of the concentration gradient. Also, at the focal plane the two voxels are the closest, thereby, they provide physical support for adhesion.

Another scenario is depicted in Figure 6-5 (b). Here, the focal plane is below the substrate, thereby, the linking initiates at the substrate/resist interface and forms ripple structures at the bottom of the channels (see Figure 6-7).

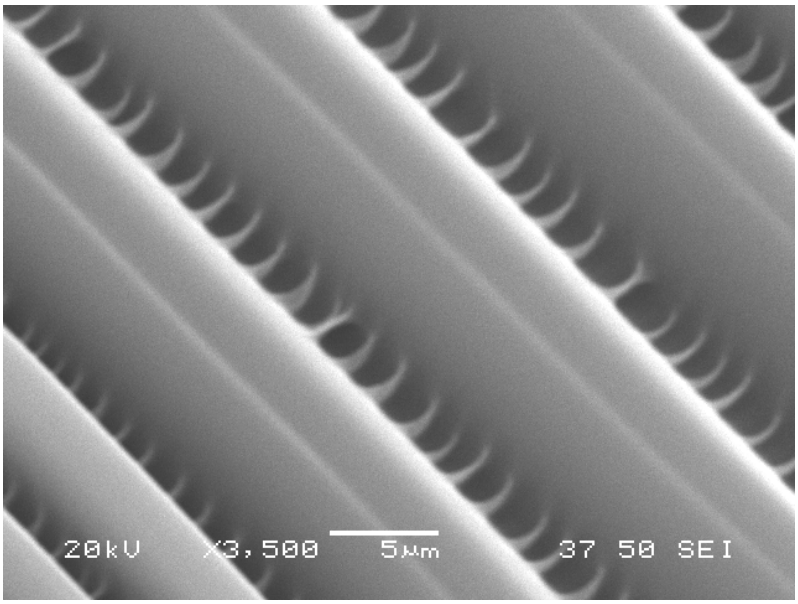

Figure 6-7: Ripple at the bottom of the channel, 2.48 ps, 26 MHz, 274mW, 150 mm/s

The growth in the axial direction is again determined by the radical concentration that is reduced while moving away from the focal plane. In the actual experiments, the location of the focal plane is difficult to control and maintain due to the lack of automated focusing mechanisms. Therefore, in some samples co-existence of roofs and ripples can be observed, as shown in Figure 6-8.

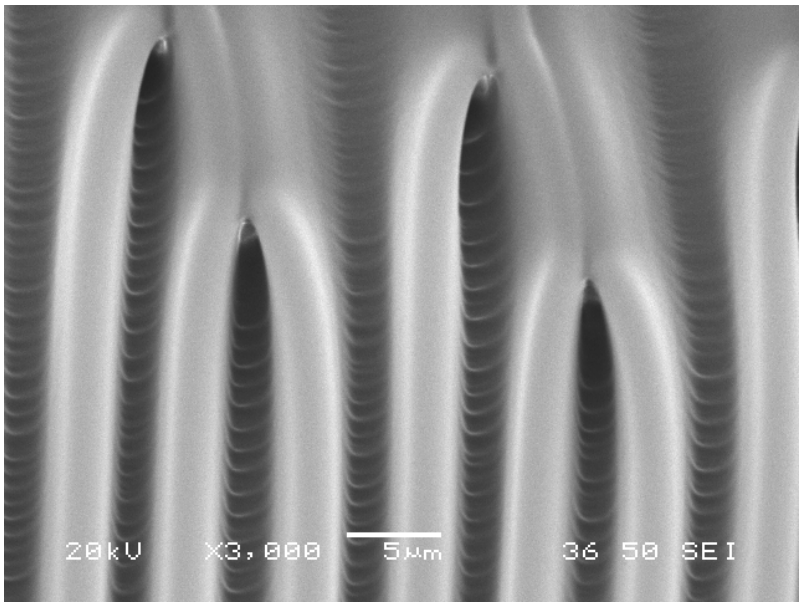

Figure 6-8: Co-existing roofing and ripples 2.48 ps, 26 MHz, 230mW, 150 mm/s

The arrays of fluidic channels with various laser parameters are created with the attempt to link the two adjacent ribs on the top and control the height and the width of enclosed channel in between. In addition, the channels precise width and the height can also be achieved by precisely positioning the focal point with high precision nano-positioning stages or laser beam steering mechanisms. Nonetheless, selection of appropriate process parameters is crucial in creating successful linkage. Figure 6-9 presents two channel arrays created at various laser parameters.

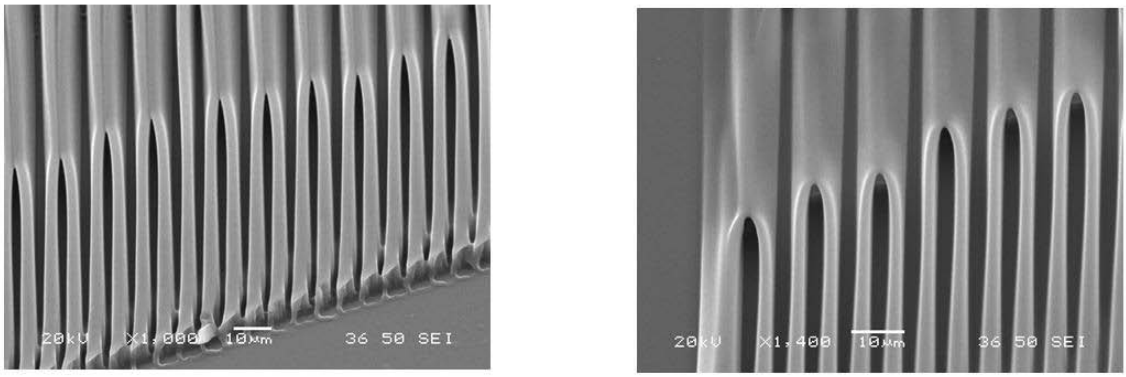

(a) (b)

Figure 6-9: Enclosed fluidic channel arrays 2.48 ps, 26 MHz, 300 mm/s (a)932 mW (b) 587 mW

6.5 PARAMETRIC EFFECTS

6.5.1 EFFECT OF LASER PULSE WIDTH

Laser pulse width is the most significant laser parameter in sub-sequent polymerization. One way to look at the pulse width is the irradiation time for the resist. For the irradiating laser beam, 214 fs, 1.45 ps and 3.57 ps pulse widths are used to investigate pulse width effect on the linking mechanism. With longer pulse width, the irradiation time is extended, and as a result, the radical generation is sufficiently increased at the focal area. The peak intensity in picosecond laser is less in comparison to the femtosecond, because in picosecond laser the pulse energy is distributed over longer pulse duration. Hence, the TPA polymerization region in picosecond laser is not as confined to the close vicinity of the focal spot as in the case of femtosecond laser. However, providing high enough energy by increasing laser power for picosecond laser, TPA polymerization is achievable. In picosecond, the pulse energy is less localized and the concentration of active radicals has greater distribution for a given laser spot. Therefore, the sub-activated region is significantly evident in picosecond laser exposure and therefore the

probability of linking via sub-sequent polymerization is considerably high. As the pulse width increases, the active radical concentration as well as its diffusion increases in the radial direction due to the energy distribution. Figure 6-10 (a)-(c) shows channels fabricated with pulse width of 428 fs, 1.42 ps, and 2.48 ps, respectively. As the pulse width increases, the sub-activated region starts to expand resulting in the channel transforms from a tall-narrow (with an apex on top) to a uniform circular profile (see the comparison of channels profile in Figure 6-10).

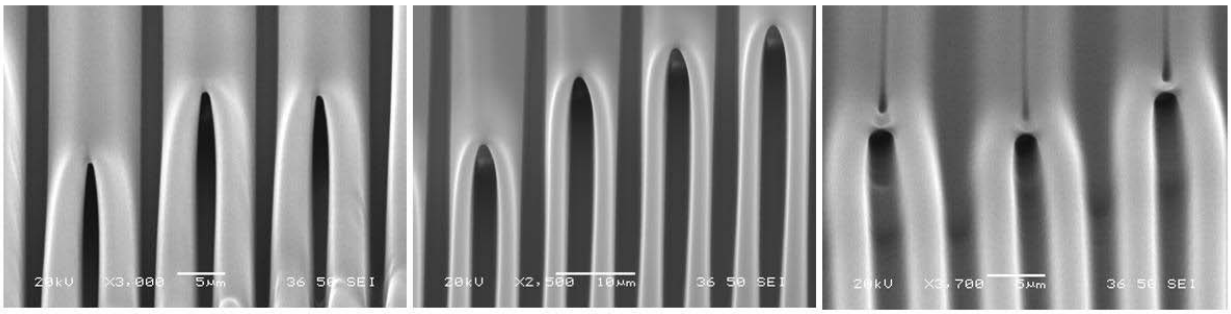

Figure 6-10: Enclosed fluidic channels (a) 428 fs, 26MHz, 455mW, 100 mm/s (b) 1.42 ps, 26MHz, 587mW, 100 mm/s (c) 2.48 ps, 26MHz, 320mW, 100 mm/s

6.5.2 EFFECT OF SCAN SPEED

Other than controlled spacing between the ribs and an optimal spot size, the width of the ribs and the height of the micro-channels can also be controlled dynamically manipulating the laser average power and the scan speed, as a measure of the laser fluence and the exposure time, respectively. With constant repetition rate, the two consecutive laser spot separation, R ($R=V/f$, Eqn. (4.4)), is smaller for low scan speed. If the value of R is less than the spot size, there will be an overlap ($\%Overlap = (1-R/2\omega_0) \times 100$, Eqn. (4.5)) between two consecutive spots. The spot-overlap is necessary to obtain uniform, continuous ribs with well-defined edges. Figure 6-11 illustrates the three spot-overlap conditions and their determining effects on the final

polymerized ribs. The slower scan speed with tighter resolution and greater spot-overlap results in a higher degree of polymerization. Also, the linearity of the ribs significantly improves with high percent spot-overlap, which is necessary to have good sidewalls in fluidic channels.

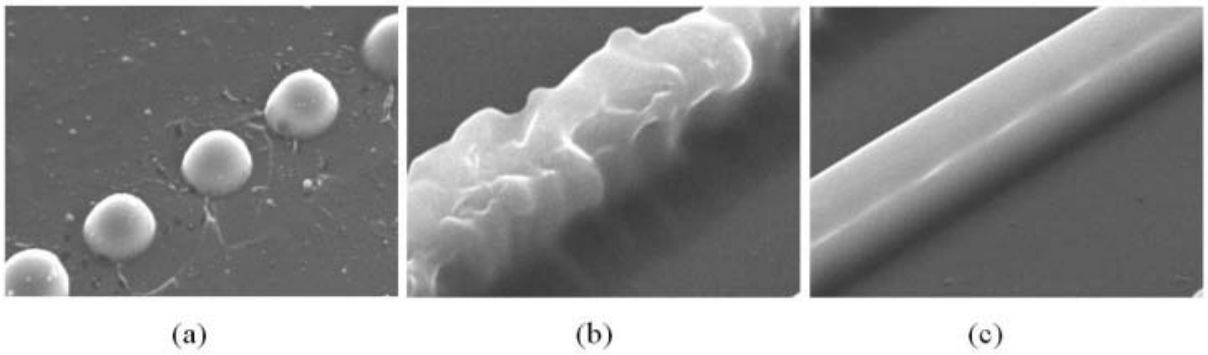

Figure 6-11: Polymerized ribs with spot-overlap (a) no spot-overlap (b) 55% spot-overlap (c) 90% spot-overlap

6.5.3 EFFECT OF LASER REPETITION RATE

The time period from the end of the first pulse until the second pulse arrives is called a dark period. The free radical chain polymerization reaction takes place during this period because of longer time duration available to complete polymerization, in comparison to time duration of the pulse interaction [50]. Therefore, it is essential for the degree of polymerization and can be controlled by manipulating the pulse repetition rate. For a given scan speed, the effective N_{eff} is proportional to the repetition rate (see Eqn. (4.3)). The N_{eff} for 26 MHz and 13 MHz was calculated to be 56 pulses and 28 pulses, respectively for the scan speed of 300 mm/s. The conversion ratio of the chain of monomers from active radicals increases as the number of pulses increases. Hence, for 26 MHz the active radical concentration is greater than for 13 MHz. However, the laser fluence decreases as the repetition rate increases. The resist is likely to polymerize even with low laser fluence, if the N_{eff} is high enough to provide sufficient

concentration of active radicals required to start photoinitiation. This phenomenon can be further explained by the Gaussian energy distribution of laser pulse. Figure 6-12 shows the Gaussian shaped intensity profile for effective machining spots [63]. The laser effect of multiple laser pulses focused into the same point will accumulate, if the dark period is shorter than the cooling time. Thus, if the single pulse energy is too low to induce photoinitiation, it can be induced by multiple pulses with high pulse repetition rate (shorter dark period), because of the accumulation phenomenon.

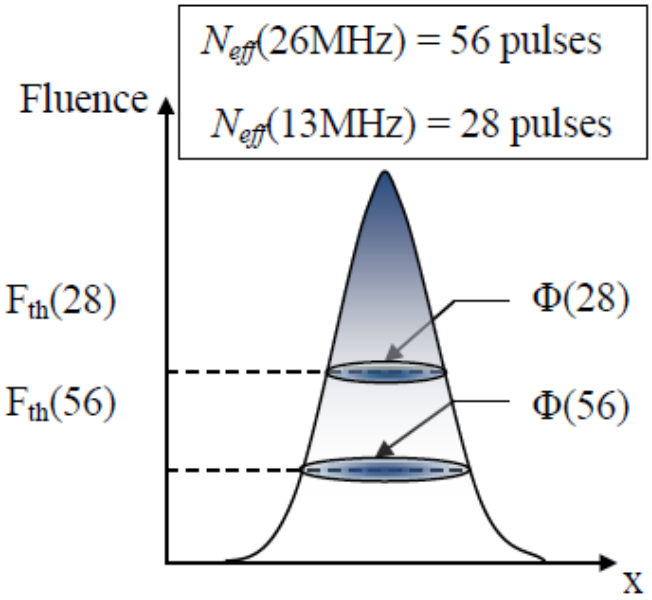

Figure 6-12: The effective spot size increases with increasing N_{eff}

In Figure 6-12, the lower intensity outer edge of the beam does not polymerize for N_{eff} of 28, because the accumulation of laser fluence is not sufficient to overcome the photoinitiation threshold fluence. In contrast, the outer edge for N_{eff} of 56 is polymerized with a high enough repetition rate to have a large enough accumulation of laser fluence. The diagram also illustrates the reduction in the threshold fluence with increase in N_{eff}. Thus, at a given fluence value, the

machine spot diameter for 56 pulses, $\Phi(56)$, is greater than the effective machining spot for 28 pulse, $\Phi(28)$, resulting in a greater area of exposure. At a given offset between two adjacent ribs, scan speed, and pulse energy, the probability of linking ribs is higher for larger N_{eff}, at which there will be a greater overlap of sub-activated regions. Therefore in our experiment, the repetition rate of 26 MHz was proven to be much more successful in generating enclosed channels.

6.6 SUMMARY

Realizing the true potential of microfluidic devices, many researchers have developed numerous techniques to fabricate fluidic channels. Nevertheless, most of these techniques are only capable of creating open fluidic channels. The open channels require additional post-processing so that they can be enclosed or sealed to avoid evaporation of the sample and chemical reagent. A single step fabrication of self-enclosed fluidic channels based on TPA polymerization has been proposed and successfully demonstrated. In this process, an ultrafast laser is used to polymerize parallel pairs of ribs and crosslink two adjacent ribs via sub-sequent polymerization to form hollow channel in between. For the first time, the model of the sub-sequent polymerization is presented and discussed. Laser parameters such as pulse energy, pulse width, repetition rate along, with process parameters, the scan speed and line offset were investigated for greater controllability of the process. Finally, the proposed method is, again a simple, fast and inexpensive process like the previous two processes proposed in Chapter 4 and 5. Nonetheless, the method proposed in this chapter is capable of producing the enclosed fluidic channels in a single step, which eliminate any post-processing of enclosing or sealing the channels; thereby, this can be a very attractive method for rapid prototyping for LOC and μTAS.

CHAPTER 7

SUMMARY, CONCLUSIONS AND FUTURE WORK

7.1 SUMMARY

Lab-on-a-chip and μTAS technologies represent a revolution in laboratory experimentation, bringing the benefits of miniaturization, integration, and automation to many research-based industries. Fluidic channels are the essential feature of any microfluidic devices. This research work is intended to develop new fabrication processes for the rapid prototyping of fluidic channels.

The currently employed fabrication processes were investigated and reviewed along with identification of the advantages and the limitations of each of these techniques. The processes are categorized into two main classes based on the fluidic channels material; inorganic materials and polymeric materials. In addition, the processes are further divided based on the fabrication techniques developed in IC manufacturing. Fabrication techniques of inorganic fluidic channels include various types of lithography and thin-film processes. Fabrication of polymeric fluidic channels includes techniques such as hot embossing, injection molding, casting and laser ablation.

Choosing the effective technique plays an important role in a relatively new area of research such as microfluidics. Due to the increase in demand for designing and prototyping various microfluidic devices, new fabrication methods are needed to substitute the lithography based methods initially adopted from IC fabrication to complement the demands of prototyping.

The femtosecond laser microfabrication technique is identified to be most capable of achieving the desired function of versatility, high quality and least number processing steps, along with being capable of producing true 3D features.

Even though the feasibility of TPA polymerization induced by the femtosecond lasers in creating microfluidic features has been predicted for a while now, the rapid prototyping applications of this technique is awaited due to the challenges faced in terms of laser parameters, inadequate experimental studies in this area and the lack of improvements in robustness of laser processing suitable for rapid prototyping. The physical process of laser-polymer interaction is indeed very complicated and involves a variety of different phenomena, underlying the different aspects of laser induced polymerization. These processes were successfully studied and also the mechanisms and phenomena involved in the laser induced polymerization for two distinctive polymers SU-8 and ORMOCER were explained.

This thesis shows that the femtosecond laser polymerization by the technique of TPA is a simple, fast and inexpensive process for rapid prototyping of microfluidic channels applicable to microsystems and microfluidic devices such as MEMS, LOC, μTAS and biochips. Unlike other lithography processes, it does not require any mask and it is configurable to design requirements, thereby it is suitable for rapid prototyping. For this research work, a high repetition rate femtosecond laser capable of producing high output power was chosen due to the critical requirements of high photon flux and photon flux density in order to induce TPA. General models for the experimental setup were developed after studying the capabilities of the proposed laser system. Three distinctive approaches were taken for the laser exposure scheme to create fluidic channels governed by different phenomena. The laser parameters like pulse width,

repetition rate and scan speed were thoroughly evaluated to study the influence of these parameters on resolution and the size of side walls of fabricated fluidic channels.

For the first study, an extremely simple idea of creating fluidic channels confined between two polymerized ribs is investigated and reported. The laser is scanned in the pattern of parallel lines with fixed pitch. The exposed lines turn into ribs after polymerizations. The laser parameters and the process parameters are evaluated to maximize the controllability of the process and reduce the width of the channel (i.e. the spacing between two ribs). It is also demonstrated that SU-8 has a threshold pronounced behavior and it decreases linearly with increase in repetition rate. Femtosecond laser with repetition rate of 4.33 MHz, 8.67 MHz, 13 MHz and 26 MHz found to have the photoinitiation threshold of 0.989 J/cm^2, 0.819 J/cm^2, 0.734 J/cm^2, and 0.400 J/cm^2, respectively. Experimental results showed that the high repetition rate is preferred to obtain minimum channel width due to the increase in polymerization construability of the ribs. Fluidic channels as narrow as 110 nm are successfully fabricated. Even though this method is proven to be very effective in creating fluidic channels down to the nanometer scale, it has its drawbacks in the ability to efficiently maintain a constant channel width for two dimensional fluidic networks. The major reason for such deficiency is because of the scan speed variance between two scan paths for the enclosing ribs.

The second study is conducted to overcome the limitation of the first process. Instead of creating a channel between two parallel ribs, this time the channel is engraved in the center of the rib via polymerization assisted ablation. This method is primarily based on a well-known direct material ablation phenomenon. Nevertheless, the TPA polymerization assisted ablation, utilized in this study, is investigated and reported for the first time. Polymerization assisted ablation

presents greater opportunity in ablating resist with low laser power in comparison to direct ablation of the resist. In addition, TPA assisted ablation also improves the feature size and spatial resolution with superior control compared to direct ablation.

The third and final study is conducted concentrating on creating enclosed channels. The previous two methods are capable of producing open channels which have to be enclosed or sealed by post processes, such as, thermal bonding, solvent bonding, adhesive bonding or chemical bonding. By doing so, not only does the fabrication cost and time increase, but also the process becomes more and more complex. In this study, an alternative process of creating self-enclosed fluidic channels is proposed. Similar to the first method, the channel is created between two polymerized ribs. However, this time the polymerization is controlled such that two adjacent ribs are crosslinked on top via sub-sequent polymerization forming a hollow channel in between. This study also proposed a model of sub-sequent polymerization. Also, the effects of laser parameters such as the pulse energy, pulse width, repetition rate along with process parameters, the scan speed and line offset were investigated.

7.2 CONCLUSIONS

Microfluidics, the manipulation of liquids and gases in channels is a rapidly growing research area that has the potential to influence a variety of industries from clinical diagnostics to drug discovery. The need for innovative fabrication methods for rapid prototyping of biochips, μTAS and LOC devices is continuously growing; hence the main objective of the thesis was to investigate and propose novel fabrication processes to overcome the shortcomings of the lithography methods inherited from microelectronics fabrication. All the objectives outlined for this research study are successfully achieved.

- Three novel and distinctive fabrication processes for fluidic channels based on TPA polymerization are successfully demonstrated focusing on different desirables. The first method is suitable for creating channels down to the nanometer scale. The second method is capable of creating two dimensional fluidic networks. The final method eliminates the post-processing to enclose the channels.
- The photoinitiation threshold fluence for SU-8 decreases linearly with respect to repetition rate. Also, the pulse energy and the laser fluence can be precisely controlled for the high repetition rate resulting in a feature with higher spatial resolution.
- TPA polymerization assisted ablation can be achieved at significantly less energy due to the lowered ablation threshold after polymerization. In addition, linear nature of the absorption after initial polymerization presents excellent controlling and predicting the ablating area.
- Self-enclosed channels can be created using TPA polymerization when polymerized sidewalls are crosslinked on top via the sub-sequent polymerization technique. Sub-sequent polymerization can result when there is an overlap of sub-activated region, which is resulted due to the concentration gradient of the active radicals. The combination of laser pulse width, repetition rate and scan speed, providing the sufficient overlap of the sub-activated region, are achievable to enclose channels at the top.

7.3 FUTURE WORK

This research has achieved promising results for fabricating fluidic channels in three simple ways utilizing the TPA polymerization phenomenon. The resist used here, SU-8 and ORMOCER, both are commercially available. However, this study can be extended to various

kinds of other photoresists with special photoinitiators designed for the available laser parameters. By doing so, the polymerization efficiency, resolution and aspect ratio can be enhanced.

One of the most attractive characteristics of TPA polymerization is its ability to generate true 3D structures. During this research study, piezoscanner was used to scan the laser beam in *XY* plane. A motor driven stage can be used to focus the laser in *Z* direction to create 3D features. Therefore, all necessary components, such as, microwells, nozzles, pumps, valves and channels can be fabricated in a single step.

From the second experimental study, it can be concluded that the threshold fluence can be determined for the given repetition rate, scan speed, and focal spot radius if the material constants *C* and *b* are known. These constants can be found experimentally but their relationship with the photoresist's properties should be established for further in-depth analysis.

Finally, TPA has great potential to create 3D channels with different cross section profiles because of its ability to polymerize only at the focal length in thick resist. Future work will be focused on creating 3D channels with desired cross section profiles using the property of within-volume-polymerization of TPA.

REFERENCE

[1] S. Deffree. IC insights cautious, but still sees 2008 growth. EDN September 29, 2008. <http://www.edn.com/article/CA6600386.html> [Accessed April 19].

[2] P. Abgrall, A.-. Gué. "Lab-on-chip technologies: Making a microfluidic network and coupling it into a complete microsystem - A review" *J Micromech Microengineering.* **17.** 5 (2007).

[3] D. Erickson. "Towards numerical prototyping of labs-on-chip: Modeling for integrated microfluidic devices" *Microfluid Nanofluid.* **1.** 4 (2005) 301-318.

[4] J.O. Foley, et al. "Concentration gradient immunoassay. 2. computational modeling for analysis and optimization" *Anal Chem.* **79.** 10 (2007) 3549-3553.

[5] P. Auroux, D. Iossifidis, D.R. Reyes, A. Manz. "Micro total analysis systems. 2. analytical standard operations and applications" *Anal Chem.* **74.** 12 (2002) 2637-2652.

[6] D.R. Reyes, D. Iossifidis, P.-. Auroux, A. Manz. "Micro total analysis systems. 1. introduction, theory, and technology" *Anal Chem.* **74.** 12 (2002) 2623-2636.

[7] S.C. Terry, J.H. Jerman, J.B. Angell. "A gas chromatographic air analyzer fabricated on a silicon wafer" *IEEE Trans Electron Devices.* **26.** 12 (1979) 1880-1886.

[8] A. Manz, N. Graber, H.M. Widmer. "Miniaturized total chemical analysis systems: A novel concept for chemical sensing" *Sens Actuators, B Chem.* **1.** 1-6 (1990) 244-248.

[9] M.A. Burns, et al. "An integrated nanoliter DNA analysis device" *Science.* **282.** 5388 (1998) 484-487.

[10] R. Fan, et al. "DMA translocation in inorganic nanotubes" *Nano Lett.* **5.** 9 (2005) 1633-1637.

[11] J.T. Mannion, C.H. Reccius, J.D. Cross, H.G. Craighead. "Conformational analysis of single DNA molecules undergoing entropically induced motion in nanochannels" *Biophys J.* **90.** 12 (2006) 4538-4545.

[12] M. Zwolak, M. Di Ventra. "Electronic signature of DNA nucleotides via transverse transport" *Nano Lett.* **5.** 3 (2005) 421-424.

[13] D.T. Chiu, et al. "Patterned deposition of cells and proteins onto surfaces by using three-dimensional microfluidic systems" *Proc Natl Acad Sci U S A.* **97.** 6 (2000) 2408-2413.

[14] Y. Liu, et al. "Electrophoretic separation of proteins on a microchip with noncovalent, postcolumn labeling" *Anal Chem.* **72.** 19 (2000) 4608-4613.

[15] S. Takayama, et al. "Patterning cells and their environments using multiple laminar fluid flows in capillary networks" *Proc Natl Acad Sci U S A.* **96.** 10 (1999) 5545-5548.

[16] D.V. McAllister, M.G. Allenand M.R. Prausnitz. "Microfabricated microneedles for gene and drug delivery" (2000).

[17] P.M. Sinha, et al. "Nanoengineered device for drug delivery application" *Nanotechnology.* **15.** 10 (2004).

[18] M. Foquet, et al. "DNA fragment sizing by single molecule detection in submicrometer-sized closed fluidic channels" *Anal Chem.* **74.** 6 (2002) 1415-1422.

[19] O.A. Saleh, L.L. Sohn. "Quantitative sensing of nanoscale colloids using a microchip coulter counter" *Rev Sci Instrum.* **72.** 12 (2001) 4449-4451.

[20] O.A. Saleh, L.L. Sohn. "An artificial nanopore for molecular sensing" *Nano Lett.* **3.** 1 (2003) 37-38.

[21] S.C. Jacobson, A.W. Moore, J.M. Ramsey. "Fused quartz substrates for microchip electrophoresis" *Anal Chem.* **67.** 13 (1995) 2059-2063.

[22] B. He, N. Tait, F. Regnier. "Fabrication of nanocolumns for liquid chromatography" *Anal Chem.* **70.** 18 (1998) 3790-3797.

[23] M. Tokeshi, T. Minagawa, T. Kitamori. "Integration of a microextraction system on a glass chip: Ion-pair solvent extraction of fe(II) with 4,7-diphenyl-1,10-phenanthrolinedisulfonic acid and tri-n-octylmethylammonium chloride" *Anal Chem.* **72.** 7 (2000) 1711-1714.

[24] T. Pan, R.T. Kelly, M.C. Asplund, A.T. Woolley. "Fabrication of calcium fluoride capillary electrophoresis microdevices for on-chip infrared detection" *J Chromatogr A.* **1027.** 1-2 (2004) 231-235.

[25] S. Berry. "Honey I've shrunk biomedical technology!" *Trends Biotechnol.* **20.** 1 (2002) 3-4.

[26] P.C. Simpson, A.T. Woolley, R.A. Mathies. "Microfabrication technology for the production of capillary array electrophoresis chips" *Biomed Microdevices.* **1.** 1 (1998) 7-25.

[27] G.T. Kovacs. *Micromachined transducers sourcebook* **1st** McGraw-Hill Science/Engineering/Math, (1998).

[28] R. Divakar, D. Butler and I. Papautsky. "Room temperature low-cost UV-cured adhesive bonding for microfluidic biochips" *International Conference on Chemical and Biochemical Analysis Systems (UTAS)*, Monterey, CA, October 21-25, (2001).

[29] E. Di Fabrizio, et al. "X-ray lithography for micro-and nano-fabrication at ELETTRA for interdisciplinary applications" *J Phys Condens Matter.* **16.** 33 (2004).

[30] H.N. Chapman, et al. "First lithographic results from the extreme ultraviolet engineering test stand" *J Vac Sci Technol B Microelectron Nanometer Struct.* **19.** 6 (2001) 2389-2395.

[31] C.K. Harnett, G.W. Coates, H.G. Craighead. "Heat-depolymerizable polycarbonates as electron beam patternable sacrificial layers for nanofluidics" *J Vac Sci Technol B Microelectron Nanometer Struct.* **19.** 6 (2001) 2842-2845.

[32] A. Hibara, et al. "Nanochannels on a fused-silica microchip and liquid properties investigation by time-resolved fluorescence measurements" *Anal Chem.* **74.** 24 (2002) 6170-6176.

[33] H. Yanagi, Y. Kawai. "Organic field-effect transistor with narrow channel fabricated using focused ion beam" *Jpn J Appl Phys Part 2 Letter.* **43.** 12 B (2004).

[34] H. Cao, J.O. Tegenfeldt, R.H. Austin, S.Y. Chou. "Gradient nanostructures for interfacing microfluidics and nanofluidics" *Appl Phys Lett.* **81.** 16 (2002) 3058.

[35] L.J. Guo, X. Cheng, C.-. Chou. "Fabrication of size-controllable nanofluidic channels by nanoimprinting and its application for DNA stretching" *Nano Lett.* **4.** 1 (2004) 69-73.

[36] V. Studer, A. Pépin, Y. Chen. "Nanoembossing of thermoplastic polymers for microfluidic applications" *Appl Phys Lett.* **80.** 19 (2002) 3614.

[37] M. Köhlerand W. Fritzsche. Nanotechnology: An introduction to nanostructuring techniques **2nd ed** Germany: Wiley-VCH, (2007).

[38] B.A. Peeni, et al. "Planar thin film device for capillary electrophoresis" *Lab Chip Miniaturisation Chem Biol.* **5.** 5 (2005) 501-505.

[39] G. Lee, et al. "Microfabricated plastic chips by hot embossing methods and their applications for DNA separation and detection" *Sens Actuators, B Chem.* **75.** 1-2 (2001) 142-148.

[40] S. Maruo, O. Nakamura, S. Kawata. "Three-dimensional microfabrication with two-photon-absorbed photopolymerization" *Opt Lett.* **22.** 2 (1997) 132-134.

[41] A. Doraiswamy, et al. "Two photon induced polymerization of organic-inorganic hybrid biomaterials for microstructured medical devices" *Acta Biomater.* **2.** 3 (2006) 267-275.

[42] S. Maruo, K. Ikuta, H. Korogi. "Submicron manipulation tools driven by light in a liquid" *Appl Phys Lett.* **82.** 1 (2003) 133-135.

[43] S. Maruo, K. Ikuta, H. Korogi. "Force-controllable, optically driven micromachines fabricated by single-step two-photon microstereolithography" *J Microelectromech Syst.* **12.** 5 (2003) 533-539.

[44] M. Göppert-Mayer. *Ann Phys.* **9.** (1931) 273-294.

[45] W. Kaiser, C.G.B. Garrett. "Two-photon excitation in CaF2: Eu2+" *Physical Review Letters.* **7.** 6 (1961) 229-231.

[46] J.P. Fouassier. Photoinitiation, photopolymerization and photocuring: Fundamentals and applications New York: Hanser, (1995).

[47] M. Rumi, et al. "Two-photon absorbing materials and two-photon-induced chemistry" (2008).

[48] Z. Huang. One vs two-photon excitation. www.belfield.cos.ucf.edu <http://belfield.cos.ucf.edu/one%20vs%20two-photon%20excitation.html> [Accessed April 19].

[49] S.M. Kuebler, M. Rumi. "Nonlinear optics -- applications: Three-dimensional microfabrication" *Encyclopedia of Modern Optics.* (2004) 189-206.

[50] C. Lee, et al. "Fabricating high-aspect-ratio sub-diffraction-limit structures on silicon with two-photon photopolymerization and reactive ion etching" *Appl Phys A.* **79.** 8 (2004) 2027-2031.

[51] H. Sun, et al. "Shape precompensation in two-photon laser nanowriting of photonic lattices" *Appl Phys Lett.* **85.** 17 (2004) 3708-3710.

[52] J. Serbin, et al. "Femtosecond laser-induced two-photon polymerization of inorganic-organic hybrid materials for applications in photonics" *Opt Lett.* **28.** 5 (2003) 301-303.

[53] R. Pal, et al. "An integrated microfluidic device for influenza and other genetic analyses" *Lab Chip Miniaturisation Chem Biol.* **5.** 10 (2005) 1024-1032.

[54] W.H. Teh, et al. "Effect of low numerical-aperture femtosecond two-photon absorption on (SU-8) resist for ultrahigh-aspect-ratio microstereolithography" *J Appl Phys.* **97.** 5 (2005) 1-11.

[55] L. Shah, A.Y. Arai, S.M. Eaton, P.R. Herman. "Waveguide writing in fused silica with a femtosecond fiber laser at 522 nm and 1 MHz repetition rate" *Opt.Express.* **13.** 6 (2005) 1999-2006.

[56] X. Liu, D. Du, G. Mourou. "Laser ablation and micromachining with ultrashort laser pulses" *IEEE J Quantum Electron.* **33.** 10 (1997) 1706-1716.

[57] K. Venkatakrishnan, et al. "Femtosecond pulsed laser direct writing system" *Opt Eng.* **41.** 6 (2002) 1441-1445.

[58] S.W.P. Turner, M. Cabodi, H.G. Craighead. "Confinement-induced entropic recoil of single DNA molecules in a nanofluidic structure" *Phys Rev Lett.* **88.** 12 (2002) 1281031-1281034.

[59] Z.R. Chowdhury, R. Fedosejevs. "Two photon absorption coefficients and processing parameters for photoresists" *Microsyst Technol.* **14.** 1 (2008) 59-67.

[60] K. Venkatakrishnan, B. Tan, B.K.A. Ngol. "Submicron holes in copper thin film directly ablated using femtosecond pulsed laser" *Opt Eng.* **40.** 12 (2001) 2892-2893.

[61] K. Venkatakrishnan, et al. "Effect of scanning resolution and fluence fluctuation on femtosecond laser ablation of thin films" *Appl Phys A.* **77.** 5 (2003) 655-658.

[62] T.H.R. Crawford, A. Borowiec, H.K. Haugen. "Femtosecond laser micromachining of grooves in silicon with 800 nm pulses" *Appl Phys A.* **80.** 8 (2005) 1717-1724.

[63] P.T. Mannion, et al. "The effect of damage accumulation behaviour on ablation thresholds and damage morphology in ultrafast laser micro-machining of common metals in air" *Appl Surf Sci.* **233.** 1-4 (2004) 275-287.

[64] E.N. Glezer, E. Mazur. "Ultrafast-laser driven micro-explosions in transparent materials" *Appl Phys Lett.* **71.** 7 (1997) 882-884.

[65] H. Sun, et al. "Real three-dimensional microstructures fabricated by photopolymerization of resins through two-photon absorption" *Opt Lett.* **25.** 15 (2000) 1110-1112.

[66] K. Venkatakrishnan, S. Jariwala, B. Tan. "Maskless fabrication of nano-fluidic channels by two-photon absorption (TPA) polymerization of SU-8 on glass substrate" *Opt Express.* **17.** 4 (2009) 2756-2762.

[67] M. Castaño-Álvarez, M.T. Fernández-Abedul, A. Costa-García. "Poly(methylmethacrylate) and topas capillary electrophoresis microchip performance with electrochemical detection" *Electrophoresis.* **26.** 16 (2005) 3160-3168.

[68] Y. Yang, C. Li, K.H. Lee, H.G. Craighead. "Coupling on-chip solid-phase extraction to electrospray mass spectrometry through an integrated electrospray tip" *Electrophoresis.* **26.** 19 (2005) 3622-3630.

[69] T.B. Stachowiak, et al. "Fabrication of porus polymer monoliths covalently attached to the walls of channels in plastic microdevices" *Electrophoresis.* **24.** 21 (2003) 3689-3693.

[70] J. Wang, et al. "Towards disposable lab-on-a-chip: Poly(methylmethacrylate) microchip electrophoresis device with electrochemical detection" *Electrophoresis.* **23.** 4 (2002) 596-601.

[71] R.T. Kelly, T. Pan, A.T. Woolley. "Phase-changing sacrificial materials for solvent bonding of high-performance polymeric capillary electrophoresis microchips" *Anal Chem.* **77.** 11 (2005) 3536-3541.

[72] Z. Meng, S. Qi, S.A. Soper, P.A. Limbach. "Interfacing a polymer-based micromachined device to a nanoelectrospray ionization fourier transform ion cyclotron resonance mass spectrometer" *Anal Chem.* **73.** 6 (2001) 1286-1291.

[73] D.C. Duffy, J.C. McDonald, O.J.A. Schueller, G.M. Whitesides. "Rapid prototyping of microfluidic systems in poly(dimethylsiloxane)" *Anal Chem.* **70.** 23 (1998) 4974-4984.

[74] J.C. McDonald, et al. "Fabrication of microfluidic systems in poly(dimethylsiloxane)" *Electrophoresis.* **21.** 1 (2000) 27-40.

[75] T. Fujii. "PDMS-based microfluidic devices for biomedical applications" *Microelectron Eng.* **61-62.** (2002) 907-914.

[76] P. Mao, J. Han. "Fabrication and characterization of 20 nm planar nanofluidic channels by glass-glass and glass-silicon bonding" *Lab Chip Miniaturisation Chem Biol.* **5.** 8 (2005) 837-844.

[77] W. Li, et al. "Sacrificial polymers for nanofluidic channels in biological applications" *Nanotechnology.* **14.** 6 (2003) 578-583.

[78] Q. Xia, K.J. Morton, R.H. Austin, S.Y. Chou. "Sub-10 nm self-enclosed self-limited nanofluidic channel arrays" *Nano Letters.* **8.** 11 (2008) 3830-3833.

[79] U. Bilitewski, M. Genrich, S. Kadow, G. Mersal. "Biochemical analysis with microfluidic systems" *Anal Bioanal Chem.* **377.** 3 (2003) 556-569.

[80] H.A. Reed, et al. "Fabrication of microchannels using polycarbonates as sacrificial materials" *J Micromech Microengineering.* **11.** 6 (2001) 733-737.

[81] G. Witzgall, et al. "Single-shot two-photon exposure of commercial photoresist for the production of three-dimensional structures" *Opt Lett.* **23.** 22 (1998) 1745-1747.

[82] H. Sun, et al. "Scaling laws of voxels in two-photon photopolymerization nanofabrication" *Appl Phys Lett.* **83.** 6 (2003) 1104-1106.

[83] N. Uppal, P.S. Shiakolas. "Modeling of temperature-dependent diffusion and polymerization kinetics and their effects on two-photon polymerization dynamics" *Journal of Micro-Nanolithography Mems and Moems.* **7.** 4 (2008) 043002.